1
Glass-Transition Phenomena in Polymer Blends

Ioannis M. Kalogeras

University of Athens, Faculty of Physics, Department of Solid State Physics, Zografos 15784, Greece

1.1
Introduction

The ever-increasing demand for polymeric materials with designed multifunctional properties has led to a multiplicity of manufacturing approaches and characterization studies, seeking proportional as well as synergistic properties of novel composites. Fully integrated in this pursuit, blending and copolymerization have provided a pair of versatile and cost-effective procedures by which materials with complex amorphous or partially crystalline structures are fabricated from combinations of existing chemicals [1–3]. Through variations in material's composition and processing, a subtle adaptation of numerous chemical (corrosion resistance, resistance to chemicals, etc.), thermophysical (e.g., thermal stability, melting point, degree of crystallinity, and crystallization rate), electrical or dielectric (e.g., conductivity and permittivity), and manufacturing or mechanical properties (dimensional stability, abrasion resistance, impact strength, fracture toughness, gas permeability, recyclability, etc.) can be accomplished effortlessly. It is therefore not surprising the fact that related composites have been widely studied with respect to their microstructure (e.g., length scale of phase homogeneity in miscible systems, or type of the segregation of phases in multiphasic materials) and the evolution of their behavior and complex relaxation dynamics as the material traverses the glass transformation range [4–7].

The reversible transformation of amorphous materials (including amorphous regions within semicrystalline polymers) from a molten or rubber-like state into a stiff and relatively brittle glassy state is denoted as "glass transition" (or "liquid–glass transition"). Originally, this term was introduced to describe the striking changes in thermodynamic derivative properties (e.g., heat capacity, compressibility, and thermal expansivity) that normally accompany the solidification of a viscous liquid, such as a polymer melt, during cooling or even compression. In time course, however, the term "glass transition" acquired a broader meaning and is now frequently

Encyclopedia of Polymer Blends: Volume 3: Structure, First Edition. Edited by Avraam I. Isayev.

employed for describing "any phenomenon that is caused by a timescale (on which some interesting degree of freedom equilibrates) becoming longer than the timescale on which the system is being observed" [6]. The conventional route to the glassy state of matter is the (rapid) cooling of a melt, provided that crystalization is bypassed. Interestingly, melt mixing provides one of the most common techniques for the large-scale preparation of compression or injection molded polymer blends. The freezing-in of a structural state during cooling, commonly referred to as glassification or vitrification, corresponds to a loss of the state of internal equilibrium possessed by the initial liquid. The vitrification process occurs over a narrow temperature interval, the so-called glass transformation range, over which the characteristic molecular relaxation time of the system changes by some 2–2.5 orders of magnitude, reaching the order of 100 s (the laboratory timescale). In macromolecular substances, this relaxation time is connected with the time response of cooperative (long-range) segmental motions. For convenience, the glass transformation region is traditionally represented by a single value, denoted as the "glass-transition temperature" (T_g) [7]. Because of the range of temperature involved and also because of its history, path, and cooling (or heating) rate dependences, assigning a characteristic T_g to a system becomes frequently a problematic task. Nonetheless, when appropriately measured, the glass-transition temperature is very reproducible and has become recognized as one of the most important material properties, directly relating to several other thermophysical and rheological properties, processing parameters, and fields of potential application [8].

Nowadays, polymer engineering largely relies on chemical and compositional manipulation of T_g, in an attempt to target particular technological or industrial requirements. A notable paradigm provides meticulous studies on the physical stabilization of active pharmaceutical ingredients (typically, poorly soluble drugs, but potentially also of proteins or other compounds) in the form of binary or ternary solid dispersions/solutions with biologically inert glassy polymers, with the aim of increasing their solubility, dissolution rate, bioavailability, and therapeutic effectiveness [9]. Significant improvements in the performance of related systems are frequently accredited to a combination of factors, including the effects of hydrogen-bonding networks or ion–dipole intercomponent interactions (i.e., stabilizing enthalpic contributions), and strong crystallization-inhibitory steric effects owing to the high viscosity of the polymeric excipient [10]. The implementation of solid-state glassy formulations as a means to preserve the native state of proteins (biopreservation) entails a higher level of complexity in behavior, since chemical and physical stabilization heavily relies on manipulating the local anharmonic motions of the individual protein molecules (fast dynamics) in addition to their slow (glass-transition) dynamics [11]. The established practice in the preservation of proteins primarily focuses on hydrated solid-state mixtures of proteins with glass-forming disaccharides (e.g., trehalose or sucrose) or polyols (e.g., glycerol), serving as lyoprotectants. Still, processing problems such as surface denaturation, mixture separation, and pH changes that lead to physical and chemical degradations, in addition to degradations occurring on storage, make clear that manufacturing of alternative solid-state formulations remains a challenging issue. In this pursuit, however, one

has to take into account the complex internal protein dynamics and the fact that in order to successfully maintain protein's structural integrity the selected glass-forming polymer will have to sustain a strong and complicated hydrogen-bonding network (around and to the protein) that will effectively couple matrix dynamics to the internal dynamics of the protein molecules [11]; the adaptability in local structures and chemical environments, offered by polymers' blending, might provide a viable solution to the problem.

While general consensus exists as to the usability of glass transitions in exploring molecular mobilities, molecular environments, and structural heterogeneities in segmental length scales, conflicting arguments still appear regarding the interpretation of fundamental phenomenological aspects of the transition itself. The nature of the glass transition remains one of the most controversial problems in the disciplines of polymer physics and materials science, and that in spite of the in-depth experimental and theoretical research conducted hitherto [12–14]. The difficulty in treating glass transitions even in relatively simple linear-chain amorphous polymers is caused by the almost undetectable changes in static structure, regardless of the qualitative changes in characteristics and the extremely large change in the timescale. Given the significance of this subject, this chapter begins with an overview of important aspects of the phenomenology of glass formation. To address the perplexing behavior encountered when a system passes through its glass transformation range, a number of theoretical models approach this phenomenon using arguments pointing to a thermodynamic or a purely dynamic transition. Although we have not arrived at a comprehensive theory of supercooled liquids and glasses, it is frequently recognized that the observed glass transitions are not *bona fide* phase transitions, but rather a dynamical crossover through which a viscous liquid falls out of equilibrium and displays solid-like behavior on the experimental timescale. Basic notions and derivations of common theoretical models of the glass transition are presented in Section 1.2, with particular reference to early free volume and configurational entropy approaches, in view of their impact on the development of "predictive" relations for the compositional dependence of the T_g in binary polymer systems. Note that regardless of the multitude of treatments we clearly lack a widely accepted model that would allow *ab initio* calculation of the glass-transition temperature. Most theoretical approaches simply allow a prediction of changes in T_g with – among other variables – applied pressure, degree of polymerization (molar mass) or curing (cross-linking), and composition. Important chemical factors that influence the affinity of the components and the magnitude of T_g in polymer blends, in addition to manufacturing processes or treatments that are typically used for manipulating the glass-transition temperature of polymer composites, are briefly reviewed in Section 1.3.

The largely experimentally driven scientific interest on glass transitions in composite materials is equipped with a collection of experimental methods and measuring techniques, with the ability to probe molecular motions at distinctly different length scales [15–17]. Most of them introduce different operational definitions of T_g, and some of them are endorsed as scientific standards. In Section 1.4, fundamental aspects of important experimental means are presented,

with emphasis placed on the relative sensitivity and measuring accuracy of each technique, and the proper identification and evaluation of glass transitions in multicomponent systems. Typically, the broadness of the glass-transition region is indicative of structural (nano)heterogeneities, whereas its location can be adjusted by appropriate variations in composition and the ensuing changes in the degree of interchain interactions or material's free volume. Given the diversity of chemical structures of the polymers used and the wide range of dynamic asymmetries and molecular affinities explored, it is not surprising the wealth of information on polymers' miscibility and the number of phenomena revealed in related studies. Two general cases are distinguished experimentally: *single-phase* and *phase-separated* systems. In the first case, for instance in a pair of miscible polymers or in random copolymers (i.e., with random alternating blocks along the macromolecular chain), a single – although rather broad – glass-transition region is recorded by most experimental techniques. The glass-transition behavior associated with phase separation, a situation characterizing the vast majority of engineering polymer blends, their related graft, and block copolymers, as well as interpenetrating polymer networks, demonstrates an elevated level of complexity; multiple transitions, ascribed to pure component phases and regions of partial mixing, are common experimental findings. Issues related to miscibility evaluations of polymer blends, such as the determination of the length scale of structural heterogeneity using different experimental approaches, are discussed in Section 1.5. The theoretical foundations and practical examples from the analysis of experimental data for miscible systems are critically reviewed in Section 1.6. The applicability ranges of important theoretical, semiempirical, or purely phenomenological mixing rules used for describing the compositional dependence of T_g are explored, with examples demonstrating the physical meaning of their parameters. A number of case studies, involving intermolecularly hydrogen-bonded binary blends and ternary polymer systems, are presented in the Section 1.7. This chapter ends with a summary of general rules relating the results of glass-transition studies with structural characterizations and miscibility evaluations of polymer blends, as well as typical requirements for reliable determinations of T_g in polymeric systems.

1.2 Phenomenology and Theories of the Glass Transition

1.2.1 Thermodynamic Phase Transitions

What seems to be a long-standing and exceptionally puzzling question is whether the physics of glass formation can be understood considering a purely dynamical origin with no thermodynamic signature, or necessitates thermodynamic or structural foundation. Customarily, the apparent glass-transition phenomenon in appropriately prepared amorphous materials (e.g., several

oxides, halides, salts, organic compounds, metal alloys, and numerous polymeric systems) is considered to be a kinetic crossover, and the most remarkable phenomena – structural arrest and dynamic heterogeneities – are strongly linked to molecular dynamics. Purely kinetic explanations, however, overlook the thermodynamic aspects of the phenomenology of glass formation and its deceptive resemblance to a second-order phase transition. Formally, as "phase transition" we consider the transformation of a thermodynamic system from one phase or state of matter to another, produced by a change in an intensive variable. The traditional classification scheme of phase transitions, proposed by Paul Ehrenfest, is based on the behavior of free energy (F) as a function of other state variables (e.g., pressure, P; volume, V; or temperature, T). Under this scheme, phase transitions are labeled by the lowest derivative of the free-energy function that is discontinuous at the transition. Thus, *first-order* phase transitions exhibit a discontinuity in the first derivative of the free energy with respect to some thermodynamic variable. In the course of heating, during a first-order transition the material absorbs a certain amount of heat (called the *latent heat of transition*) and undergoes a change in its constant-pressure heat capacity C_P. Typical examples are various crystal–liquid–gas phase transitions (e.g., melting or freezing, boiling, and condensation), which involve a discontinuous change in density (ρ), the first derivative of the free energy with respect to the chemical potential. On the other hand, *second-order* phase transitions are continuous in the first derivative of the free energy, but exhibit discontinuity in a second derivative of it. The order–disorder transitions in alloys and the ferromagnetic phase transition are typical examples. Passing through such transitions the material will undergo a change in its heat capacity, but no latent heat will be present.

The order of a phase transition can be defined more systematically by considering the thermodynamic Gibbs free-energy function, G. In a first-order phase transition, the G (T, P) function is continuous, but its first derivatives with respect to the relevant state parameters,

$$S = -\left(\frac{\partial G}{\partial T}\right)_P, \quad V = \left(\frac{\partial G}{\partial P}\right)_T \quad \text{and} \quad H = -\left(\frac{\partial (G/T)}{\partial (1/T)}\right)_P, \tag{1.1}$$

are discontinuous across the phase boundary (Figure 1.1; the symbol S denotes entropy, and H stands for enthalpy). In a similar way, in a second-order phase transition the above functions are continuous, but their derivatives with respect to the relevant state parameters, isobaric heat capacity, compressibility, κ_T, and isobaric expansivity (also called the coefficient of thermal expansion), α,

$$C_P = -T\left(\frac{\partial^2 G}{\partial T^2}\right)_P = T\left(\frac{\partial S}{\partial T}\right)_P = \left(\frac{\partial H}{\partial T}\right)_P \tag{1.2a}$$

$$\kappa_T = -\frac{1}{V}\left(\frac{\partial^2 G}{\partial P^2}\right)_T = -\frac{1}{V}\left(\frac{\partial V}{\partial P}\right)_T \tag{1.2b}$$

$$a = \frac{1}{V}\left(\frac{\partial}{\partial T}\left(\frac{\partial G}{\partial P}\right)_T\right)_P = \frac{1}{V}\left(\frac{\partial V}{\partial T}\right)_P, \tag{1.2c}$$

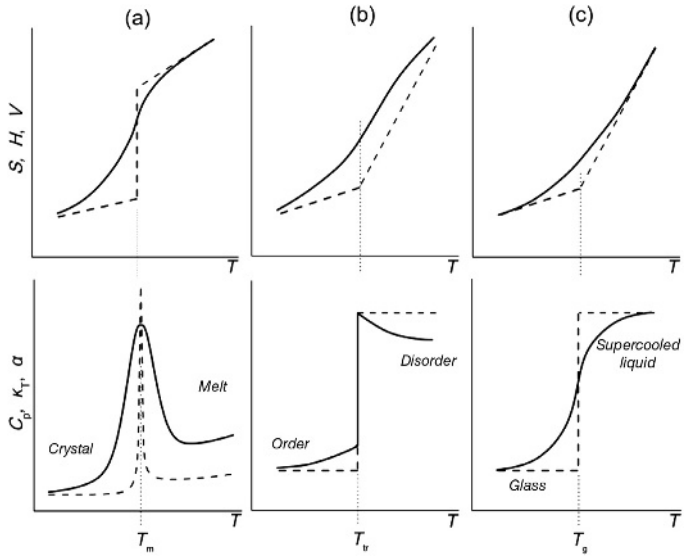

Figure 1.1 Schematic representation of thermodynamic responses. (a) First-order phase transition: consider, for example, melting of a crystal with defects (—) or of a perfect infinite crystal (--). (b) Second-order transition: transition dominated by intermolecular cooperative phenomena (—), or having only intermolecular cooperative phenomena (--). (c) Glass transition: experimental response (—), and ideal response in an infinately slow experiment (--).

are discontinuous across the phase boundary. Figure 1.1 compares the thermodynamic signatures of the classic first- and second-order transitions with the response of the experimental glass transition. Parameters such as α and C_p, and many other properties of inorganic glasses and glassy polymers exhibit a gradual change in slope in the glass-transition temperature, and any such (rounded) step or kink can be used to define T_g (see Section 1.4). This behavior is to be contrasted with the peak or the discontinuity expected, respectively, for genuine first- or second-order phase transformations. The latter is also characterized by a single ordering parameter determining the position of equilibrium in the relaxing system, with the jumps of the above parameters connected via the Ehrenfest ratio

$$\Pi_E \equiv \frac{1}{VT}\frac{\Delta C_p \Delta \kappa_T}{(\Delta\alpha)^2} = 1. \tag{1.3}$$

At the glass-transition temperature, however, the same ratio (known as the Prigogine–Defay ratio) is greater than unity [18,19]. Arguments like the above cast considerable doubt on the validity of models (e.g., configurational entropy models or the random first-order transition [RFOT] theory), postulating the existence of some type of an underlying thermodynamic transition (see Section 1.2.4).

1.2.2
Structural, Kinetic, and Thermodynamic Aspects

One of the most intriguing questions in theoretical physics today is whether the glass is a new state of matter or just a liquid that flows too slowly to observe. The defining property of a structural glass transition for a polymer melt, observed on cooling from a sufficiently high temperature, is the increase of shear viscosity (η) by more than 14 orders of magnitude, without the development of any long-range order in structure. The typical X-ray or neutron diffraction studies of glassy solids, for example, reveal broad spectra of scattering lengths with no clear indication of primary unit cell structures. The "amorphous halo" of the static structure factor assessed by scattering experiments, or calculated via Monte Carlo and molecular dynamics computer simulations of amorphous cells, also shows insignificant changes when the material crosses the glass transformation range. Voronoi–Delaunay structural analyses of model amorphous systems have provided some means for distinguishing subtle differences between the rigid glass and liquid states of matter [12]. Relevant studies, however, are inconclusive as to the existence of some type of universally accepted geometric descriptor of the feeble structural changes occurring during the transition.

Contrary to the above findings, the marked change in behavior observed for thermodynamic derivative properties or physical quantities during the glass transition has provided the venue for "quantitative" descriptions of the process. Consider, for example, the shape of a typical thermal expansion curve (Figure 1.2a) [20]. In the polymer melt, the thermal expansion coefficient is almost constant, as it is again so in the glassy state but with a smaller value, similar to that of a crystalline solid. At the glass transition, there is therefore a pronounced change in the dependence of density or specific volume on

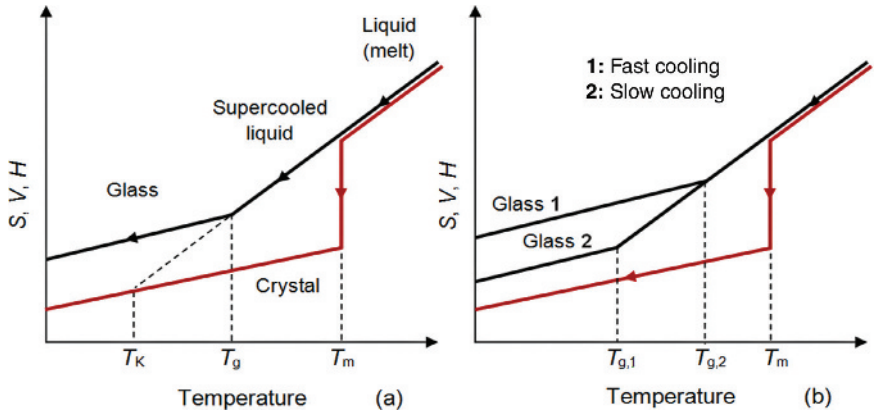

Figure 1.2 (a) Schematic illustration of the typical temperature dependence of configurational entropy, volume, or enthalpy of glasses and crystals. The glass-transition temperature (T_g), the Kauzmann temperature (T_K), and the crystal melting point (T_m) are indicated on the plot. (b) Schematic illustration of the cooling rate effect on T_g.

temperature; this constitutes the foremost identifier of the glass-transition temperature in all glass formers. Interestingly, the density of the glassy state and the location of the glass transition depend on the rate of temperature change, $q = |\mathrm{d}T/\mathrm{d}t|$. With reference to polymers, the sequence of chain conformation states traversed during a slow cooling process exhibit reduced apparent volume (i.e., higher density), and this behavior extends to lower temperatures, relative to the sequence of conformational states traversed at faster cooling. In parallel, since slower cooling rates allow for longer time for polymer chains to sample different configurations (i.e., increased time for intermolecular rearrangement or structural relaxation), the T_g decreases. The inflection point observed in the apparent volume, enthalpy, or entropy versus temperature plots of glass-forming materials marks the glass-transition temperature and demonstrates a similar cooling-rate dependence (Figure 1.2b). It is well known that variations in the heating rate produce similar effects, which are further complicated by additional aspects of the kinetics of glassy behavior (*structural recovery* effects). All these features reveal that the value of T_g, unlike the melting temperature T_m, is a rate-dependent quantity, and that the transition defines a kinetically locked thermodynamically unstable state [21], or, otherwise, a metastable state of matter [22].

Among other observations, the shape of the experimentally determined $S(T)$ dependences has provided the stimulus for early studies toward the development of an equilibrium thermodynamic framework for the description of the glass transition. With reference to the generalized behavior already depicted in Figure 1.2a, it becomes clear that in the course of supercooling the difference in entropy between the liquid and crystal phase decreases, with a precipitous decrease in heat capacity at T_g. The latter reflects the annihilation of the configurational degrees of freedom that the material possesses in the supercooled liquid state, besides the vibrational contributions found in both the crystalline and glassy ($T < T_g$) states of most materials. If the experimental curve for the entropy or heat capacity of the supercooled liquid is extrapolated to temperatures below the glass transition, it appears that there exists a temperature (the "Kauzmann temperature," T_K) at which the *configurational (excess) entropy*, S_c, that is the difference between the glass and crystal entropies, will become zero (Figure 1.3) [23,24]. Following the same extrapolation, a further reduction in temperature toward absolute zero would find the noncrystalline state to possess entropy lower than that of the stable crystal phase at the same temperature, which constitutes a violation to Nernst's theorem (the third law of thermodynamics). This paradoxical situation was first pointed out by Walter Kauzmann in 1948 [23]. If the extrapolation is valid, one is forced to admit that even for an infinitely slow cooling process, in which the liquid can reach equilibrium at any temperature, the liquid phase cannot persist below T_K. A means to sidestep the so-called Kauzmann paradox, or entropy catastrophe problem, is to consider that a thermodynamic transition to a new state of matter occurs at T_K, the *ideal glass transition*, with $T_g \to T_K$ as the rate of cooling approaches zero. The temperature T_K would thus mark a *divergence* of viscosity and the structural relaxation time of the liquid, and a breaking of the ergodicity, which might be connected with the postulated thermodynamic

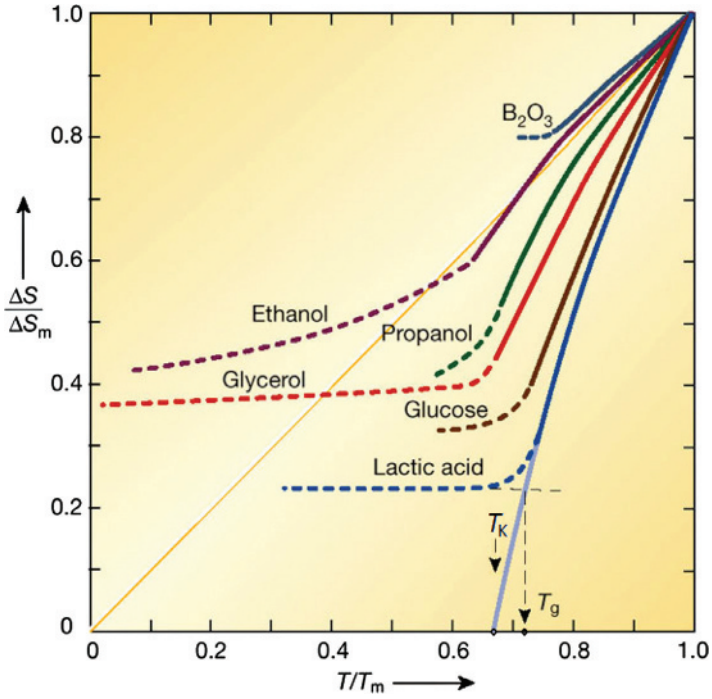

Figure 1.3 Temperature dependence of the entropy difference between several supercooled liquids and their stable crystals at ambient pressure ($\Delta S/\Delta S_m$, ΔS_m being the entropy of fusion). The thick lines correspond to experimental data in the range between T_m (normal melting point) and T_g. Extrapolation of the curve for lactic acid to lower temperatures is used to show the glass transition and the Kauzmann temperatures (at the point of intersection with the horizontal axis). From ref. [24], with permission, © 2001 Nature Publishing Group.

transition. Experimental manifestation of the phenomenon is presumably masked by the fact that, before getting to this temperature, the liquid falls out of equilibrium. Even so, it is a priori difficult to unequivocally interpret the glass-transition phenomenon as a kinetic manifestation of a second-order transition due to the absence of clear evidence showing growing thermodynamic or structural correlations as the system approaches the transition. Compelling evidence on the existence of a static correlation function that displays a diverging correlation length related to the emergence of "amorphous order," which would classify the glass transition as a standard second-order transition, is still lacking [25]. Recent experimental results on equilibrated structures (see Section 1.2.3.1) cast doubt on the validity of the expectation of a dynamic divergence response, diverging timescales, and a concomitant singulatity in the thermodynamics at some temperature well below laboratory T_gs.

Considering the glass as a *nonergodic*, *nonequilibrium*, but slowly evolving *metastable* state of matter, it is expected that its structure will undergo physical processes that will progressively decrease its specific volume, enthalpy, or

entropy, until an equilibrated structural state is attained. The principle of the minimization of the Gibbs free energy provides the thermodynamic driving force necessary for the eventual change. The underlying process of slow spatial reorganization of the polymer chains, without irreversible chemical changes, is referred to as *physical aging* (or *structural relaxation*), when it takes place at the use temperature of the polymer, and as *annealing*, when performed at a higher temperature (but below T_g). Structure equilibration is achieved quite rapidly at $T \geq T_g$, while, at considerably lower temperatures, glass configurations remain sensibly stable over extremely long periods of time. Physical aging and annealing affect all the temperature-dependent properties that change more or less abruptly at T_g [26,27]. The kinetic attribute of the glass transition is evident in the aging behavior of volumetric or enthalpic data in the glassy state. Figure 1.4 demonstrates the results of a benchmark experiment performed by Kovacs [20], involving the temperature variation of the isobaric (one atmosphere) specific volume data of poly(vinyl acetate) (PVAc). In that study, the sample was initially equilibrated volumetrically at a high temperature. Subsequently, the temperature was stepped to a lower value and the volume was measured at a specified time ($\Delta t = 0.02$ or 100 h) after quenching. Glass densification accomplished in the course of physical aging was found to produce a reduction in the specific volume of about 0.5% for aging time of 100 h at $T \approx T_g - 40\,^{\circ}\mathrm{C}$ ($T_g \approx 27\,^{\circ}\mathrm{C}$), while the longer equilibration times before the temperature change resulted in a lower T_g.

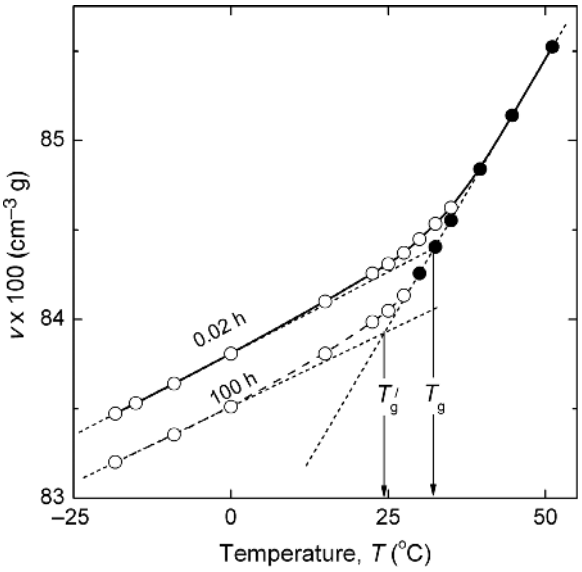

Figure 1.4 Temperature variation of the isobaric volume of PVAc. The filled symbols represent equilibrium volumes, while open symbols correspond to the volumes observed $\Delta t = 0.02$ and 100 h after quenching of the melt. The intersection of the dashed extrapolated lines marks the glass transition (fictive) temperature. Replotted data from ref. [20]; with permission © 1958 John Wiley & Sons.

Since the measured volumes depend on the temperature and rate of cooling one can also talk about the "time" and "rate" of volume recovery. The rate of volume (or enthalpy) recovery depends on the magnitude and sign of the deviation from the reference equilibrium state, and on how long the sample was allowed to remain at the preceding temperature (memory effect). Plain kinetic effects can be described using a simple kinetic theory, like the single-parameter volume (or enthalpy) relaxation model proposed by Tool [28], and Davies and Jones [29],

$$-\frac{\mathrm{d}\delta_v}{\mathrm{d}t} = q\delta\alpha + \frac{\delta_v}{\tau_v}, \tag{1.4a}$$

where $\delta_v = (V - V_{\mathrm{eq}})/V_{\mathrm{eq}}$, V_{eq} is the equilibrium state volume, and τ_v is the isobaric volume relaxation time. This model was later improved using the Doolittle equation, resulting in

$$-\frac{\mathrm{d}\delta_v}{\mathrm{d}t} = q\Delta\alpha + \frac{\delta_v}{\delta_{v_{\mathrm{g}}}}\exp\left(\frac{B}{f_{\mathrm{g}}} - \frac{B}{f}\right), \tag{1.4b}$$

where $\tau_{v\mathrm{g}}$ is a reference relaxation time and f_{g} the free-volume fraction at T_{g}. To account for the memory effects, the superposition of a number of elementary relaxation processes has been considered in the multiparameter Kovacs–Aklonis–Hutchinson–Ramos approach [30],

$$-\frac{\mathrm{d}\delta_{v,i}}{\mathrm{d}t} = q\Delta\alpha_i + \frac{\delta_{v,i}}{\tau_{v,i}} \tag{1.4c}$$

with $\delta_v = \sum_{i=1}^{N} \delta_{v,i}$ and $\Delta\alpha = \sum_{i=1}^{N} \Delta\alpha_i$. Enthalpy relaxation effects on differential scanning calorimetry (DSC) heating scans (Section 1.4.1) are most prominent when the material is isothermally held in the glassy state (20°–50° below T_{g}), for a sufficient duration of time. In addition to rate effects, the glass transition is pressure and path dependent. McKenna and Simon [14] reviewed studies related to the path dependence of T_{g} and the kinetics of glass formation. Their survey clearly demonstrates that the glass-transition temperature and its pressure dependence are functions of whether the PVT surface of the glass is obtained isobarically, by pressurizing the liquid and cooling from above T_{g}, or isochorically, using variable pressure to retain liquid volume constant until a low temperature is reached at a constant rate.

1.2.3 Relaxation Dynamics and Fragility

The relaxation dynamics in many different kinds of materials encompass contributions from various types of motional processes spanning a range of length scales, which become prominent at different temperature ranges and/or timescales. By virtue of their high densities, supercooled liquids exert strong frustration constraints on the dynamics of individual atomic/molecular entities or

"particles" (e.g., atoms, oligomeric molecules, pendant groups, short-chain segments, or even bigger parts of the chain). As temperature decreases toward T_g, a tagged particle is most likely trapped by neighbors (i.e., caged) given that the amplitude of thermodynamic fluctuations decreases following a decrease in temperature. Near the glass-transition temperature, several groups of particles may remain caged for relatively long times. For them, liberation from the cage requires collaborative rearrangement of several other particles in its environment, which themselves are also imprisoned. The volume over which cage restructuring – by cooperative motions – must occur presumably increases as the molecular packing increases (with decreasing temperature). Considering the complexity of the systems involved and the diversity of configurational changes that may cause relaxation of a polymeric material, fundamental research in each system often focuses on the description of the time evolution of the relaxation dynamics (i.e., plots of the time dependence of the relaxation or response functions), at a constant temperature, and the creation of relaxation maps (i.e., plots of the temperature dependence of the relaxation times of distinct groups of particles). Some of these issues and the pertinent concept of liquid fragility will be briefly discussed.

1.2.3.1 Relaxations in Glass-Forming Materials

For over half a century, the nature of the relaxational response of supercooled liquids and glasses has been extensively explored, in an effort to expand our understanding of the structure–property relationships in the rapidly evolving collection of glassy materials, and at the same time establish connections among experimental responses and theoretical predictions. Out-of-equilibrium studies of glassy dynamics reveal a collection of modes, extending over a broad temperature-, frequency-, or time range. At short times of observation at constant temperature, the approach to equilibrium after a given perturbation is dominated by very fast to moderately fast motions of small parts of the macromolecular chain. The picosecond dynamics of disordered materials include a *fast secondary relaxation* process, which appears as an anharmonic relaxation-like signal (a broad quasielastic scattering) in the GHz–THz region of excitation spectra [31]. This contribution is commonly ascribed to caged molecular dynamics (i.e., cage rattling) with relaxational activity displaying gas-like power-law temperature dependence [32]. Close to it, Raman and neutron scattering inelastic studies reveal a rather controversial lower frequency vibrational mode, or group of modes, known collectively as the "boson peak." Potential correlations between these early-time modes and the long-time dynamics of glass-forming materials emerge from studies relating characteristics (e.g., its intensity and frequency) of the nearly temperature-independent boson peak with the concept of liquid fragility, Kohlrausch's exponent (β_{KWW}) [33], and the cooperativity length scale (ξ_α) [34], all strongly linked to the glass-transition dynamics of disordered media. Several other important secondary processes occur on timescales much slower than cage rattling, but much faster than the structural (α) relaxation. These are related to complicated, though local, non or not fully cooperative [35] dynamics. A number

of physical origins have been proposed for the principal *slow secondary relaxation* process (in the kHz region of isothermal relaxation spectra [15–17]), the so-called Johari–Goldstein (JG) β-process, a process widely recognized as an intrinsic feature of the glassy state and frequently deemed to originate from the same complicated frustrated interactions leading to the glass transition. Of the alternative attributions proposed hitherto, it is worth mentioning its correlation with molecular motions occurring in "islands of mobility" (i.e., regions of relatively loose structure [36]), the highly restricted stepwise reorientation of practically all molecules in a system [37], and its discussion in terms of intermolecular [38] degrees of freedom or even intramolecular [39] ones. Other secondary relaxations (γ or δ, in the accepted notation for amorphous materials [15,16]) entail more trivial and system-specific motions of structural entities, usually connected with intramolecular degrees of freedom, such as simple bond rotations of lateral groups (including rotations within side groups). With the exception already noted for the modes contributing to the fast (picosecond) dynamics of disordered materials, all other secondary mechanisms are commonly regarded to involve relaxation jumps over asymmetric double-well potentials (e.g., Gilroy–Phillips model [40]). The temperature dependence of the respective relaxation times can thus be well described by a simple exponential Arrhenius-type equation, that is,

$$\tau(T) = \tau_0 \exp\left(\frac{E_{\mathrm{act}}}{k_\beta T}\right), \tag{1.5}$$

where τ_0 is the pre-exponential factor (or Arrhenius prefactor) and k_β is the Boltzmann constant. The apparent activation energy, E_{act}, is typically determined by internal rotation barriers (intramolecular part) and the environment of the relaxing unit (intermolecular part, linked to the stereochemical configuration of the chains). Broad distributions of relaxation times and a strongly temperature-dependent width (presumably due to a Gaussian distribution of barrier heights) are common features of signals related to the JG mode [41]. In several cases, by extrapolating to high temperatures the Arrhenius line, the slow β-mode seems to result from bifurcation of the structural relaxation mode (α-relaxation, Figure 1.5), which encompasses cooperative segmental motions on much longer length scales.

The abrupt retardation of molecular mobility in the course of vitrification is an important facet of the relaxation dynamics of disordered systems. Various experimental results and simulations indicate that the structural relaxation of a supercooled liquid is a dynamically and spatially heterogeneous process with a strongly non-Arrhenius relaxation behavior. Dynamic heterogeneity describes the spatial heterogeneity of the local relaxation kinetics, manifested by the coexistence of "slow" and "fast" mobility regions of limited length within a material [42–44]. Different assumptions that introduce heterogeneity in supercooled liquids exist, including the old concept of liquid-like cells that create liquid-like clusters (Cohen–Crest model), the conception of a solid glass with a small fraction of fluidized domains of extremely high mobility (Stillinger–Hodgdon

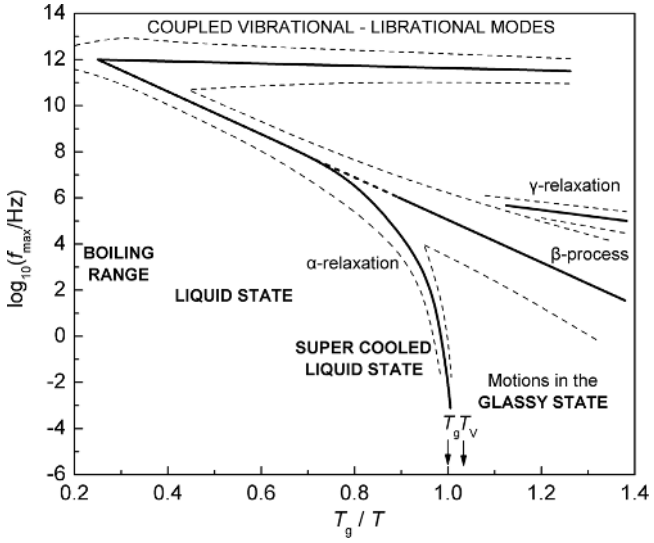

Figure 1.5 Schematic illustration of the temperature dependence of characteristic relaxation frequencies of representative oscillatory and relaxational modes of motion found in glass-forming polymer liquids. The thick lines indicate the trend of the most probable frequencies, while thin dashed lines indicate typical half-widths of the respective bands. Note the increasing separation (decoupling) of the vibrational and structural relaxation times as the temperature decreases approaching T_g. A further decoupling of characteristic motions occurs near and below T_g, giving rise to the JG β-process.

model), and the hypothesis of the existence of small distinguishable subvolumes in the system that relaxes statistically independent of their environment. The terminology germane to these regions includes the influential "cooperatively rearranging region(s)" (CRR(s)) introduced in the Adam–Gibbs model, the concept of "entropic droplets," and the "domains" of locally preferred structures, advocated by thermodynamic treatments of glass formation (see Section 1.2.4.3). So far, most techniques provide indirect estimates of the relevant cooperativity length scale, by invoking thermodynamic fluctuation formulae, combined with an appropriate set of *ad hoc* assumptions, to obtain ξ_α from the available experimental data, or by simply introducing external perturbations (e.g., confinement in finely regulated nanometer-sized geometries) [43,45–47]. In the subvolume of each CRR, for example, the density, the temperature, the entropy, and the energy (E) are somewhat different, and their mean square fluctuations $\langle \Delta\rho^2 \rangle$, $\langle \Delta T^2 \rangle$, $\langle \Delta S^2 \rangle$, and $\langle \Delta E^2 \rangle$, respectively, are given by standard relations of statistical thermodynamics. Among others [47], Donth proposed to correlate these relations with the width of relaxation time distribution of the so-called α-relaxation process [41]. Each subvolume can be then considered as a thermodynamic system in metastable equilibrium with fluctuating variables having a Gaussian distribution, and a distinct glass-transition temperature (T_α) and relaxation time (τ_α). Accordingly, the relaxation time distribution can be related to the glass transition one,

with $\langle T_\alpha \rangle$ assumed to be the conventional glass-transition temperature of the system. In Donth's approach, the characteristic volume of cooperativity at T_g (V_α) and the number of segments in the cooperative volume (N_α) can be estimated by

$$V_\alpha \propto \xi_\alpha^3 = \frac{\Delta(1/C_V)}{\rho(\delta T)^2} k_B T_g^2 \tag{1.6a}$$

and

$$N_\alpha = \frac{\rho N_A \xi_\alpha^3}{M_0}, \tag{1.6b}$$

respectively, with N_A the Avogadro number, $(\delta T)^2$ the mean square temperature fluctuation related to the dynamic glass transition of a CRR, C_v the isochoric heat capacity with $\Delta(1/C_v) \approx \Delta(1/C_p) = (1/C_p)_{glass} - (1/C_p)_{liquid}$, and M_0 the molar mass of the repeat unit (monomer). Theoretical claims [46], thermodynamic treatments starting from volume, temperature, and entropy fluctuations [41,47], and extensive use of sensitive experimental probes of dynamic and spatial heterogeneity [43,47] – including results based on the Boson peak frequency [34] – have provided values for ξ_α in the range ~1–4 nm [35]. In parallel, the cooperativity length scale and N_α (of the order of 100 near T_g) appear to increase as temperature decreases near T_g [31].

The strongly non-Arrhenius temperature behaviors for the structural relaxation dynamics and the viscosity of glass-forming liquids at temperatures exceeding T_g are well documented (Figure 1.5). Both are frequently interpreted in terms of the empirical Williams–Landel–Ferry (WLF) [48] or Vogel–Fulcher–Tammann–Hesse (VFTH) [49] equations, which were later rationalized in terms of free-volume (or configurational-entropy) concepts. The WLF equation is expressed as

$$\log_{10} \alpha_T = \frac{-C_1(T - T_r)}{C_2 + (T - T_r)}, \tag{1.7a}$$

where α_T is called the temperature shift factor (generally known as the reduced variables shift factor), T_r is a reference temperature, and C_1 and C_2 are constants. The shift factor is related to the viscosity, $\alpha_T = \eta(T)/\eta(T_r)$, relaxation times, $\alpha_T = \tau(T)/\tau(T_r)$, and several other mechanical (e.g., tensile strength and compliance) or dielectric (e.g., permittivity and electric modulus) relaxing quantities. When T_g is taken as the reference temperature, the following form is obtained:

$$\log_{10} \alpha_T = \frac{-17.44(T - T_g)}{51.6 + (T - T_g)}. \tag{1.7b}$$

By averaging data for various types of synthetic high polymers, the values of $C_1 = 17.44$ and $C_2 = 51.6$ K were derived and applauded as "universal" constants for linear amorphous polymers of any chemical structure. Their usability in complex polymeric systems must be treated with cautiousness, since a different set of values is to be expected when distinct dynamic processes and/or substances are explored. Despite these shortcomings, Eq. (1.7b) introduces some important

kinetic aspects of the glass-transition phenomenon. For instance, if the time frame of an experiment is decreased by a factor of 10 near T_g, this equation reveals an increase of the glass-transition temperature of about 3°. Of particular interest in dynamic experiments is the temperature dependence of the structural α-relaxation times, $\tau_\alpha(T)$, for which the WLF temperature dependence is expressed as

$$\tau_\alpha(T) = \tau(T_r)\exp\left(\frac{-C_1(T - T_r)}{C_2 + (T - T_r)}\right) \tag{1.8}$$

and the mathematically equivalent VFTH equation has the form

$$\tau_\alpha(T) = \tau(\infty)\exp\left(\frac{C}{T - T_V}\right), \tag{1.9}$$

where $C = C_1(T_r - T_V)$ is a material parameter and $T_V = T_r - C_2$ denotes the so-called Vogel temperature (at which the relaxation time is *extrapolated* to diverge). In the absence of deep arguments regarding the underlying physics of glasses, the VFTH equation is mostly regarded an entirely heuristic modification of the Arrhenius rate law to include a finite divergence temperature. Even though the physical meaning of the Vogel temperature has not been clearly defined [41], the universality of the VFTH equation in a wide temperature range (T_g to $T_g + 100$ K) makes clear that T_V is a significant parameter for the dynamics of the glass transition. A survey of the literature provides evidence of a weak connection between T_V and T_K ($T_V \approx T_K$ [50]), with T_V generally found to be approximately 30°–50° (depending on system's fragility) below conventional laboratory T_gs. In practice, the glass-transition temperature can be obtained by extrapolating the Arrhenius plot constructed for the structural relaxation times or characteristic frequencies (plots of $\log\tau$ or $\log f_{max}$ versus $10^3/T$, with $f_{max} = 1/2\pi\tau$), using Eq. (1.8) or (1.9) along with the usual convention $\tau(T_g) = 100$ s [51].

Theoretical treatments, computer simulations, and a number of experimental results strongly argue in favor [52] or against [53–55] the existence of a dynamic divergence phenomenon – a behavior also referred to as "super-Arrhenius" – at some temperature above absolute zero. The "geological" ages required for a material to attain equilibrium far below T_g preclude, in general, extensive testing of the above conjecture. Recent data on the temperature dependence of the shift factor obtained by dielectric spectroscopy for PVAc [54], using samples aged to equilibrium as much as 16° below the calorimetric glass-transition temperature, demonstrate, for example, an Arrhenius sub-T_g behavior in contradiction to the predictions made by classic theories. Further work on a Cenozoic (20 million years old) Dominican amber [55] was able to probe equilibrium dynamics nearly 44° below T_g, and subsequently present more stronger experimental evidence of nondiverging dynamics at far lower temperatures than previous studies. Notice that several other functions may well provide adequate description of the super-Arrhenius behavior of glass-forming liquids, showing either a divergence at zero temperature (e.g., the Bässler-type law, $\tau_\alpha(T) \sim \exp(A/T^2)$ [56]) or no divergence at all (e.g., the DiMarzio–Yang formula, $\tau_\alpha(T) \sim \exp(-AF_c/k_\beta T)$, where F_c is the configurational part of the Helmholtz free energy [57]).

1.2.3.2 The Concept of Fragility

In an attempt to establish some link between the observed thermodynamic behaviors of glass-forming systems and the temperature dependences of several dynamical quantities, Angell introduced the concept of *liquid fragility* [58]. In Angell's classification scheme, the word "fragility" is used to characterize the rapidity with which a liquid's properties (such as $\eta(T)$ or $\tau(T)$) change as the glassy state is approached, in contrast to its colloquial meaning that most closely relates to the brittleness of a solid material. Over the years, fragility has become a useful means of characterizing supercooled liquids, despite the criticism on some inferences of the concept [59]. The term "strong" liquid suggests a system with relatively stable structure and properties (such as the activation energy barriers associated with viscosity or the structural relaxation time) that do not change dramatically in going from the liquid into the glass, while a "fragile" liquid behaves in a reverse manner. Formally, fragility reflects to what degree the temperature dependence of a dynamic property of the glass former deviates from the Arrhenius behavior. One way of evaluating fragility is to construct fragility plots (Angell plots), where the logarithm of a dynamical quantity is plotted versus T_g/T (Figure 1.6) [60]. Several parameters have been introduced, at different theoretical contexts and with varying level of success, for characterizing quantitatively the fragility of glass-forming liquids (e.g., see treatments of Doremus [59], Bruning and Sutton [61], and Avramov [62]). The most common definition of fragility is the fragility parameter (or steepness index), m, which characterizes the slope of a dynamic quantity (X) with temperature as the material approaches T_g from above [63],

$$m = \left(\frac{\partial \log_{10} X}{\partial (T_g/T)}\right)_{T=T_g}. \tag{1.10}$$

Bearing in mind the non-Arrhenius temperature dependence of τ_α, for example, Eq. (1.10) takes the form

$$m_{\mathrm{VFTH}} = \left(\frac{\partial \log_{10} \tau_\alpha}{\partial (T_g/T)}\right)_{T=T_g} = \frac{C/T_g}{(\ln 10)\left(1 - \frac{T_V}{T_g}\right)^2}, \tag{1.11a}$$

which provides an estimate of the fragility index in terms of the Vogel temperature. Considering the expression of the relaxation time given by the Tool–Narayanaswamy–Moynihan formula [28,64], another dynamic estimate of the fragility index can be obtained from DSC experiments with different heating rates, through a relation that links m with the apparent activation energy of structural relaxation Δh^*,

$$m_{\mathrm{DSC}} = \frac{\Delta h^*}{RT_g \ln 10}. \tag{1.11b}$$

The fragility can be intuitively related to the cooperativity of atomic motions in the glassy state (anticipating an increase in cooperativity with increasing m)

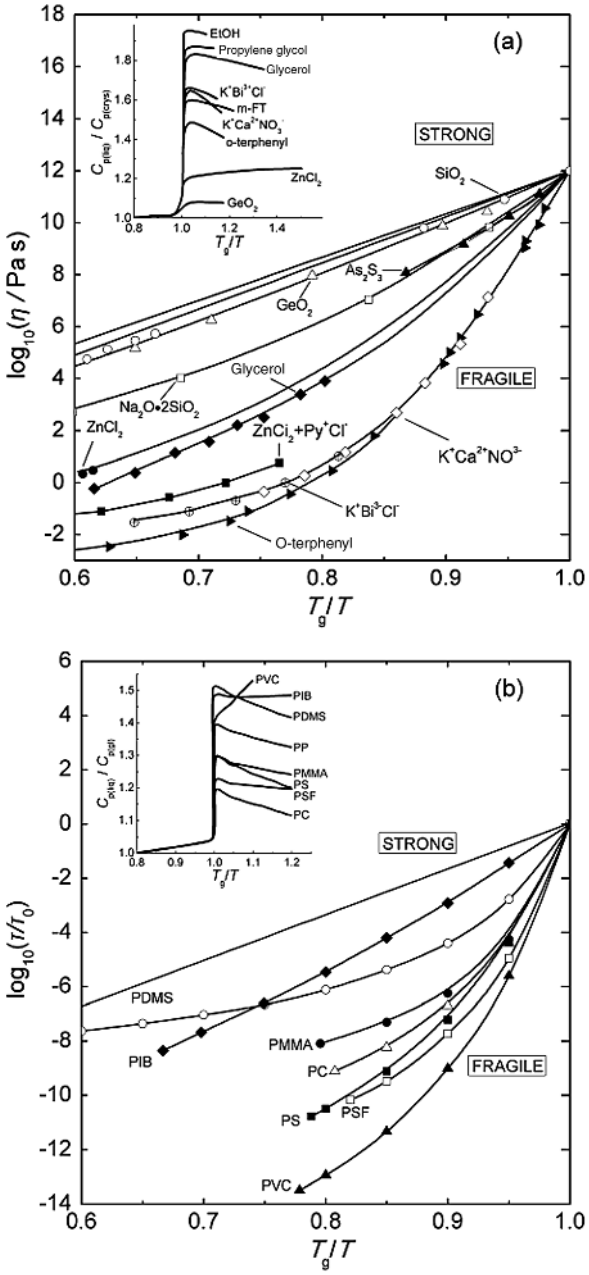

Figure 1.6 Fragility plots of glass-forming liquids (Figure 1.6a) and polymers (Figure 1.6b). Following the established practice, in the first plot T_g is roughly defined for each system by the relation $\eta(T_g) = 10^{13}$ poise (10^{12} Pa·s), while in the second plot, T_g is defined as the temperature at which the segmental relaxation time $\tau(T_g)$ equals 100 s. Insets show the heat capacity changes at the glass transition for selected systems (replotted from data appearing in ref. [60], with permission © 2001 AIP Publishing LLC).

[41,45], as well as to the breakdown of the Stokes–Einstein relation between viscosity and diffusion coefficient [65]. In that respect, several studies explore the validity of empirical relationships among components of the fragility parameter [34,66] and the length scale of cooperativity or spatial variations in dynamics. For example, by applying the chain rule of differentiation

$$m = \left(\frac{\partial \log_{10}\tau_\alpha}{\partial\left(\frac{T_g}{T}\right)}\right)_P\Bigg|_{T=T_g} = \left(\frac{\partial \log_{10}\tau_\alpha}{\partial\left(\frac{T_g}{T}\right)}\right)_V\Bigg|_{T=T_g} + \left(\frac{\partial \log_{10}\tau_\alpha}{\partial P}\right)_T\Bigg|_{T=T_g} \times \left(\frac{\partial P}{\partial\left(\frac{T_g}{T}\right)}\right)_V\Bigg|_{T=T_g}$$

one separates the conventional (isobaric) fragility parameter into two terms

$$m = m_V + \frac{\Delta V^\#}{k_B \ln 10} \times \frac{\alpha_T}{\kappa_T} \tag{1.12}$$

with $\Delta V^\#$ denoting the activation volume at T_g. Following the above treatment, Sokolov and coworkers [34] suggested that the isochoric (constant density) fragility, m_V, characterizes the pure thermal contribution to fragility that bears no connection to the length scale of dynamic heterogeneities. The second term of Eq. (1.12) encompasses the volume contribution to fragility, that is, the effect due to the temperature-induced change of density under isobaric conditions. Given the correlation evidenced between the cooperativity volume ξ_α^3 and $\Delta V^\#$ [34], this term is likely to depend directly on cooperativity. A relationship between parameters characterizing the stretching of the relaxation function and isochoric fragility is also probable [66]. Other studies provide pieces of evidence for possible correlations between the conventional (atmospheric pressure) estimates of the fragility parameter and molecular or structural properties of the material, such as its chemical composition, the type of bonding, intermolecular interactions, or the degree of microphase separation [67].

The values of m range from ~250 [68] for very fragile glass-forming liquids (e.g., ionic systems, organic materials, or polymers with nondirectional intermolecular bonding) to the theoretically low limit of ~16 [69] for very strong glass formers (the network oxides SiO_2 and GeO_2, BeF_2, etc. [70]). Highly fragile materials demonstrate narrow transitions, while those with lower fragility indices have relatively broader transitions. The roles of chemical structure, composition, and main-chain stiffness in the glass-forming tendency of polymers [71] and polymer blends [51], as well as possible correlations among the "dynamic fragility" index and thermodynamic measures of liquid fragility ($m_T = \Delta C_p$, $C_{p(liq)}/C_{p(gl)}$, $C_{p(liq)}/C_{p(crys)}$, or $1 + \Delta C_p/S_c$, all determined at $T = T_g$, typically used to assert "thermodynamic fragility" [60,72]), are issues in debate [73]. As suggested by the Adam–Gibbs theory (see Section 1.2.4), kinetically fragile liquids are expected to have large configurational heat capacities [6], resulting from their configurational

entropy changing rapidly with temperature. Strong glass-forming liquids are resistant to temperature-driven changes in the medium-range order. Therefore, the amount of configurational entropy in the liquid is small, as is the change in heat capacity at T_g. Even though the heat capacity changes shown in the inset of Figure 1.6a support the positive correlation between m and ΔC_p, more recent data appear contradicting. Huang and McKenna [60] classified the experimental m versus ΔC_p dependences into three groups: polymeric glasses with a negative correlation (Figure 1.6b) [72], small-molecule organics and hydrogen-bonding small molecules with no correlation, and inorganic glass formers with a positive one [74]. There are also several reports demonstrating that thermodynamic and kinetic fragilities are not strongly correlated [75], especially when polymeric systems are considered. In view of that, a system concluded to be kinetically fragile will not necessarily be also thermodynamically fragile. Finally, a direct correlation between fragility indices and the average size of the CRRs is frequently considered [41,45,76].

1.2.4 Theoretical Approaches to the Glass Transition

1.2.4.1 General Overview

The intriguing phenomenology of the glass transition has been the driving force of intense efforts aiming to establish firm theoretical perspectives with wide quantitative support for the microscopic and relaxational behavior of liquids in the glass transformation range. The marked decrease in molecular mobility as a system passes through its glass-transition temperature has led several researchers to construct early theories of glass transition based on concomitant changes of conjugate thermodynamic variables, such as the free volume and the configurational entropy. The defect diffusion [77], free volume [78], and configurational entropy [44,79,80] approaches, all dating back to the 1960s, remain in the forefront of current interest about the glass transition. While these early theories fall short in properly defining – among other properties and phenomena – the molecular motions involved in the glass-transition mechanism [13], they are still frequently invoked in interpretations of experimental results. A number of more recent theories and elaborate concepts, including the potential energy landscape (PEL) picture [24,81,82], the coupling model (CM) [13], the mode-coupling theory (MCT) [83–85], and the RFOT [86] theory, the configuron percolation model (CPM) [87–89], as well as the concepts of kinetic constraints [90,91] and geometric frustration [92], have provided an amplification of our perceptions on the glass-transition phenomenon and more plausible explanation of certain experimental observations. Still, irrespective of the intense theoretical efforts to handle the glass-transition phenomenon employing arguments resembling thermodynamic or purely dynamic transitions, we have not yet arrived at a comprehensible theory of supercooled liquids and glasses. Their behavior near the glass transition has been described, but not all that behavior is thoroughly explained by a single theoretical concept [85]. Elements of certain theoretical frameworks

and some insight into their strengths, flaws, capabilities, and limitations will be provided in the following paragraphs; the reader is referred to a – regretfully condensed – list of review papers [13,25,85,93–95] for a comprehensive account of the available theoretical approaches.

1.2.4.2 Energy Landscapes and Many-Molecule Relaxation Dynamics

In a seminal 1969 paper, Goldstein [81] put forward the notion that atomic motions in a supercooled liquid comprise high-frequency vibrations in regions of deep potential energy minima in addition to less frequent transitions to other such minima. In an amplification of this concept, Stillinger and coworkers [24,82] formulated the PEL picture of glassy systems, a multidimensional surface describing the dependence of the potential energy on the coordinates of the atoms or molecules. Their conception provided a "topographic" view of phenomena associated with glass formation, along with a valuable theoretical background in the pursuit of distinguishing among vibrational and configurational contributions to the properties of a viscous fluid.

In the phenomenological PEL approach of Stillinger and Weber [24], an N-particle system is represented by a potential energy function $\mathrm{U}(\vec{r}_1, \vec{r}_2, \ldots, \vec{r}_N)$ in the $3(N-1)$-dimensional configuration space. The energy of the disordered structure is partitioned into a discrete set of "basins" connected by saddle points – a picture that represents the complicated dependence of potential energy (or enthalpy) on configuration [96]. Each basin contains a metastable local (single) energy minimum and each corresponds to a mechanically stable arrangement of the system's particles. In terms of PEL, relaxations ascribed to short-time molecular motions are considered to occur via intrabasin vibrations (harmonic oscillations) about a particular structure, while long-time molecular motions are considered to take place via occasional activated jumps over saddle points into neighboring basins. In an amplification of this concept, the picture of "metabasins" has been introduced [97], with each metabasin consisting of several local minima ("inherent structures") separated by similar low-energy barriers. Jumps within the superstructure of a metabasin are connected with secondary relaxation events (Figure 1.7a), while much slower collective molecular motions (i.e., "ergodicity restoring" processes related to the glass transition) are considered to proceed via infrequent jumps between neighboring metabasins, separated by large barriers relative to $k_\beta T$. While the PEL is suitable for modeling glass-transition behavior under isochoric conditions, almost all experimental studies of glass formation are performed under constant pressure conditions. To that end, an enthalpy landscape approach [98] has conveyed an extension of PEL to an isothermal–isobaric ensemble, allowing for changes in both particle positions and the overall volume of the system. In all energy landscape models (potential-energy, free-energy, or enthalpy variants [97,98]), the dynamics are to a certain degree cooperative, since transitions between two minima engage the coordinates of all particles of some localized region. Related frameworks have contributed a certain degree of understanding of the nature of the glass transition and the glassy state of matter. It has been suggested, for example, that it is not possible for the

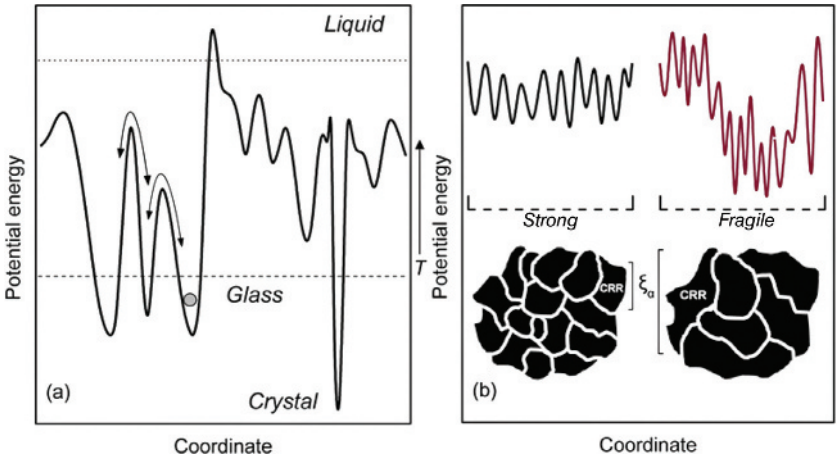

Figure 1.7 (a) Schematic illustration of a 1D PEL. At a given temperature, the system can visit the configurations between the dashed line and the solid curve. In the glassy state, the system is trapped in a metastable state performing harmonic oscillations. Jumps between neighboring basins (arrows) are related to the β relaxation, while α relaxation involves jumps into neighboring metabasins. (b) Hypothetical forms of the PEL and their relation to the strong/fragile character of a material described in terms of the average size of the CRRs.

configurational entropy of a supercooled liquid to vanish at a finite temperature, since some transitions are always allowed between basins, but only at absolute zero temperature, when it is confined to just a single microstate. Stillinger further extended the concept of a single Kauzmann temperature to multiple "Kauzmann points" in the temperature–pressure plane of a system [82,99]. Although the above statements suggest that the ideas of the "Kauzmann paradox" and the purported "ideal glass transition" are illusive, mere results of improper extrapolations [99] and lacking experimental corroboration [100], several counterarguments cannot be ignored [46]. Worthy of note is also the proposed connection between liquid fragility (as well as between the sharpness and strength of the glass transition [98]) and the topography of the underlying potential energy or enthalpy landscapes, which relates the behavior of strong or fragile liquids to landscapes of rather uniform roughness or highly nonuniform topography, respectively (Figure 1.7b) [82].

Energy landscapes contribute to our understanding of the processes observed during the evolution of molecular dynamics from short to very long times [97]. These encompass contributions from a range of modes, starting from fast vibrations and localized motions and progressively entering the time window of cooperative molecular motions. General characteristics of this behavior are schematically illustrated in Figure 1.8, for the case of the relaxation function, $\Phi(t)$, a pattern closely resembling the time dependence of the density fluctuation autocorrelation function at constant temperature. A phenomenological description of the distinctly nonexponential time dependence of the long-times primary

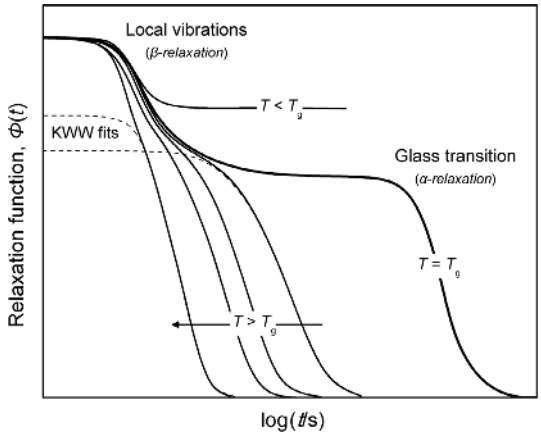

Figure 1.8 Schematic illustration of the time variation of the relaxation function. Note the different response in the ergodic (supercooled liquid, $T > T_g$) and the nonergodic (glassy, $T < T_g$) states of the system.

relaxation (glass transition) is provided by a function having the *Köhlrausch–Williams–Watts* (KWW) stretched exponential form [101]

$$\Phi_\alpha(t) = \exp\left[-\left(\frac{t}{\tau_\alpha}\right)^{\beta_{\mathrm{KWW}}}\right], \tag{1.13}$$

with $0 < \beta_{\mathrm{KWW}} \leq 1$. Parameter β_{KWW} delivers a convenient measure of the width of the dispersion of the α-relaxation and the extent of the many-molecule relaxation dynamics, both critically controlled by intermolecular interactions and spatial constraints. Nonexponentiallity is typically accounted for by two fundamentally different – yet, experimentally indistinguishable – scenarios: the material is considered either to comprise a set of heterogeneous environments with exponential relaxation activity but distinctly different characteristics among different environments (e.g., a scenario equivalent to a distribution of relaxation times), or to be entirely homogeneous with each molecule relaxing nearly identically with an intrinsically nonexponential manner.

Many-molecule relaxation is a central element of the CM, a general theory of relaxation presented by Ngai [13]. Even though this approach is clearly not a complete theory of the glass transition, it has successfully tackled problems originating from prior oversimplified or even illusive considerations of nontrivial interactions between relaxing units in glass-forming materials and the inadequate description of their many-molecule relaxation dynamics. The idea behind CM is the picture of a cooperative system of identical relaxing species (such as ions in a viscous conductor or entangled polymer chains). At short times, the particles can be considered to be noninteracting and thus the relaxation rate is constant, while after some critical time, t_c, the molecules interact more strongly and thus the relaxation becomes slowed down. In terms of the

CM, the characteristics of the structural relaxation are correlated with the aspects of the processes that have transpired before it, which include the caging of the molecules (picosecond dynamics) and the universal JG β-process [36]. A rational outcome of the notion that the α-relaxation process originates from the relaxation of individual molecules is to consider that, at sufficiently short times, the many-molecule relaxation is reduced to isolated local motions independent of each other. These correspond to the primitive relaxation of the CM, which can be seen as part of the faster processes in the relaxation spectrum. The model sets forth a relation between τ_α and the primitive relaxation time (τ_p), or equivalently the JG relaxation time (τ_{JG}), via the coupling parameter n (with $n = 1 - \beta_{KWW}$) characterizing the primary relaxation, of the form [13]

$$\tau_\alpha(T,P) = \left[t_c^{-n}\tau_p(T,P)\right]^{1/(1-n)} \approx \left[t_c^{-n}\tau_{JG}(T,P)\right]^{1/(1-n)}. \quad (1.14)$$

The CM predicts the short-time behavior to be essentially Debye. Although the temperature and pressure dependences of τ_α and τ_p (or τ_{JG}) are not given or derived, the applicability of Eq. (1.14) has been successfully tested for a wide range of glass formers. The stronger dependence of $\tau_\alpha(T, P)$ compared to that of $\tau_p(T, P)$ or $\tau_{JG}(T, P)$ is expressed by the superlinear factor $1/(1-n)$ and relates to the longer length scale of the motions involved. The CM also provides an explanation of changes in the relaxational behavior of glass formers – including the component dynamics of mixtures or the dynamics of nanoconfined polymers – in terms of the temperature dependence of n or the width of the α-relaxation. Of the cases compiled by Ngai [13], here is only mentioned the projected crossover of the temperature dependence of τ_α from one VFTH equation to another, at some temperature $T_B > T_g$, coincident with the apparent onset of bifurcation of τ_{JG} from τ_α, and the onset of decoupling of the translational and orientational motion, which are all related to the small values of n at $T > T_B$ and its more rapid increase with decreasing temperature below T_B. Ngai and Rendell [13] mention that an explanation of the heterogeneous picture of relaxation in terms of spectra or distributions of relaxation times is incompatible with the model. They argue that interactions perturb the relaxation in a way as to make it inherently nonexponential and not that it arises from superposition of single exponential (Debye) processes. A main limitation of the CM is connected with the absence of a detailed explanation of the potential relaxation mechanisms in molecular level and how these exactly contribute to the overall macroscopic behavior.

1.2.4.3 Approaches with an Underlying Avoided Dynamical Transition

The most famous purely dynamical approach to the glass transition is the MCT, a mean-field treatment of the phenomenon based on a microscopic theory of the dynamics of fluids [83–85]. The theory exploits the idea of a nonlinear feedback mechanism in which strongly coupled microscopic density fluctuations lead to structural arrest and diverging relaxation time at a critical point, with no singularity observed for the thermodynamics. The physical picture adopted by the originally developed scenario of the *idealized* MCT (*i*MCT) attributes the viscous slow-down with decreasing temperature to a so-called cage effect, that is, the

assumption that each particle in a dense fluid is kinetically constrained (confined) in a cage formed by neighboring particles. At low temperatures, the probability of occurrence of a strong spontaneous density fluctuation, large enough to liberate a particle from its cage, appears insignificant. In consequence, as the temperature gets lower and the system gets denser, structural arrest occurs because particles can no longer leave their cage even at infinite time. Within the MCT, fast secondary relaxations are related to relatively rapid local motions of molecules trapped inside cages, while the slow process of the breakup of a cage itself contributes to the structural relaxation. Large-scale spatial motion typical of a fluid can only proceed cooperatively, that is, one of the caging particles has to make way, which can only happen if one of its neighbors moves, and so on. One of the main predictions of the *i*MCT is that dynamical freezing and a transition from an ergodic to a nonergodic state occurs at a critical temperature T_{MCT} ($\sim 1.2T_g$). Above T_{MCT}, where ergodicity is obeyed, all regions of phase space are accessible, while below T_{MCT}, where structural arrest occurs, parts of phase space remain inaccessible. At $T = T_{MCT,}$ the *i*MCT visualizes the "self" part of the intermediate scattering function, $F_s(k, t)$, to decay (in the limit $t \to \infty$) to a finite, nonzero, number called the *nonergodicity parameter*. For temperatures exceeding T_{MCT}, the *i*MCT predicts that the scattering function decays to zero in two steps (β- and α-regimes), with the decay of the correlation function at long times approximated by the stretched exponential KWW function (see Figure 1.8). Approaching T_{MCT} from above, the structural relaxation time (and viscosity) scales in a power-law fashion

$$\tau_\alpha(T) \propto (T - T_{MCT})^{-\gamma}, \tag{1.15}$$

where T_{MCT} is a critical temperature for the onset of the glass transition, and the exponent $\gamma > 1.5$.

The *idealized* mode-coupling approach successfully describes key aspects of the relaxation dynamics of moderately supercooled liquids, with its main achievement involving the prediction of the two-step relaxation process that emerges as temperature decreases, in agreement with experimental studies and simulation results. Nevertheless, the dynamic arrest and the predicted singularity at the purported critical temperature of the model bear no connection to the laboratory glass transition or a transition to an "ideal" glass state of matter. Experiments clearly provide no evidence of critical singularities above T_g in real systems (e.g., molecular liquids and colloids), while at the shortcomings of this theory one has to count the complete neglect of heterogeneities [47]. Later revisions offered an *extended* version of the theory (*e*MCT), in which inclusion of flux correlators, besides the density correlators, introduced "phonon-assisted hopping processes" that can restore ergodicity below T_{MCT}. These changes generated a "rounding" of the singularity, due to the existence of secondary couplings that allow activated processes to occur lower than T_{MCT}. The debatable robustness of the *e*MCT to describe dynamical correlations and some aspects of dynamic heterogeneities in the regime $T_g \leq T < T_{MCT}$ suggests that at least in its present form it does not provide a complete theory of the glass transition and, therefore, a particular means of predicting the transition from liquid to glass.

Even so, the mathematical formalism and analysis offered by *e*MCT is acknowledged as a useful starting point in the description of novel systems with unknown behavior (for a review, see Berthier and Biroli [25]).

A different approach offers a group of simple lattice models of glasses, collectively described as kinetically constrained models (KCMs), which are characterized by a trivial equilibrium behavior, but interesting slow dynamics due to restrictions on the allowed transitions between configurations. These models rely on a Hamiltonian for noninteracting entities (spins or particles on a lattice) combined with specific constraints on the permitted motions of any such entity. Their perspective on the glass-transition problem assumes that most of the interesting properties of glass-forming systems are dynamical in origin, and all explanations develop without recourse to any complex thermodynamic behavior. This viewpoint contradicts essential thermodynamic arguments adopted by a number of theoretical treatments (see the following section). Central physical assumptions in most KCMs appear to be the supposition of sparse mobility for the particles (i.e., the atomic motions are deemed to principally involve small amplitude vibrations and not diffusion steps) and the notion of insignificant contribution of static correlations in system dynamics. With appropriate choices of the constraints and explicit mechanisms (e.g., taking into consideration "facilitation" processes), several KCMs provide a natural explanation of the super-Arrhenius slowdown of dynamics and dynamical heterogeneities (e.g., nonexponentiallity) as a consequence of local, disorder-free interactions, notably without the emergence of finite temperature singularities [90]. The super-Arrhenius temperature dependence of the relaxation time is often described by a Bässler-type expression (see Section 1.2.3.1), for temperatures much below an "onset" that marks the beginning of facilitated dynamics with sparse mobile regions. Despite their reliance on local constraints, the implementation of a form of dynamical frustration enables the KCMs to describe cooperative dynamics, aging phenomena, and ergodicity breaking transitions [91]. At low temperatures (or high densities), a struggle between the scarcity of mobility defects (excitations, vacancies) and their need to facilitate motion at neighboring regions is taken into account, leading to a hierarchical collective relaxation. Whether the KCMs provide the correct theoretical framework to explain the glass transition is highly debatable. Among their serious shortcomings stands out the fact that neither glass-transition's phenomenology related to thermodynamics is acknowledged nor are the nontrivial static correlations (argued to accompany the increase of relaxation time in fragile glass formers) properly addressed. Furthermore, these models provide no information either on the slow β-relaxation or on fast relaxation processes and pertinent anomalous vibrations, and, more importantly, on their acknowledged ties to the structural relaxation mechanism.

1.2.4.4 Models Showing a Thermodynamic (or Static) Critical Point

Several statistical–mechanical or mean-field treatments of glass formation build on the premises of the existence of an avoided, or unreachable, thermodynamic (e.g., configurational entropy and random first-order theories), or static (free-volume theories) critical point. Probably the oldest related phenomenological treatment is

provided by free-volume theories, which consider that molecular mobility is controlled by the free volume, while the glass is regarded a frozen metastable state of matter, described by an additional kinetically controlled internal order parameter [78,102,103] and a P–V–T equation of state. Many different models of the glass transition that rely on the concept of free volume [78,104] exist, including the simple kinetic (hole) theories [66]. While not identical, these models consider molecular motions in the bulk state of polymeric materials to depend on the presence of structural voids, also known as "vacancies" or "holes" of molecular size (~0.02–0.07 nm^3), or imperfections in the packing order of molecules. These holes are collectively described as "free volume," a term also used to describe the excess volume that can be redistributed freely without energy change [78]. (It is worth noticing, however, that the free volume available for molecular movement does not coincide with the total empty space in the material, which corresponds to the difference between the geometric volume of all segments and the total volume.) The concept that local rearrangement motions in dense systems require some empty space, which can be taken by atoms involved in this motion, is intuitively appealing: in the liquid state, where the free volume is large, molecular movements occur easily and the rearrangement of chain conformations is practically unconstrained, while, following a decrease in temperature, the free volume shrinks until it is too small to allow large-scale molecular motions. As thermal expansion and viscoelastic relaxation of a solid or rubber-like material can be rationalized in terms of changes in the temperature-dependent free volume, the viscoelastic behavior of polymers and related composites has been extensively studied – with variable success – in relation to free-volume variations [105–107]. Evidence on the significance of free-volume theories and support of the hypothesis that T_g is inversely proportional to free volume is often encountered in the studies of binary polymer systems (e.g., see Figure 1.9 for miscible polyethylene oxide [PEO] + phenolic blends [108]).

Most theories based on the free-volume concept state that the glass transition is characterized by an iso-free-volume fraction state, that is, they consider that "the glass transition temperature is the temperature below which the polymers have a certain universal free volume" [109]. The total volume of the material, V, obeys the relation

$$V = V_0 + V_f, \tag{1.16}$$

where the limiting or occupied volume, V_0, is associated with the hardcore or incompressible molecular volume (molecular volume at zero thermodynamic temperature or extremely high pressure) and significant volume fluctuations (from thermal motion; i.e., bond vibrations and librations). The free volume at temperatures below T_g (denoted by V_f^*) is considered nearly constant, and increases only as the glass-transition temperature is exceeded. In the latter temperature range, free volume can be expressed as

$$V_f = V_f^* + (T - T_g)\frac{\delta V_f}{\delta T}, \tag{1.17}$$

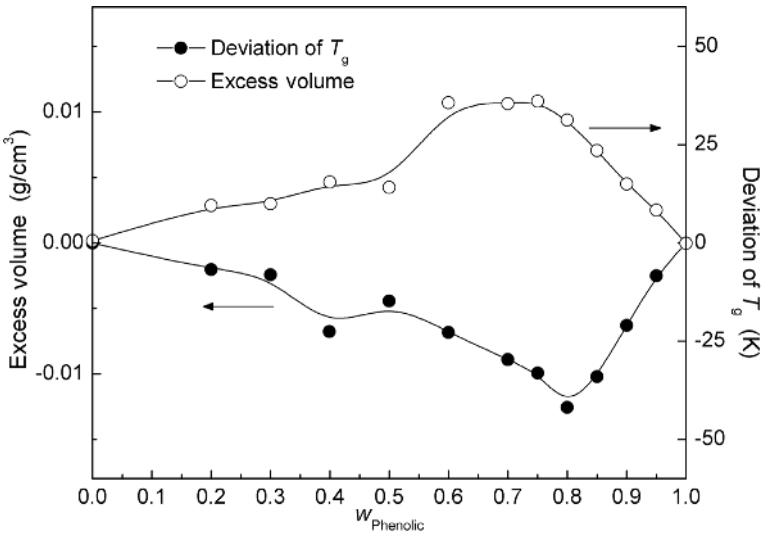

Figure 1.9 Composition-dependent deviations from the linear mixing rules for the glass-transition temperature (positive deviation) and mixture's volume (negative deviation) in miscible PEO + phenolic blends. Adapted and replotted from ref. [108], with permission © 2000 Elsevier.

and by dividing by V, one gets the relation

$$f = f_g + \alpha_f(T - T_g), \tag{1.18}$$

where $f = V_f/V$ is the fractional free volume at some temperature, f_g is the fractional free volume at T_g, and α_f is the thermal expansion coefficient of the free volume. Studying a wide range of polymers, Simha and Boyer [110] supported the iso-free-volume hypothesis for the glass transition and derived the value of $f_g = 0.113$. The starting point of the treatment provided by Williams, Landel, and Ferry [48] is that at $T > T_g$ the internal mobility of the system, represented by viscosity, is related to the fractional free volume by an empirical relationship, which is based on the Doolittle equation [102]

$$\eta = A \exp\left(B \frac{V_0}{V_f}\right), \tag{1.19}$$

with A and B material specific constants. With the approximation of $f = V_f/V \approx V_f/V_0$, valid given that $V_0 \gg V_f$, Eq. (1.19) can be written in the form $\ln \eta = \ln A + B/f$. If $\eta(T)$ denotes viscosity at a temperature T and $\eta(T_g)$ corresponds to the viscosity at the glass-transition temperature, the temperature shift factor (α_T) is given by

$$\ln a_T = \ln\left(\frac{\eta(T)}{\eta(T_g)}\right) = B\left(\frac{1}{f} - \frac{1}{f_g}\right). \tag{1.20}$$

By combining Eqs. (1.18) and (1.20), and after appropriate rearrangement in a $\log_{10}$ functional form, one obtains

$$\log_{10} a_T = \frac{-\dfrac{B}{2.303 f_g}(T - T_g)}{\dfrac{f_g}{\alpha_f} + (T - T_g)}. \tag{1.21}$$

The constant B was found by Doolittle to be of the order of unity. A direct comparison between Eqs. (1.21) and (1.7b) suggests the existence of *universal* values for both the fractional free volume at T_g ($f_g \approx 0.025$) and the thermal expansion coefficient of the free volume ($\alpha_f = f_g/51.6 \approx 4.8 \times 10^{-4}\,K^{-1}$). An immediate inference of the above treatment is that the glass-transition temperature is reached when the fractional free volume attains the limiting low value of 0.025 (more precisely 0.025 ± 0.009 for most polymers). Several equation-of-state models, such as the statistical–mechanical Simha–Somcynsky hole theory [103], permit the determination of V_f. The latter, however, is better determined experimentally, given the serious discrepancies often encountered in theoretical derivations [111]. Positron annihilation lifetime spectroscopy (PALS) [112], for example, provides values for the free-volume fraction in the range 0.02–0.11, in reasonable agreement with theoretical estimates [104,110].

Free-volume theories lack the ability to provide connections among relaxation characteristics of glass-forming liquids and important macroscopic thermodynamic properties, notably the configurational entropy and its temperature derivative, the isobaric heat capacity. A thermodynamic perspective to the glass-transition phenomenon may be provided by considering the glass as a thermodynamic phase, an assumed "fourth state of aggregation of matter" [8]. The assumption of an underlying true second-order phase transition (in the Ehrenfest notation), due to a change in the configurational entropy, has led to various phenomenological entropic treatments, most notably the Gibbs–DiMarzio [79] and Adam–Gibbs [44] theories. Strong motivation for their development provided the crisis that emerges when the entropy of a supercooled liquid is extrapolated toward low temperatures. Recall that the so-called Kauzmann's paradox is avoided by the glass transition, since the entropy has a smooth change (as experimentally evidenced) due to an underlying phase transition. The theoretical derivation of the statistical–mechanical theory of Gibbs and DiMarzio was based on the Flory [113] and Huggins [114] lattice model. The model develops by first calculating the number of ways that n_y linear polymer chains of y monomer segments each (y-mers) can be placed in a diamond lattice with n_0 unoccupied holes. Each chain has a lowest energy shape and the more the shape deviates from it, the greater the internal energy of the molecule. The ensuing configurational partition function, describing the location of holes and polymer molecules, has the form

$$Q = \sum_{f, n_y, n_0} \Omega\left(f_1 n_y \ldots, f_i n_y \ldots, n_0\right) \exp\left[-\frac{E\left(f_1 n_y \ldots, f_i n_y \ldots, n_0\right)}{k_\beta T}\right], \tag{1.22}$$

where $f_i n_y$ is the number of molecules packed in conformation i, E in the internal energy of the system, and Ω is the microcanonical partition function (i.e., the total number of ways that the n_y molecules can be packed into $yn_y + n_0$ sites on the quasi-lattice). Knowledge of the partition function allows the configurational entropy to be determined from the relation

$$S_c(T) = k_\beta T \left(\frac{\partial \ln Q}{\partial T} \right)_{V,n} + k_\beta \ln Q, \tag{1.23}$$

through which several derivations and property calculations become possible. While several of its predictions are in agreement with experimental data (e.g., the molecular mass dependence of T_g), the validity of the theory remains rather questionable in the absence of rigorous mathematical justification of critical assumptions (e.g., the actual form of the microcanonical partition function). In an effort to reconcile thermodynamic arguments with purely dynamical aspects of the phenomenon, it has been postulated that, although the observed glass transitions show clear manifestations of a kinetic phenomenon, the underlying true transition features equilibrium properties that are difficult to observe experimentally. This aspect was considered in the Gibbs–DiMarzio approach by defining a new transition temperature, T_2, at which the configurational entropy of the system reaches a critically low value $S_{c,0}$ [57] ($S_{c,0}(T_2) = 0$ in ref. [79]). T_2 is clearly not an experimentally measurable quantity; calculations place it approximately 50° below the glass-transition temperature observed at ordinary measuring times. In effect, T_2 is considered to be the lower limit value that T_g would reach in a hypothetical experiment of infinite timescale.

A somewhat different phenomenological approach to an "entropy-vanishing" glass-transition model has been presented by Adam and Gibbs [44]. The idea behind their molecular-kinetic theory is that the liquid consists of regions that rearrange as units, independently of their environment, when experiencing a sufficient fluctuation in enthalpy. Each related subsystem of the material is referred to as a cooperatively rearranging region (CRR) and has a size determined by the number, z, of molecules included (monomeric segments in polymers' case). The temperature-dependent relaxation times for a viscous material are determined from the probabilities for cooperative rearrangements to take place. A structural rearrangement is activated with a barrier height ($\Delta\mu$) proportional to the lower limit number $z^*(T)$ of segments within the hypothetical critically sized CRR with a nonvanishing transition probability. The structural relaxation time is inversely proportional to the average transition probability, providing the relation

$$\tau_\alpha(T) = \tau_\infty \exp\left(\frac{z^* \Delta\mu}{k_\beta T} \right), \tag{1.24}$$

where τ_∞ is a constant. At high temperatures, the molecular displacements are taken to be entirely noncollective, and the barrier height reduces to a constant Arrhenius activation energy. The size of the CRR depends on temperature and is determined by the configurational entropy of the liquid, while an increase in the dynamic cohesive length, ξ_α, is anticipated with decreasing temperature. A link to

the Gibbs–DiMarzio theory is provided by the hypothesis that $z^*(T)$ is simply inversely proportional to the (molar) configurational entropy, $z^*(T) = N_A s_c^*/S_c(T)$, where s_c^* is the configurational entropy of the critically sized CRR. By combining the latter equations, configurational entropy and structural relaxation time (or the shear viscosity) in the liquid state are now connected through the relation

$$\tau_\alpha(T) = \tau_\infty \exp\left(\frac{A}{TS_c}\right). \tag{1.25}$$

As temperature decreases and larger units progressively form, S_c decreases until it approaches zero at some temperature T_0 (generically close to T_2 and T_K [54]). At this point, relaxation times and viscosity diverge, and a second-order thermodynamic transition is suggested to occur. The validity of Eq. (1.25) has been tested in numerous experimental studies (which, typically, use the excess entropy of the liquid over the crystal in the place of S_c) and computer simulations (where S_c is directly assessed) [115]. Adam and Gibbs [44] used their entropic theory to derive a WLF-type formula for the temperature shift factor. Furthermore, considering that the configurational entropy can be calculated from the relation

$$S_c(T) = S_c(T_0) + \int_{T_0}^{T} \frac{\Delta C_p}{T} \mathrm{d}T \tag{1.26a}$$

and roughly assuming a hyperbolic form for the configurational part of the specific heat ($\Delta C_p \sim 1/T$), it follows that

$$S_c(T) \propto \frac{T - T_0}{T}, \tag{1.26b}$$

from which Eq. (1.25) further derives the VFTH equation (with T_0 replacing T_V). One of the limitations of the Adam–Gibbs theory is that it provides no information regarding the size or number of CRRs in the system, because s_c^* is not specified, except as a formal lower limit that provides, in practice, no useful insight at the microscopic level. As an extreme limit, the entropy of the smallest region capable of undergoing a rearrangement is obtained by the Boltzmann relation as $s_c^* = k_\beta \cdot \ln 2$, given that a minimum of two configurations must be available for a rearrangement to take place. Adopting this value, $\Delta\mu$ and z^* may be evaluated from experimental data. However, the low values deduced for $z^*(T_g)$ in a number of glass formers suggest that the Adam–Gibbs theory, if valid, might be more appropriate for local processes transpiring before the glass transition [13].

An elaborate mean-field approach to glass formation is given by the RFOT theory [86]. Within this framework, vitrification is described analogous to crystallization, with the difference that the system is frozen into a set of aperiodic structures instead of a periodic crystalline structure. This theoretical ensemble ties together intelligibly aspects of several prior concepts, notably, the *unreachable* thermodynamic transition postulated by the configurational entropy theories, the emergence of a complex free-energy landscape with numerous energy minima, and the *avoided* dynamical

singularity of the MCT. In this way, a low-temperature thermodynamic transition, at T_K, to an ideal glass phase (accompanied by a discontinuous jump in the order parameter, but no latent heat) is postulated to exist along with a high-temperature ergodicity breaking dynamical transition, at T_{MCT}. These two coexisting critical points are separated by a regime in which an exponentially large (in system size) number of metastable free-energy states (configurations) dominate the thermodynamics while trapping the dynamics. Support for the above phenomenology has been found in several standard liquid models when treated within mean field-like approximations (see reviews by Berthier and Biroli [25], and Cavagna [116]). The thermally activated hopping mechanisms that take control in the regime $T_K < T < T_{MCT}$ are described in a nonperturbative way. Phenomenological arguments only exist [117], backed by microscopic computations [118], which describe liquid dynamics below the crossover at T_{MCT} as a "mosaic state," while a dynamical scaling theory based on "entropic droplets" (domains of synergetic molecular motions, with linear size ξ^*) is considered as temperature approaches T_K. The entropic droplets are formed and stabilized by the competition between a favorable driving force (i.e., an increase of the configurational entropy) and an unfavorable surface mismatch penalty. The mosaic length scale ξ^*, characteristic of the mosaic cells and entropic droplets, represents the length scale above which any consideration of metastable states becomes inappropriate. Assuming that thermal activation over energy barriers grows with size as $(\xi^*)^{\psi}$, with $\psi \geq \theta$, the super-Arrhenius $\tau_\alpha(T)$ dependence is given by [118]

$$\ln\left(\frac{\tau_\alpha}{\tau_0}\right) = C\frac{Y}{k_\beta T}\left(\frac{Y}{T \cdot S_c(T)}\right)^{\frac{\psi}{d-\theta}}, \tag{1.27}$$

where C is a constant, Y is a "bare" energy scale (in appropriate units), d is the dimension of space, and ψ and θ are two critical exponents. The latter are predicted to obey the relation $\psi \approx \theta = 3/2$, in $d = 3$ [117], providing an Adam–Gibbs-type formula for the relaxation time with the configurational entropy per particle, $s_c(T)$, vanishing at the ideal glass transition T_K. Several other nontrivial derivations of the RFOT, frequently based solely on phenomenological arguments [119], address issues such as the decoupling between translation and rotation, nonexponential relaxation (i.e., $\beta_{KWW} < 1$) and its connection with fragility, the specific heat jump at the glass transition, and the accelerated segmental dynamics close to free surfaces [120]. The reader is referred to an excellent review by Berthier and Biroli [25] for a detailed discussion of several limiting approximations and missing links between the pieces of this "patchwork" theory, as well as potential weaknesses of the RFOT construction in providing the description of finite-dimensional systems.

Reference to some form of space fragmentation into dynamically and/or spatially heterogeneous zones (described, for example, as "regions," "spheres," "domains," or "droplets") appears also in the frustration-limited domains (FLDs) theory. Through a series of tentative assumptions [121], this approach directly addresses glass formation in terms of the real space at the molecular level [92]. Its critical assumptions include the existence of a locally preferred structure in a

liquid (i.e., a domain-level molecular arrangement that minimizes some local free energy), the unfeasibility for this local structural order to expand over the entire system (i.e., the domain size is limited by frustration, or equivalently, the ordered domains are deemed separated by domains of topological defects), and the possibility to build an conjectural system in which the effect of frustration can be suppressed or disabled. In the context of liquids and glasses, frustration is attributed to a competition between a short-range propensity for expansion of a locally preferred order and global constraints that prohibit the periodic tiling of space with the particular local structure. Considering a system that organizes itself, at low temperatures and finite frustration level, into a mosaic of domains corresponding to some local order, its dynamics will involve restructuring of the domains in a thermally activated manner, using arguments similar to those adopted within the mosaic picture of RFOT. Under rather generic conditions, frustration produces a "narrowly avoided critical point," that is, the ordering transition that may possibly exist at some temperature T^* (above T_g) in the absence of frustration may disappear when an infinitesimal degree of frustration is introduced. The crossover temperature, T^*, marks the onset of an anomalous supermolecular (collective) behavior and it can be used to establish a scaling description of several collective properties of glass-forming liquids. In relation to the existence of a pertinent heterogeneity length scale, for example, let us consider the free energy of a domain (of volume L^3), given by

$$F(L, T) = c_1(T)L^2 - c_2(T)L^3 + c_3(T)L^5. \tag{1.28}$$

The bulk free-energy gain inside the domain (second term) is modified by the strain free energy due to frustration (last term), and this strain induces breaks in the order that give rise to surfaces with free energy $c_1 \cdot L^2$ (first term). By minimizing the free energy per unit volume, $F(L,T)/L^3$, one finds that the characteristic radius of the domains scales as $(c_1/c_3)^{1/3}$, and that their size increases when temperature decreases without showing any divergence [121]. The presence of structured domains, whose size is finely tuned by the amount of frustration, readily connects to fundamental phenomena occurring in glass formers, such as cooperativity, dynamic heterogeneity, and spatial fluctuations, which directly rationalize – at least qualitatively – nonexponential relaxation, decoupling phenomena, and liquid fragility. Relaxation times (and shear viscosity), for example, are predicted to exhibit a distinctive super-Arrhenius temperature dependence at $T < T^*$, of the form

$$\tau_\alpha(T) = \tau_\infty \exp\left(\frac{E_\infty}{T} - \frac{\Delta E(T)}{T}\right). \tag{1.29}$$

The term $\Delta E(T) = BT^*(1 - T/T^*)^{8/3}$ describes the energetic requirement for restructuring the FLDs, and is thus assumed to be zero above T^*, yielding a simple exponential behavior. The four adjustable parameters (τ_∞, E_∞, B, T^*) of Eq. (1.29) can be obtained by fitting of experimental data. The fragility of a glass former is quantified by the value of parameter B, which is inversely proportional to the degree of frustration [93]. A major weakness of this theory is the missing

identification of the locally preferred structure for molecules of nonspherical shapes, the structural elements of most real fragile materials. It is very likely that the postulated formation – on supercooling – of tetrahedral or icosahedral local order (or even of hexagonal bond orientational local order) in three-dimensional one-component liquids with atoms interacting via spherically symmetric pair potentials [122], has little to do with the behavior of ordinary molecular liquids and polymers.

1.2.4.5 Percolative Phenomena in Glass Formation

Both liquids and glasses have a topologically disordered distribution of elementary particles, without perceptible differences in their translation-rotation symmetry. Their structure cannot be described in terms of repeating unit cells, as the unit cell of any amorphous material would comprise all *particles* (atoms or molecules) due to nonperiodicity. A number of approaches to the glass-transition phenomenon build on alternative structure descriptions [12], such as the consideration of the bond system rather than the set of particles. For each state of matter, one may define a set of bonds, that is, introduce a bond lattice model, which is the congruent structure of its chemical bonds. The bond lattices of glasses and liquids have different symmetries, in contrast to the symmetry similarity of particles in the liquid and glassy states of matter. Structural signatures in the form of percolation thresholds of the Delaunay networks [123] and an increase in icosahedral ordering near T_g [124] have been observed by computer simulations of amorphous solids and simple liquids. Interesting observations have emerged from studies of the percolation thresholds of networks of the Delaunay simplices of different "coloring," with each color denoting the Delaunay sites of identical form (i.e., with identical metric properties). For example, in a molecular dynamics study of the configurations of liquid, supercooled, and quenched (glassy) rubidium, Medvedev and coworkers [123] showed that the Delaunay simplices develop macroscopic aggregates in the form of percolative clusters. In the liquid state, low-density atomic configurations form a cluster that goes across the whole material. This macroscopic structural organization permits extensive motions, like those observed in shear flow. In contrast, in the glassy state nearly tetrahedral high-density configurations contribute to the formation of clusters that percolate across the whole glass.

The CPM explains the glass transition in terms of a percolation-type phase transition, a percolation effect in the system of broken bonds connected with the formation of percolation clusters made of *configurons* [87]. A "configuron" is defined as a fundamental configurational excitation in an amorphous material that involves breaking of a chemical bond and the concomitant strain-releasing local adjustment of centers of atomic vibration. At absolute zero temperature broken bonds are absent, while the concentration of thermally activated broken bonds (configurons) is expected to increase with temperature, accompanied by a loss in material's rigidity. Since configurons weaken the bond system, the higher their content the lower the viscosity of the system becomes. Based on the percolation theory, when the concentration of configurons exceeds the threshold level,

these will form a macroscopic so-called percolation cluster of broken bonds, which penetrates the whole volume of the disordered network. The percolation cluster is a dynamic structure postulated to develop at the glass-transition temperature. The critical temperature at which the percolation level is achieved can be found assuming that the configurons achieve their universal critical density, $p(T_g) = p_c$, given by the percolation theory. Although no symmetry changes are evidenced in the atomic distribution, there is a symmetry breaking expressed by a stepwise variation of the Hausdorff–Besikovitch dimensionality of bonds at the glass transition: from 3 (canonical Euclidean space), in the glassy state, the dimension of bonds reduces to 2.55 ± 0.05 in the liquid state (fractal network geometry).

Within the CPM, the resemblance of the glass-transition phenomenon to a second-order phase transformation, as a consequence of a change in symmetry, is treated in terms of the Landau–Ginsburg theory. Important role in the latter theory plays the order parameter, which equals zero in the disordered phase and has a finite value in the ordered phase. The density of the percolation cluster of configurons changes from a nonzero value in the liquid state to zero in the glassy state, and thus offers a suitable order parameter. As temperature approaches T_g, the CPM reveals diverging behavior for several parameters, such as the correlation length [$\xi(T) = \xi_0/|p(T) - p_c|^n$, with a critical exponent $n = 0.88$], the thermal expansion coefficient, and the heat capacity (both proportional to $\sim 1/|T - T_g|^{0.59}$). A direct anticorrelation between the fragility ratio, introduced by Doremus [59], and the configuron percolation threshold has been postulated to exist [87], and explained considering that in fragile materials the configurons are larger (delocalized). Important thermodynamic parameters of the configurons (e.g., the configuron formation enthalpy and entropy, H_d and S_d, respectively) can be extracted from the temperature dependence of the shear viscosity of amorphous materials [88]. These can be further used to predict the glass-transition temperature from the relation

$$T_g = \frac{H_d}{S_d + R \ln\left[(1 - p_c)/p_c\right]} \tag{1.30}$$

and also to numerically access T_g at arbitrary cooling rates [89]. Unfortunately, while a number of successful predictions have been reported for oxide glasses, the effectiveness of Eq. (1.30) is restricted due to the large uncertainties in the determination of the required thermodynamic parameters (five coefficients concurrently determined in fits of $\eta(T)$) and specific model approximations. Interestingly, the configuron model of viscosity results in a two-exponential $\eta(T)$ equation, a functional form similar to that originally proposed by Douglas [125] for the universal description of viscosity data at all temperatures, which can be readily approximated (within narrow temperature intervals) by known theoretical or heuristic functions.

An alternative approach offers the two-order-parameter model of Tanaka [126]. This model considers the glass transition as being controlled by the competition (due to the incompatibility in their symmetry) between long-range density

ordering toward crystallization and short-range bond ordering toward the formation of long-lived rigid structural elements (designated as "locally favored structures"). The supercooled liquid is described as a frustrated metastable liquid state consisting of metastable solid-like islands, in a sea of short-lived random normal-liquid structures, which exchange each other dynamically at the rate of the structural relaxation time. Depending on the type of measurement, T_g can be defined either as the temperature at which the average lifetime of the metastable islands exceeds the characteristic observation time or as the temperature where percolation of long-lived metastable islands occurs. The average fraction of locally favored structures is regarded as a suitable measure of fragility (with a higher fraction indicating a stronger liquid), while extensive reasoning addresses the crossover from the noncooperative to the cooperative regime and the origin of the non-Arrhenius behavior of the structural relaxation.

At present, approaches like those mentioned above simply provide an interesting, yet incomplete, picture of glass formation, given the fact that they can address only a narrow range of its plethoric phenomenology.

1.3 Manipulating the Glass Transition

The glass-transition temperature reflects the ease by which polymer chains commence waggling and break out of the rigid glassy state into the soft rubbery state in the course of heating. Its location is thus primarily regulated by *intrinsic characteristics* of the macromolecular system (Section 1.3.1), typically related to the chemical structure (main-chain structure, tacticity, type of pendant groups, etc.), chain conformations, and the degree of polymerization (molecular mass). Knowledge of the potential influence of each of these factors is a prerequisite – but clearly not the only – for appropriate selection of the components in binary and ternary mixtures and the preparation of polymer composites with finely adjusted properties and structural characteristics. Besides blending, which is comprehensively treated later in this chapter, reference should also be made to a number of technologically important *externally controllable processes* (application of pressure, orientation processes, presence of additives, electron-beam irradiation, etc.), *chemical reactions* (copolymerization, curing), or *physical phenomena* (aging, crystallization), with a substantial bearing on the glass structure and the temporal response (during storage or service life) of engineering polymeric materials (Section 1.3.2).

Guidance for targeted polymeric molecular design may come from explicit theoretical and simulation methodologies that aim to predict material's properties from its molecular details. Freed and coworkers [127], for example, developed a generalized entropy theory that combines the lattice cluster theory – for a semiflexible-chain polymer fluid – with the Adam–Gibbs model for the structural relaxation time. Their model provided a rational, predictive framework for calculating the essential properties (including T_g and fragility) of glass-forming fluids as a function of their molecular architecture, bond stiffness, cohesive

interaction energy, pressure, molar mass, concentration and structure of additives, and so forth. The estimates appear to corroborate several of the experimentally established general trends discussed below. Simulation approaches, on the other hand, usually employ either quantitative structure–property relationship (QSPR) models (where structural and quantum-chemical descriptors of perceived significance along with group additive methods are typically used in relevant estimations [128,129]) or atomistic modeling techniques (where full atomic detail of the polymers is considered, as in molecular dynamics simulations [130]). For selected polymers, interesting information on various structure–property dependences, such as the variation of T_g with chain stiffness and substituent volume [131] or the type of the polymerization initiator [132], has been derived from QSPR studies.

1.3.1 Effects of Chemical Structure

The location of the glass transformation range is representative of the flexibility of polymer chains, which in turn is determined by the degree of freedom with which their segments rotate along the backbone. As a result, low T_gs are typical of linear polymers with single covalent bonds and a high degree of rotational freedom about σ bonds in the main chain, while stiffening groups along the backbone (e.g., aromatics and cyclic structures) reduce chain flexibility and increase intermolecular cohesive forces. For instance, the incorporation of a *p*-phenylene ring (Ph) into polyethylene's (PE) monomeric unit gives poly(*p*-xylylene) [(—CH_2—Ph—CH_2—)$_n$], with a glass-transition temperature (≈+80 °C) significantly elevated compared to that observed in various commercial PEs (−130 °C to −80 °C). Tacticity has considerable bearing on the rotational energy requirements of the backbone. In the case of mono- and disubstituted vinyl polymers, (—CH_2—CXY—)$_n$, for example, Karasz and MacKnight [133] indicate that steric configuration affects T_g only when the substitutes are different, and neither of them is hydrogen. Based on the Gibbs–DiMarzio theory of the glass transition, the increase observed going from isotactic and highly syndiotactic polymers can be related to the larger difference among the energy levels between rotational isomers in syndiotactic chains. In monosubstituted vinyl polymers, where the other substitute is hydrogen, the energy differences between the rotational states of the two pairs of isomers are comparable and the effect of tacticity is weak (e.g., polystyrene[PS] and poly(vinyl acrylate)s; Table 1.1). If the different tactic configurations of a single disubstituted vinyl polymer are considered, the glass-transition temperature appears to increase with the increasing content of syndiotactic triads. This trend is clearly demonstrated by poly(*N*-vinyl carbazole) (PVK) (i.e., T_g = 126 °C, 227 °C, and 276 °C, for isotactc (i-), atactic (a-), and syndiotactic (s-) PVK, respectively) [134]), poly(methyl methacrylate) (PMMA) [16,135], and several other poly(vinyl methacrylate)s (Table 1.1).

The chemical nature (e.g., polarity and ionicity), bulkiness, and flexibility of the groups attached to a polymer chain are often used to adjust its glass-transition

Table 1.1 Effect of tacticity on the glass-transition temperatures for various poly(vinyl acrylate)s and poly(vinyl methacrylate)s [1,136].

	T_g (°C)				
	Poly(vinyl acrylate)s		Poly(vinyl methacrylate)s		
Side chain	Isotactic	Atactic[a)]	Isotactic	Atactic[a)]	Syndiotactic
Methyl	10	8	43	105	160
Ethyl	−25	−24	8	65	120
n-Propyl		−44		35	
Isopropyl	−11	−6	27	81	139
n-Butyl		−49	−24	20	88
Isobutyl		−24	8	53	120
sec-Butyl	−23	−22		60	
Cyclohexyl	12	19	51	104	163

a) Atactic specimens with high syndiotactic content.

temperature. Pendant groups endorsing stronger intermolecular forces are responsible for polymers of higher T_g. The polar carbon chloride bond in poly(vinyl chloride) (PVC), for example, is the source of stronger intermolecular (dipole–dipole) interactions, compared to the relatively weak van der Waals forces present in polypropylene (PP); the large difference of $T_g^{(PVC)} - T_g^{(PP)} \approx +100\,°C$, among the atactic forms of these polymers, is an immediate consequence of the substitution. The upshift is even stronger when the Cl— groups are completely substituted by OH— (+105 °C) or CN— (+117 °C) groups, owing to the establishment of an extensive network of hydrogen-bonding interactions. Large and inflexible groups normally bring about an increase in chain's rigidity. Bulky groups, such as the benzene ring, may even hook up on neighboring chains and restrict rotational freedom (physical cross-linking), with a concomitant increase in polymer's T_g. Ample experimental evidence exists in the case of monosubstituted vinyl polymers [5,7,134], with the glass-transition temperatures following an increasing trend after substituting the hydrogen atom by progressively bulkier, stiffer, and/or more polar pendant groups: $T_g \leq -80\,°C$ (for X = H), $T_g = -10\,°C$ (X = —CH_3), 31 °C (X = —O—CO—CH_3), 85 °C (X = —OH), $T_g = 100–130\,°C$ in *p*-methyl, 2-methyl, or *p*-chloro styrene containing polymers, $T_g = 130–150\,°C$ when biphenyl or napthalene pendant groups are introduced, and $T_g > 170\,°C$ in poly(*n*-vinyl pyrrolidone) and PVK [7,134]. Moreover, changes in the number of successive methanediyl (—CH_2—) or methyl (—CH_3) groups in the aliphatic sequence of the flexible pendant groups in polyvinyl acrylates [137], methacrylates [133], and several other linear-chain polymers [138] have been extensively used to regulate chain's packing and system's T_g. Typically, by increasing the length of the aliphatic chain, free volume (at a given temperature) increases and the frictional interaction between chains is lowered [16]. Examples illustrative of the above behavior are presented in Table 1.2, for several

Table 1.2 Effect of the pendant group length of the glass-transition temperature of typical linear-chain thermoplastic polymers.

Alkyl	T_g (°C)			
	Poly(*n*-alkyl methacrylate)s	Poly(vinyl *n*-alkyl ether)s		
	TD (*V* – *T*) [133]	DMA (1 Hz) [106]	TD (*L* – *T*) [140]	TD (*V* – *T*) [139]
Methyl	105	−10	−22	
Ethyl	65	−17	−33	−42
n-Propyl	35	−27		
n-Butyl	20	−32	−56	−54
n-Pentyl				−66
n-Hexyl	−5		−74	
n-Octyl	−20		−80	−80
n-Dodecyl	−65			

poly(*n*-alkyl methacrylate)s [133], of the general formula $(—CH_2—CCH_3(OX)—)_n$, and poly(vinyl *n*-alkyl ether)s [106,139,140], $(—CH_2—CH(OX)—)_n$, with X representing the *n*-alkyl group. The predictions of the generalized entropy theory [127] for polymer chains with stiff backbones and flexible side groups (e.g., poly(*n*-alkyl methacrylate)s and poly(*n*-α-olefin)s [141]) are in line with the experimental trends.

It is also worth stressing the modulation of the flexibility of a pendant group by the compactness of its isomers. The different isomeric forms of the butyl radical in poly(vinyl butyl ether)s is an interesting example: T_g increases from −32 °C in the case of poly(vinyl *n*-butyl ether) to −1 °C in poly(vinyl isobutyl ether), and, finally, to 83 °C in poly(vinyl *tert* butyl ether), which accommodates the most compact isomer [142]. Mixed dependences may appear in more complex chain structures, attributable to coalescent counteracting effects. In different classes of polyphosphazenes [143,144], for example, in the region of short alkyl groups the response is regulated by an increase in free volume, with the short side groups acting as chain ends [144]. Above the side-chain length associated with each T_g minimum, a further addition of methylene groups enhances intermolecular interactions, presumably due to a physical cross-linking action of the longer alkyl side groups [144,145]. For chains with flexible backbones and stiff side groups, theoretical predictions reveal a strong increase in the glass-transition temperature with increasing length of the side groups [127].

Main chain's length and polarity have also significant bearing on the glass-transition temperature. The latter is very dependent on the degree of polymerization up to a value known as the critical T_g or the critical molar mass [1]. In most cases, the strong dependence persists only up to $M_n \sim 10^4$, with no appreciable effect being seen for longer chains. The theoretical treatments of Fox and Flory [109] and Somcynsky and Patterson [146] suggest a linear dependence of

T_g on the inverse molar mass of a homopolymer, expressed as

$$T_g = T_g^{\infty} - \frac{K}{M_n}. \tag{1.31}$$

In this relation, K is a constant depending on the polymer, M_n is the number-averaged molecular mass of the homopolymer, and T_g^{∞} is the glass-transition temperature of a linear chain of "infinite" length. For PVC, for example, Pezzin and coworkers [147] reported values of $T_g^{\infty} = 78\,^{\circ}\mathrm{C}$ and $K = 8.05 \times 10^4$ (for $3 \times 10^3 \leq M_n \leq 10^5$). Equation (1.31) can be deduced from the free-volume theory, taking into account that terminal (end) groups bring about more free volume than the internal ones [148]. More satisfactory description of the experimental pattern has been reported using functional forms deriving from the statistical–mechanical Gibbs–DiMarzio [80] theory. For commercial polymers, the influence of M_n variation on T_g is insignificant and is almost always overtaken by other factors. Note also that a decrease in chain's flexibility frequently stems from an increase in the density and/or the strength of interchain interactions. The first effect is illustrated in the gradual change of the glass-transition temperature of PE from $-7\,^{\circ}\mathrm{C}$ to $137\,^{\circ}\mathrm{C}$, with chlorination levels increasing from 28.2% to 77.4% [149].

1.3.2 Externally Controlled Processes or Treatments

1.3.2.1 Pressure Effects

The measurement of changes in the glass-transition temperature with pressure variations has become an important topic of polymer science, and new experimental studies and theoretical interpretations of pressure effects are in development [150]. In practical terms, interest is primarily directed toward the studies of product failure at high-pressure applications, while polymer engineering seeks information on the pressure dependence of the glass transition of polymers – in part – as a result of its involvement in the commercial large-scale production or treatment of polymer mixtures (e.g., in hot-melt extrusion and compression molding). In general, T_g in polymers increases with increasing pressure (Figure 1.10 [150,151]), as expected from the generalized Ehrenfest relations applied to the glass–liquid transformation [152] and in accordance with predictions of free-volume theories of the glass transition [1]. The change is roughly described by the relation deriving if one considers the continuity of volume at the transition,

$$\left(\frac{\partial T_g}{\partial P}\right)_T = \frac{\Delta\kappa_T}{\Delta\alpha}, \tag{1.32}$$

while a much better description of a wider collection of experimental data [153] is provided by the second Ehrenfest relation, which considers continuity of entropy at the transition,

$$\left(\frac{\partial T_g}{\partial P}\right)_T = VT\frac{\Delta\alpha}{\Delta C_p}. \tag{1.33}$$

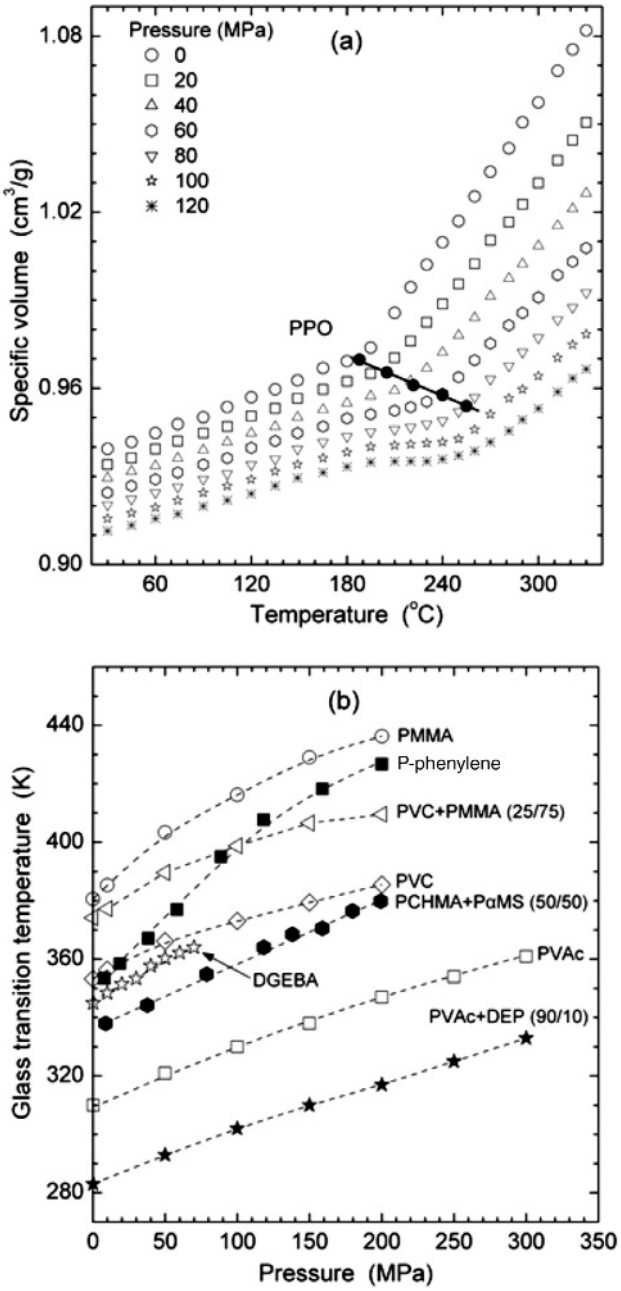

Figure 1.10 (a) Dependence of the specific volume versus temperature and pressure, reported for PPO. The solid circles represent $T_g(P)$ as determined from the intersection of the liquid and glassy $V(T)$ data [150]. (b) Pressure dependence of T_g reported for various glass formers [151], with permission © 2007 American Chemical Society.

The latter relation has been recently shown by Schmelzer [19] to be derived using an entropy-based approach for viscous flow and relaxation (Adam–Gibbs model). For all glass formers, the change in T_g with pressure is linear at low pressures, but the pressure coefficient of the glass-transition temperature decreases with increasing pressure. The empirical relation proposed by Andersson and Andersson [154]

$$T_g = k_1 \left(1 + \frac{k_2}{k_3} P\right)^{1/k_2} \tag{1.34}$$

with k_1, k_2, and k_3 material constants, is frequently used to describe experimental data. A rough estimate considers an increase of the glass-transition temperature at a rate of around 20°–25° per kbar of pressure [1]. In view of that, the stiffening effect of pressure (vitrification) becomes important only in the case of applications at very high pressures, as well as in engineering operations where the polymer is processed near T_g.

1.3.2.2 Crystallization Effects

Polymers with a high tendency for crystallization are anticipated if their molecular geometry permits the formation of specific molecular orientations. As the glass-transition phenomenon activates only in the amorphous regions of a partially crystalline material, the intensity of the signal is controlled by both the degree of crystallinity and the formation of a "rigid amorphous fraction" (RAF) [155,156]. The latter term is often used to distinguish strongly hindered (often presumed immobile) chains at the amorphous–crystalline interface from mobile chains in the remaining amorphous phase (the "mobile amorphous fraction" (MAF); see also Section 1.7.2). As a consequence of the need to accommodate flexible molecules of typically 1–100 μm length into micro- or nano-sized intercrystallite regions, a crossing of the interface by the long molecules is rather common. This produces a strong coupling between crystalline and amorphous phases and a dependence of molecular mobility on segment's proximity to crystallite surfaces. Because of that, the main glass-transition signal in semicrystalline polymers is broader than that of the amorphous ones and extends toward the high-temperature side [27]. Surprisingly, the transition temperature may either increase [5] or decrease with increasing degree of crystallinity. In poly(ethylene terephthalate) (PET), for example, the amorphous specimen T_g of 65 °C changes to 92 °C in a highly crystalline material (relaxational DSC data [157]), while, in the case of poly(4-methyl-1-pentene), an increase in crystallinity from 0% to 76% is accompanied by a drop in T_g from 29 °C to 18 °C (specific volume versus temperature thermomechanical data [158]). A broadly accepted explanation for these opposite shifts is still missing. A plausible explanation, however, considers the difference in the relative densities of the amorphous and crystalline phases as the determining factor [7]. In many polymers, the coupling observed at the interface also causes a separate glass transition for the RAF. This portion of the polymer may lose its rigid character below the melting temperature of the surrounding crystals, within the melting region, or even above the melting temperature [156].

When a molten polymer is subjected to stretch during processing, orientation of the chains occurs accompanied by a significant rise of its glass-transition temperature. Highly oriented materials, such as films or fibers, can yield an apparent T_g, that is, by as much as 30° higher than that of the unoriented amorphous material [159,160]. Even stronger dependences are observed when orientation coexists with, or promotes, crystallization [159]. A common interpretation of these changes is based on the decrease of the free volume with increasing orientation, as chains in the amorphous phase are constrained in relatively close-packed elongated forms.

1.3.2.3 **Plasticizer Effects**

In order to improve the flexibility, processability, and utility of a given polymer, it is often necessary to decrease its glass-transition temperature. This can be accomplished by the addition of low-molecular-mass chemical compounds ("diluents"), mostly nonvolatile and chemically inert liquids, referred to as *plasticizers* [161]. A plasticizer may be considered as a substance, breaking intermolecular bonds in a polymer network, or even as a lubricant, reducing intermolecular friction and by this increasing deformability of the structure [162]. The ensuing reduction of the cohesive forces between neighboring polymer chains facilitates molecular rotations with a concomitant decrease in T_g. From the perspective of free-volume theories, plasticizer molecules may be considered to increase free volume by pushing apart neighboring chains, permitting the translational and rotational mobility of their segments to be retained to temperatures lower than those in the pure polymer. In contrast to molecular plasticizers that decrease the stiffness of the glassy polymer (lowering modulus and tensile strength, followed by an increase in elongation), some chemical compounds act as *antiplasticizers*, increasing the material's stiffness while they produce a (softer) depression of T_g. The addition of an antiplasticizer has been determined by Riggleman and coworkers [163] to cause significant changes in the long-wavelength properties, which are associated with an enhanced packing efficiency in the glass state (e.g., a decrease in κ_T) and increased material stiffness (i.e., an increase in shear modulus, bulk modulus, and Poisson ratio). The efficiency of any potential plasticizer/antiplasticizer is expected to depend on its polarity, solubility parameter, stiffness, density, and loading (weight, volume, or molar fraction). These factors manipulate the relative importance of the enthalpic and entropic contributions to the glass-transition temperature. An analysis of the issue, based again on the generalized entropy theory, exemplifies the significance of diluent's molecular properties [141]: plasticization is favored by small additives whose cohesive energies are less than the cohesive energy of the host polymer (i.e., only weak attractive interactions between the diluent and the polymer matrix are present), while antiplasticization is promoted in the opposite case. Absorbed water often functions as a plasticizer on many hydrophilic materials (e.g., polyamides, starches, and sugars), while the simultaneous occurrence of plasticization and antiplasticization effects (yet in

different concentration ranges) is not uncommon in hydrated amorphous food matrices [164]. Weakly polar esters are good plasticizers because they tend to be miscible with many polar and nonpolar polymers. The most commonly used plasticizers are obtained from phthalic acid and include diethyl, dibutyl, and n-dioctyl phthalates. Smaller and/or more flexible diluents generally depress T_g more than the larger ones. In terms of application, however, low-molecular-mass plasticizers present some disadvantages, caused by their volatility and tendency for diffusion within the final product (and subsequent leaching), potentially posing environmental dangers. This fact has provoked the development of polymeric plasticizers, formed by polymers of low T_g and miscible with the base polymer [2], which provide materials with longer service times. A typical example is PVC plasticized with acrylonitrile butadiene rubber or copolymers of ethylene vinyl acetate [165].

1.3.2.4 Filler Effects

Several properties, such as the thermal stability, mechanical strength, or electrical conductivity of a polymeric material, can also be regulated by incorporating microscopic or nanoscopic inorganic fillers. Particulate systems typically involve polymers with finely dispersed clays, alumina, silica, silver or gold nanoparticles, carbon blacks, carbon nanofibers, and single-wall or multiwall carbon nanotubes [166]. The level of adjustment in the properties of the host matrix is determined by a number of factors, including the nature, size, amount (load), and surface chemistry of the filler, as well as the level of interaction between the components. In a number of studies [166,167], a loosened molecular packing of the polymer chains in the presence of the nanoparticles results in enhanced molecular mobility and a lower T_g for the composite. In contrast, wetted nanoparticle interfaces experiencing strong attractive interactions (as a rule, hydrogen bonding) with the polymer bring about moderate-to-strong upshifts in the glass-transition temperature [168]. The presence of a rigid amorphous polymer fraction around the nanoparticles has been well documented [39,169,170]. Calorimetric and dielectric results from different filler–polymer combinations suggest that the constraint in segmental mobilities does not extend throughout the material but affects only an interfacial layer with a thickness of a few nanometers. In some cases, this interfacial layer has been identified as totally immobilized [169], while in others, an additional glass transition emerges as a separate signal at higher temperature, or as shoulder at the high-temperature flank of the relaxation peak (e.g., in poly(dimethyl siloxane) + SiO_2 nanocomposites [171]). Interparticle spacing efficiently modulates the apparent glass-transition temperature of the nanocomposite [172–174], with different shifts recorded even in the same particulate system depending on the state of dispersion. This is clearly illustrated in the current thermograms of natural rubber–silica nanocomposites (Figure 1.11), where finely dispersed silica produces a small systematic increase of T_g compared to the neat rubber, while no change or a marginal decrease is observed for aggregated silica nanoparticles [175].

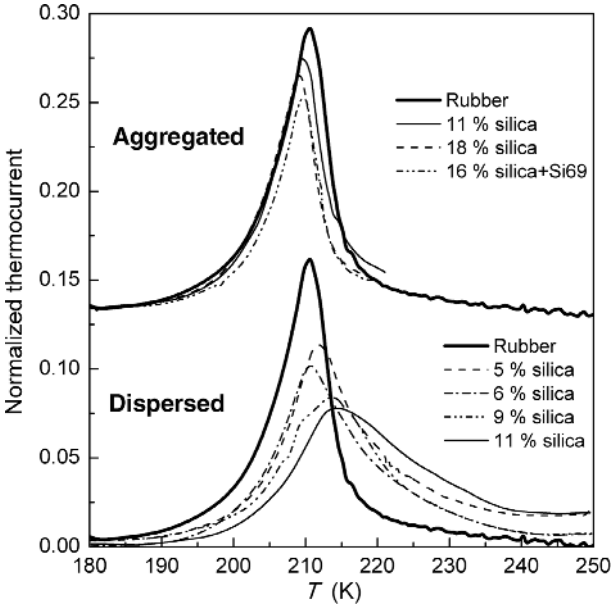

Figure 1.11 Normalized TSC spectra of natural rubber-silica nanocomposites, in the temperate range of the glass transition of the polymer matrix. For clarity, the group of spectra referring to systems with aggregated silica nanoparticles is vertically upshifted. After ref. [175], with permission © 2011 Elsevier.

1.3.2.5 Cross-linker Effects

Cross-linking of neighboring chains can be performed in a number of ways. The widely used "normal" cross-links involve strong covalent bonding of the polymer chains together into one molecule, while the weaker "reversible" cross-links found, for example, in several thermoplastic elastomers, rely on noncovalent or secondary interactions (typically hydrogen bonding and ionic bonding, respectively) between neighboring polymer chains. The stabilizing action of noncrystalline (e.g., in styrene-butadiene block copolymers) or crystalline (e.g., in thermoplastic copolyesters) domains within a composite material also provides a type of "physical" cross-linking. When normal cross-links are present, with an increasing cross-link density of the material the glass-transition temperature increases (and ΔC_p decreases) since the segmental mobility becomes progressively hindered to a higher degree. The effect of cross-linking on T_g bears some analogies to that imposed by an increase in molecular mass. Typically, the introduction of cross-links into a polymer is accomplished by the addition of a cross-linking agent, which can be regarded as a comonomer. The copolymer effect and the effect of cross-linking itself were combined by Fox and Loshaek [176] into the form of the equation

$$T_g = T_g^{\infty} - \frac{K}{M_n} + \frac{K^*}{M_c}, \tag{1.35}$$

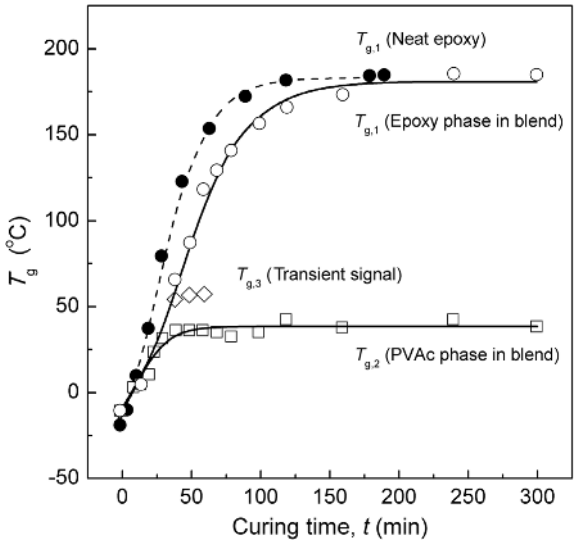

Figure 1.12 Glass-transition temperatures versus curing time for immiscible PVAc + epoxy resin blends, cured at 180 °C: (●) $w_{PVAc} = 0$ (neat epoxy resin), (○, ◇, □) blend with $w_{PVAc} = 0.05$. Phase separation after the first ~30 min of curing is evident from the appearance of multiple T_gs and the opacity in the blends. After ref. [180], with permission © 2007 John Wiley & Sons.

in which K^* is a constant and M_c is the number-average molar mass of the chains between cross-links, a parameter inversely proportional to the number of cross-links per gram of material [148]. Cross-linking is a rather common route for the preparation of molecular structures intended for applications where strength and rigidity are important. In thermosetting polymers, for example, a prepolymer in a soft solid or viscous state changes irreversibly into an infusible, insoluble polymer network by a chemical reaction known as "curing." The degree of cure (α_c), also known as fractional conversion, is a key parameter in determining the end-use properties (stiffness, creep, etc.) of the material. The glass-transition temperature is highly sensitive to the degree of cure: its value increases significantly as the curing reaction proceeds to completion (Figure 1.12), due to the progressive establishment of a three-dimensional network of bonds. Several theoretical approaches to modeling the T_g versus conversion relationship during isothermal cure have been proposed for thermosetting materials [177–179]. For example, based on thermodynamic considerations, Venditti and Gillham [179] suggested the relation

$$\ln(T_g) = \frac{(1-\alpha_c)\ln(T_{g,0}) + \lambda\alpha_c \ln(T_{g,\infty})}{(1-\alpha_c) + \lambda\alpha_c}, \tag{1.36}$$

where $T_{g,0}$ and $T_{g,\infty}$ are the glass-transition temperatures of the uncured mixture ($\alpha_c = 0$) and the fully cured network, respectively, and $\lambda = \Delta C_{p,\infty}/\Delta C_{p,0}$ ($\Delta C_{p,0}$ and $\Delta C_{p,\infty}$ are the heat capacities of the uncured monomer mixture and the fully cured network, respectively).

1.3.2.6 Geometric Confinement Effects

Parallel to sophisticated model simulations, the glass-transition dynamics and the characteristic transition temperature of nanoscopically confined glass-forming materials have been intensively studied with the purpose of elucidating the characteristic length scale of cooperativity experimentally [181]. A strong body of scientific literature [182] has been accumulated for a number of systems, including – but not limited to – amorphous layers confined between neighboring crystal lamellae [181], polymers in clay galleries, intercalated or exfoliated clay-polymer hybrid systems [183], colloidal systems, micro/nanoemulsions, ultrathin films, multilayers, organic glass formers within controlled pore inorganic glasses, as well as binary systems (e.g., filler + polymer, diluent + polymer, and binary polymer blends [184–186]) and copolymers [187]. Of particular merit appear to be studies on the behavior of organic liquids and polymers confined in nanopores and of polymers in the form of thin films, for which striking changes are often recorded for confining dimensions below 10 nm in porous environments, and for even higher thicknesses in free-standing polymer film geometries [181,188,189]. Excellent reviews on the topic [181,182,189,190] clearly demonstrate that we are far from having achieved a final, complete, and self-consistent, picture for the behavior of glass-forming materials in confined states. Confinement-induced perturbations of the molecular relaxation dynamics and the apparent glass-transition signal, usually quantified by the shift of the transition temperature ($\Delta T_g^* \equiv T_g^{conf.} - T_g^{bulk}$) and changes in the relative strength and breadth of the respective transitions, clearly demonstrate remarkable, irregular, and often contradictory dependences on the surface chemistry of the confining system (i.e., the interfacial energy controlled by the nature of the repulsive/soft or attractive/rough surfaces), compositional, and structural characteristics of the confined phase (e.g., polarity, molecular mass, chain conformation/stereoregularity, steric hindrance, and fragility), and the topology (fractality, porosity) or degree of confinement [182,189,190]. Attempts to unify interpretations and resolve pending questions stumble on the diversity of features which real systems demonstrate (depending, among other parameters, on the type and strength of interactions between the components), and to a lower degree on conflicting results that arise from intrinsic differences between the experimental techniques employed (e.g., wide variations in sensitivity and length scale of the probe) or even subtle variations in thermal histories and sample pretreatments [182]. A matter of intense research debate, consonant with the intriguing nature of the glass-transition phenomenon and the diversity of factors controlling it, constitutes reports of different trends in the variation of the transition temperature (ΔT_g^*) with changes in the confining length obtained using different experimental techniques for nearly identical systems [189,191]. Inconclusive arguments also appear with respect to the potential influence of the molar mass of the confined polymer on the type and strength of the ΔT_g^* variation [189].

Since Jackson and McKenna [192] first observed the depression of the glass-transition temperature of organic liquids (of *ortho*-terphenyl and benzyl alcohol)

into the pores of a controlled pore glass, a number of studies on hydrogen bonded glass formers have demonstrated the glass-transition temperature to decrease [189,190], remain unchanged, or even increase with increasing confinement. This complex behavior is in part related to the interplay among *surface effects* (e.g., strong hydrogen-bonding interactions between the confined molecules and the natural (uncoated) pores) and the intrinsic or *confinement effect* (e.g., breakdown of the cooperative motion, which translates into a change in the cooperativity length scale). Hydrogen-bonded liquids confined in silanized nanopores generally display accelerated relaxation dynamics, a broadening of the relaxation function, and lower glass-transition temperatures compared to those recorded in the bulk or when confined in unsilanized pores. Matrices with hydrophilic (hard) surfaces have been found to produce diverse responses, beyond the abovementioned rather typical trend. Examples provide the bulk-like behavior observed for salol in unsilanized MCM-41 nanoporous glass [193], and the elevation of the glass-transition temperature – in selected confining dimensions only – of glycerol, ethylene glycol, and oligomeric propylene glycol in unsilanized nanoporous glasses [193,194].

The majority of published results on thin polymer films suggest that the dynamics of thin polymer layers with free surfaces (free-standing films) or in contact with repulsive/soft surfaces (softly supported films) are governed by entropic effects, including chain-end segregation, density anomalies, and disentanglement. The different energetic states of the molecules located on the free surface and in the internal (bulk) regions of any material, and in particular the existence of an enhanced mobility layer at the free surface of polymers, remain a subject of intense debate [195]. The diversity of results obtained in several investigations of ultrathin or multilayer films, binary polymer blends [186], and other systems is compounded by the fact that different length scales (or extends of cooperativity) are impacted by confinement differently [196]. Several results support the idea of Keddie *et al.* [197] that a sufficiently thin liquid-like layer adjacent to the free surface exists, with reduced T_g due to the reduced requirements for cooperative segmental mobility. de Gennes [198] has further suggested a "sliding-motions" mechanism for propagating the mobility of the near-surface segments to depths comparable to the overall size of the polymer molecules. The perturbations caused by the surface layer are thus allowed to propagate some tens of nanometers into the film interior, usually resulting in a strong reduction in T_g with decreasing film thickness (D). This variation can be described by the relation

$$T_g(D) = \frac{D(2k + D)}{(\xi + D)^2} T_g(\infty), \tag{1.37}$$

where $T_g(\infty)$ denotes the thickness-independent value determined in sufficiently thick samples, and k and ξ are model-specific constants [199]. For $2k = \xi$, Eq. (1.37) reduces to a Michaelis–Menten-type function $[T_g(D) = T_g(\infty)/(1 + \xi/D)]$, which provides a satisfactory description of several experimental dependences. In contrast, strong enthalpic forces in the vicinity of the polymer–substrate interface (e.g., hydrogen bonds between films of PMMA, poly(2-vinyl pyridine) [P2VP], or

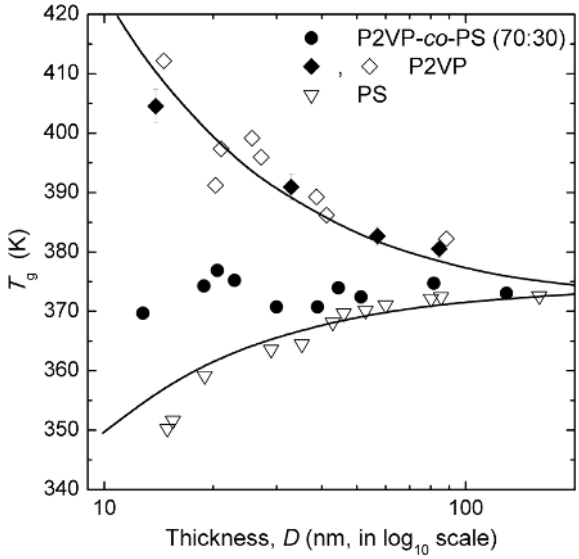

Figure 1.13 Measured and fitted glass-transition temperatures against film thickness for thin films of P2VP, PS, and poly(2-vinyl pyridine)-*co*-polystyrene (70:30), on Si substrates. Strong interaction among P2VP and the substrate is evident. Lines are data fits to Eq. (1.37). After ref. [199], with permission © 2004 Elsevier.

PVAc and native SiO_2 substrates) lead to a partial immobilization of polymer chains segments. In such cases, the local increase of the glass-transition temperature [189] is likely to produce positive values for ΔT_g^*. Reports indicate that the thickness dependence of the effective T_g of polymer blend [184,185] and copolymer [199] films (Figure 1.13) is intermediate to that recorded for neat component thin films. Data collected for miscible PS + poly(2,6-dimethyl-1,4-phenylene oxide) (PPO) [184] and PS + tetramethyl polycarbonate (TMPC) [185] mixtures on SiO_x/Si substrates manifest a strong dependence of the sign and magnitude of ΔT_g^* from blend composition. Accordingly, the increasingly positive ΔT_g^* with decreasing film thickness observed for neat TMPC gradually transforms to a negative $\Delta T_g^*(D)$ pattern, which becomes stronger as the PS content increases in the blend [185].

When a particular polymer structure is considered, and with the assumption of only marginal confinement-induced changes in its tacticity and degree of polymerization, there are strong indications for the existence of a principal underlying mechanism that operates similarly in all different types or topologies of confinement. A paradigm offers the similarities (notably observations of $\Delta T_g^* > 0$) observed in the behavior of atactic or predominantly syndiotactic PMMAs under different conditions of geometric restriction: for example, polymer in the form of supported ultrathin films (on an unsilanized/attractive SiO_2 surface) [200], polymerized *in situ* 5-nm-diameter gel-silica glass nanopores [188]

or in hydrophobic and hydrophilic 13-nm-diameter controlled pore glasses [201], containing finely dispersed SiO_2 [202] or metal (Ce, Co) nanoparticles [203], restricted between layers of organophilic montmorillonite [204], or loaded with organic bentonite [205].

1.4 Experimental Means of Determination

For a number of methods and experimental techniques, the temperature variation of different thermodynamic, physical, mechanical, or electrical properties of a material provides the means for identifying the glass transition and other transitions. From rheometry emerges the time-honored definition of T_g as the temperature at which the viscosity of the internally equilibrated supercooled liquid reaches the value of 10^{12} Pa s. Electron spin resonance (ESR) and nuclear magnetic resonance (NMR) spectroscopies permit the observation of glass transformations and T_g determinations from changes in molecular mobility (Figure 1.14 [206]). Fourier transform infrared (FTIR) and Raman spectroscopies monitor changes in molecular bonding, occurring within the temperature range of the phenomenon. Sensitive determinations of thickness-dependent glass transitions in thin homopolymer or polymer blend films are

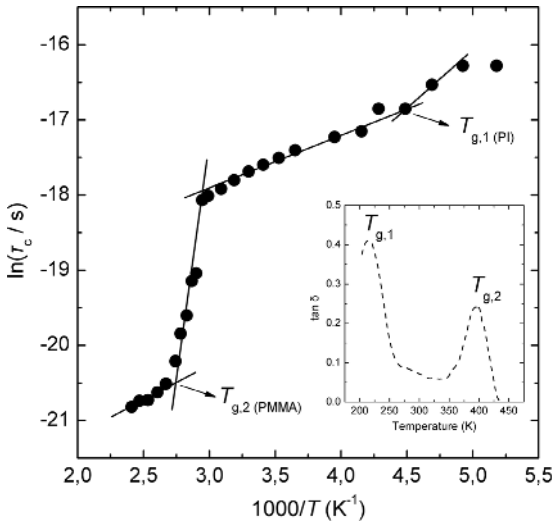

Figure 1.14 Glass transitions and ESR: Arrhenius plots of nitroxide radical (probe) rotational correlation times and loss tangent spectrum (inset) of an immiscible semi-interpenetrating polymer network based on PI and PMMA ($w_1/w_2 = 1$; 4% dicumyl peroxide, PI cross-linker). Three crossover points, the extreme ones associated with the glass transition temperatures of PI and PMMA and the intermediate related to a secondary relaxation, are indicated. The dynamic mechanical spectrum (tan δ versus T plot) is included for comparison. Compiled from plots appearing in ref. [206], with permission © 2010 Elsevier.

frequently accomplished using ellipsometry [207], X-ray or neutron reflectivity, fluorescence spectroscopy [208], Brillouin light scattering [209], and PALS [210]. The latter techniques are all sensitive to properties related to the change in polymer density at T_g. Significant results can also be extracted by combining microscopy with thermal analysis techniques (e.g., local thermal analysis [211]).

Modern thermal analysis comprises a number of sophisticated techniques, particularly efficient in performing – among other characterizations – a quantitative description of several types of thermal events and of their dependence on molecular architecture, chemical composition, or processing details. Studies devoted to glass-transition phenomena in polymer-based systems constitute an important area of related experimentation [5,17,106,107,212,213]. Nevertheless, the variability of measuring approaches and probes, the multitude of operational definitions for the glass-transition temperature, and the interrelated temperature change rate and oscillating frequency dependences of the respective signals (Table 1.3) continue to create sources of misconception in relevant

Table 1.3 Characteristics of routine thermoanalytical techniques used in studies of glass-transition phenomena in polymer-based materials.

Technique[a)]	Property measured	Operational definitions of T_g	Resolution, sensitivity
DTA	Temperature difference	Onset, midpoint, or endpoint of step change in ΔT versus T plots[b)]	Low to moderate
DSC/ MTDSC	Heat flow (differential heat flow, heat capacity)	Onset or midpoint of step change in C_p versus T plots; peak maximum in the derivative of the (reversing) heat flow versus T plots[b)]	Moderate/ high
TMA/ MTTMA	Dimension changes (thermal expansion coefficients) or softening	Point of intersection of the glassy and rubbery expansion versus T curves[b)]	Moderate/ high
DMA	Viscoelastic properties (mechanical strength, energy loss)	Temperature of the α-relaxation peak in loss modulus (E'') or damping factor ($\tan\delta$) versus T plots.[c)] Onset temperature of the storage modulus (E') drop at the transition[c)]	High
DEA	Dielectric properties and electrical relaxation (permittivity, dielectric loss, polarization change rate)	Temperature of the α-relaxation peak in loss factor (ε'') or loss tangent ($\tan\delta$) versus T plots.[c)] Onset temperature of the real part of relative permittivity (ε') rise at the transition.[c)] Temperature of the α-peak in depolarization current versus T plots[b)]	Moderate to high

a) DTA = Differential thermal analysis, TMA = Thermomechanical analysis, DMA = Dynamic mechanical analysis, DEA = Dielectric analysis.
b) Temperature change rate dependent.
c) Oscillation frequency dependent.

determinations or data comparisons. In the following sections, theoretical concepts and experimental aspects of thermal analysis techniques, emphasizing in problems encountered in glass-transition determinations in polymer blends, will be briefly presented.

1.4.1 Calorimetric Techniques

The science of calorimetry is associated with determinations of the changes in the energy of a system by measuring the heat exchanged with its surroundings in the course of physical phenomena or chemical reactions. Although somewhat dated, differential thermal analysis (DTA) is still used for heat exchange measurements, phase diagram determinations, and thermal decomposition recordings in various atmospheres of materials used in mineralogical research, environmental sciences, as well as in pharmaceutical and food industries. In the course of a typical DTA experiment, the difference in temperature between a substance (the "sample") and a reference material (a thermally inactive material, such as Al_2O_3), both placed in the same furnace and in a specified atmosphere, is monitored against time or temperature, while the temperature of the reference (T_r) and the sample (T_s) is subjected to identical linear heating cycles. The differential temperature ($\Delta T = T_s - T_r$) is plotted against program temperature (or time), providing the DTA curve. Changes in the sample, either exothermic or endothermic, can thus be detected relative to the inert reference material providing data on the transformations (e.g., glass transitions, crystallization, melting, sublimation, oxidation, and thermal degradation) that have occurred [17,214]. The DTA curve is often treated only as a *fingerprint* for identification purposes (i.e., determination of characteristic temperatures alone); quantitative results are produced only when calibration with a standard material is performed, allowing for the quantifiable conversion of ΔT to heat flow and, eventually, to heat of transition (ΔH) or the constant pressure heat capacity. Except for some high-temperature applications, in recent years DTA has been largely displaced in the field of polymer science by the more sophisticated analytical technique of DSC. In DSC, the heat flow rate difference into a substance and a reference material is measured as a function of temperature while both are subjected to a controlled temperature program. The "apparent" heat capacity of the substance, C_{app}, is related to the differential heat flow and the heating rate through the relation $dQ/dt = C_{app} \cdot (dT/dt)$, assuming that the weights of the sample and reference pans are identical. The term "apparent" is implemented here because C_{app} comprises the true heat capacity of the sample along with kinetic (time-dependent) contributions from various physical or chemical processes.

The typical DSC plots of heat flow as a function of temperature usually reveal a series of thermal effects, and the actual temperature (or temperature range) at which each thermal event appears is primarily determined by the polymer's structure. With reference to Figure 1.15, and starting from the lowest temperature onward, the first discontinuity usually observed signifies the glass transition; this appears as a rounded step or a shift of the base line, corresponding to the

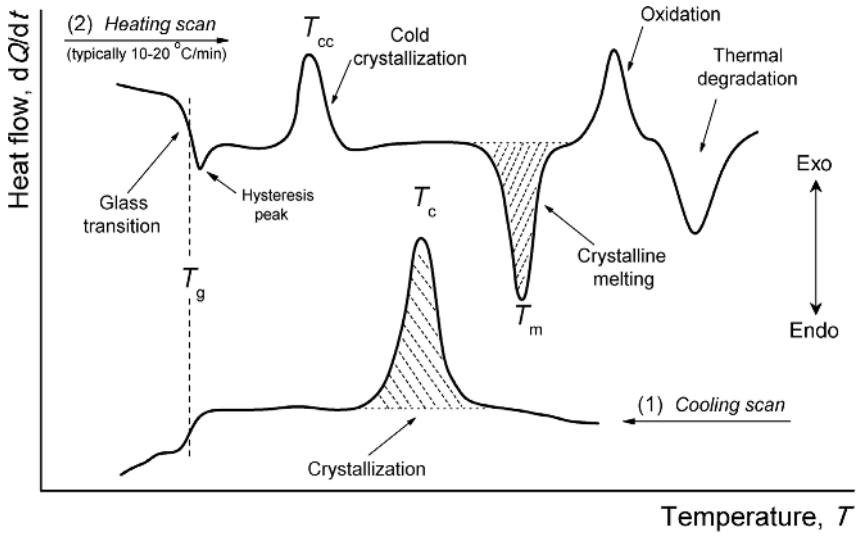

Figure 1.15 Schematic cooling (1) and heating (2) DSC curves showing a range of different transitions (glass transition, crystallization, melting) and reactions (oxidation, thermal degradation) of a typical polymer. A hysteresis peak appears in the high-temperature side of the glass transition. Possible signals from mesophase transitions (e.g., transitions between the crystalline, smectic, nematic, or isotropic phases) in polymorphic materials (liquid-crystalline polymers) are not considered here.

heat capacity difference (ΔC_p) of the sample before and after the transition. Such a step does not occur for local or normal mode relaxation processes because of the missing contribution from entropy fluctuation. Enthalpy relaxation is typically evidenced by an endothermic hysteresis peak in the high-temperature side of the glass transition, with a magnitude that strongly depends on the thermal history of the material; under some circumstances, it may even make the glass transition appear to be a melting transition (a problem particularly intense in DSC analyses of polymer blends). A controversial and rather weak liquid–liquid transition (at T_{LL}, with $T_{LL}/T_g \approx 1.1$–1.2 [215]), related to increased chain mobility and segment–segment associations, may also be present. As temperature increases, there may be a cold crystallization peak (at T_{cc}, exothermic), followed by a crystalline melting peak (T_m, endothermic). The intensity of the cold crystallization peak depends on the sample's history and ability to crystallize in the timescale of the experiment. In the course of heating, oxidation reactions (and even oxidation degradation) may appear if the experiments are not performed in inert atmosphere, in addition to thermal events related to curing chemical reactions (e.g., in elastomer formulations or thermosets). At much higher temperatures, the polymer undergoes thermal degradation, resulting in main-chain scission, cross-linking, cyclization, or loss of volatile fragments. In an inert atmosphere, the degradation pattern may be endothermic, exothermic, or both, whereas in oxygen or air, it is always exothermic.

The DSC peak area provides quantitative calorimetric information for each thermal event. The curve can be used to calculate heats (enthalpies) of transitions or reactions by integrating the peak corresponding to a given transition (e.g., the crystalline melting peak in curve 2 of Figure 1.15). There is no such heat of transition at the glass transition, since only first-order transitions have a heat of transition. The heat capacity change at the glass transition is a characteristic constant number for a given amorphous polymer. An empirical rule proposed for amorphous polymers – often called Wunderlich's rule – suggests that ΔC_p at the glass transition is around 11 J/°C·mol per mobile unit of the polymer main chain in the case of relatively small units, while for larger mobile units (such as the phenylene rings) ΔC_p may be double or triple this value [156]. It should be noted, however, that ΔC_p is strongly influenced by crystallinity and the so-called RAF in semicrystalline polymers. Detection of the temperature interval where vitrification modifies thermodynamic parameters and measurement of T_g and ΔC_p provides the most important results of a DSC scan on an amorphous or partially crystalline polymeric material. It has been suggested [212] that T_g should be measured during sample cooling, rather than in the subsequent heating run, from the intersection of the extrapolated equilibrium glass and liquid lines obtained in the enthalpy versus temperature graph. Since the sample exists in thermal equilibrium at the start of the measurement, enthalpy relaxation that often complicates T_g measurements is avoided. Instrumental drawbacks, such as poor control of the cooling rates in some differential scanning calorimeters and difficulties in performing calibration on cooling, preclude the general use of cooling curves for determining T_g. Therefore, when the glass-transition temperature is to be obtained by progressive heating of a cooled sample, and in order to minimize enthalpy relaxation effects, a cooling rate somewhat faster than that of the subsequent heating rate is recommended. A high heating rate is beneficial in detecting T_g, because the heat flow signal associated with the transition enhances, with very little corresponding increase in noise, thereby increasing resolution. Such a change produces a shift of T_g, due to a combination of thermal gradient and kinetic effects, in addition to a broadening of the transition range. In view of the above facts, and for comparison purposes, the heating and cooling rates, the breadth of the transition signal and the methodology used to extract the glass-transition temperature from the curve need to be reported along with its estimate.

Difficulties in DSC determinations of the glass-transition temperature of semicrystalline polymers or polymer blends are common since the transition can be very broad and smeared out. In such cases, derivative curves (e.g., dC_p/dT versus T plots) become useful as the heat capacity change is replaced by a more visible peak. Several methods are available for marking the "exact" location of the glass-transition temperature in a typical heating DSC curve. Figure 1.16a demonstrates five characteristic temperatures that are frequently cited throughout the literature as T_g, often without mention of the specific location actually picked. These are (1) T_b, the "onset" temperature (usually difficult to determine), which defines the point at which the first deviation from the base line on the low-temperature side is

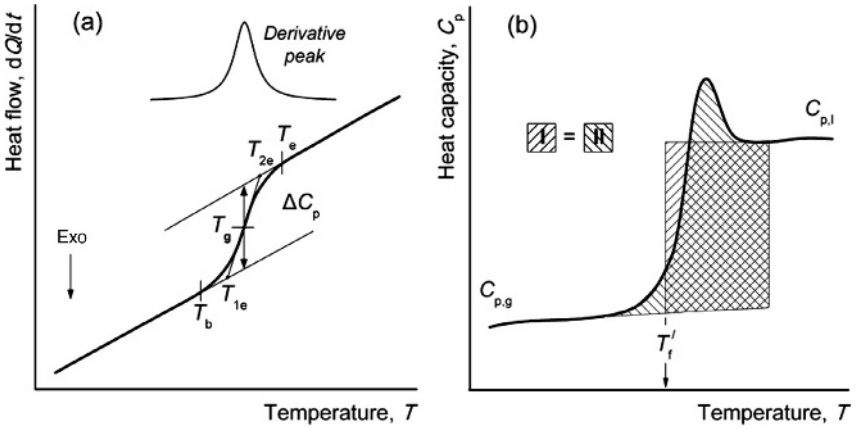

Figure 1.16 Determination of the glass-transition temperature from a heating DSC scan: (a) various T_g estimates from an idealized dQ/dt versus T curve. The height of the marker (double arrow) is proportional to ΔC_p at the glass transition. (b) Graphical representation of the procedure used to determine the limiting fictive temperature from C_p heating data. The shaded areas I and II correspond, respectively, to the left and right integrals appearing in Eq. (1.38).

observed; (2) T_{1e}, the frequently reported extrapolated onset temperature (reproducible), which is the temperature at the intersection of the extrapolated base line and the tangent taken at the point of maximum slope; (3) T_g, the temperature at the half-height of the heat capacity increase (highest reproducibility; preferred point), also called the "temperature of half-unfreezing," which is very close to the temperature at the inflection point (temperature peak in the first derivative of the C_p versus T graph); (4) T_{2e}, the extrapolated "end" temperature of the glass transition; and finally, (5) T_e, the end temperature of the glass transition, where the heat capacity dependence becomes linear again. T_{1e} is very close to the fictive temperature, T_f, which characterizes the glass. Tool [28] defined the T_f of a material in a nonequilibrium (glassy) state as the actual temperature of the same material in the equilibrium (liquid) state whose structure is similar to that of the nonequilibrium state. In that respect, the fictive temperature corresponds to the temperature at which a property of interest (enthalpy, specific volume, refractive index, logarithm of shear viscosity, etc.) when extrapolated along the glass line intersects the equilibrium liquid line [216]. The important limiting value of the fictive temperature, T_f', is obtained if the extrapolation is performed from a point deep in the glassy state after cooling at a given rate. Both T_f' (measured on heating) and T_g (measured on cooling) depend only on the cooling rate, with experimental evidence supporting their close proximity [217]. A convenient way to measure T_f' is through the area matching method from Moynihan *et al.* [216] (Figure 1.16b),

$$\int_{T_f'}^{T \gg T_g} \left(C_{p,l} - C_{p,g}\right) dT = \int_{T \ll T_g}^{T \gg T_g} \left(C_p - C_{p,g}\right) dT. \tag{1.38}$$

As indicated by Chartoff and Sircar [17], for amorphous thermoplastic polymers it is technically more significant to use the temperature at the extrapolated onset, T_{1e} ($\approx T'_f$) as the glass-transition temperature, since T_{1e} defines the initial temperature for the loss of structural properties (e.g., modulus) as the polymer softens through the glass transformation range. Therefore, T_{1e} defines both a low-temperature limit for the processing of amorphous thermoplastic polymers and an upper-use temperature. In the case of elastomers, the temperature for useful elastomeric properties lies above the glass-transition region, that is, at $T > T_e$. If the elastomer is cooled beyond T_e, it enters the glass-transition region and starts losing its elasticity, becoming progressively stiffer as the temperature decreases.

Modulated-temperature DSC (MTDSC) [218] is an important advancement of DSC. In MTDSC, the same heat-flux DSC cell arrangement is employed, but with a nonlinear heating profile applied across the sample and reference material. The heating profile results from the sinusoidal modulation (oscillation) overlaid on the traditional linear ramp, that is, temperature changes in the form

$$T(t) = T_0 + qt + A_T \sin(\omega t), \tag{1.39}$$

where T_0 is the starting temperature, q is the linear heating rate, and A_T is the amplitude of temperature modulation. The instantaneous heat flow in a modulated DSC experiment can be written as

$$\frac{dQ}{dt} = C_p(q + A_T\omega \cos \omega t) + f'(t, T) + A_k \sin \omega t, \tag{1.40}$$

where the term $q + A_T\omega \cos \omega t$ is the measured heating rate, $f(t, T)$ is the kinetic response without temperature modulation, and A_k is the amplitude of kinetic response to temperature modulation. Using Fourier's transformation analysis, the complex heat flow signal can be separated into reversing heat-capacity-related effects, which are in-phase with the temperature changes (such as glass transitions and crystalline melting), and nonreversing effects that are out of phase with the changes in temperature (e.g., cold crystallization, enthalpic relaxation, oxidation, evaporation, and thermal decomposition). Heat capacity can be calculated from the ratio of modulated heat flow amplitude to the product of amplitude of modulation temperature and frequency, while the reversing heat flow is determined by multiplying the heat capacity with average heating rate. Preference to MTDSC is supported by its ability to measure heat capacity in a simple run with increased sensitivity (five times greater than that of conventional DSC), its higher resolution (due to the very low underlying heating rate), and unique ability to separate overlapping thermal effects (due to the superimposed modulated heating profile). Examples provide the multiple glass transitions of nanoheterogeneous amorphous phases created in PEO + PMMA blends [219]. The efficacy of MTDSC to extract glass transitions masked by the rapid cold crystallization occurring in the same temperature range is also extremely useful in miscibility evaluations of polymer blends. Figure 1.17 shows, as an example, the total heat flow profile of a PET + acrylonitrile/butadiene/styrene (ABS) blend, and its separation into reversing and

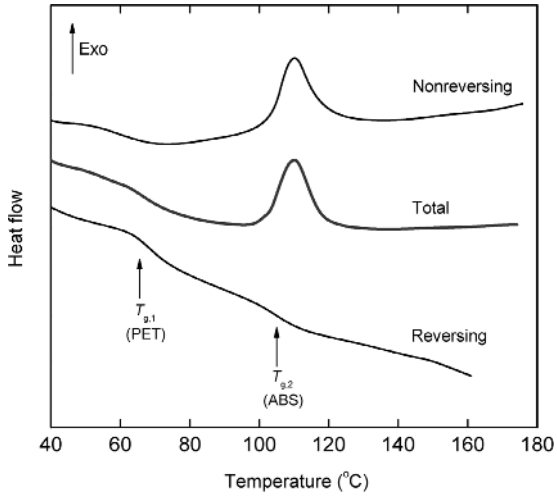

Figure 1.17 Total, reversing and nonreversing heart flow curves of an immiscible PET + ABS blend composition. Adapted and replotted from ref. [220].

nonreversing components [220]. Complete phase separation is evidenced by the existence of two well-separated glass-transition steps that appear in the curve of the reversing component of heat flow and are located within the region of the glass-transition temperatures of the constituting polymers ($T_g \approx 65\,°C$ for PET and $\approx 105\,°C$ in the case of ABS). The crystallization of PET is indicated by an exothermic peak in the nonreversing heat flow curve; the fact that the glass-transition signal of ABS is submerged in the low-temperature flang of the crystallization peak precludes its detection in a conventional DSC experiment.

1.4.2
Thermomechanical Analysis (TMA)

Thermomechanical analysis (TMA) is an established thermoanalytical technique based on the measurement of changes in sample length (L) or volume (V) as a function of temperature or time, under load at an atmospheric pressure. The technique is also referred as thermodilatometry (TD) if dimensions are measured with negligible force acting on the testing material while it is subjected to a controlled temperature program. Thermomechanical studies are usually performed under static load with a variety of probes for measuring dimensional changes in expansion/compression, penetration, tension, flexure, or shear test modes [106]. By applying special modes and different attachments, stress relaxation, creep, parallel-plate rheometry, and volume dilatometry measurements are also feasible. Polymeric materials are usually studied in the form of rigid or nearly rigid solids, or in the liquid (melt) state using special accessories. These can also be used to measure the volume changes in irregularly shaped samples or powders submerged in an inert liquid (e.g., in mercury dilatometers). The basic physical

quantities utilized in TMA is *stress*, σ, which is defined as the force applied per unit area of the material, $\sigma = F/A$, with A denoting sample's cross-sectional area, and the deformation per unit dimension caused by the applied stress and measured by the *strain*, ε. For a simple tensile experiment, strain is defined as $\varepsilon = \Delta L/L$, where ΔL is the change in length and L is the original length. When subjected to a mechanical force, materials may behave in a variety of ways. A brittle material will deform reversibly to a small amount and then fracture, while a ductile material also deforms reversibly up to a certain amount and then yield and flow under the applied force until it begins to harden under load and then fail. Up to the elastic limit, the material will return to its former shape and size when the force is removed. The slope of this linear region corresponds to Young's modulus, E, also known as *elastic modulus*, *tensile modulus*, or simply *modulus*, defined as

$$E = \frac{\sigma}{\varepsilon} = \frac{L}{A}\left(\frac{\Delta F}{\Delta L}\right)_T, \tag{1.41}$$

with $\Delta F/A$ representing the change in stress and $\Delta L/L$ the change in strain. The magnitude of E is a measure of material stiffness.

The identification of glass-transition signals in polymer-based systems (in filled, crystalline, or cross-linked materials particularly) has evolved into a routine application of TMA. The measurement of T_g is achievable with a single experiment and from the same data used to determine the linear isobaric expansivity, also known as the coefficient of linear thermal expansion (α_L),

$$\alpha_L = \frac{1}{L}\left(\frac{\Delta L}{\Delta T}\right)_p \tag{1.42}$$

or the (volumetric) coefficient of thermal expansion α ($\alpha = 3\alpha_L$ for isotropic materials). The schematic curves of expansion and penetration TMA runs are shown in Figure 1.18. During expansion measurements of amorphous and semicrystalline polymers that are not oriented, a sudden increase in expansion rate is observed above T_g, as the material shifts from a structural configuration of limited or no chain mobility to an increased chain mobility state. The point of intersection, seen as an inflection or bend, of the glassy and rubbery linear or volume expansion curves typically defines the glass-transition temperature. Note, however, that a somewhat different T_g value is seen for each mode of testing, as they each measure a different effect. The change in the slope of the expansion curves below and above T_g is related to the expansion of free volume, since the actual volume of the molecules (the hardcore or incompressible volume, corresponding to zero thermodynamic temperature or extremely high pressure) does not change appreciably around T_g. In the case of semicrystalline systems only, a further increase in temperature may result in the penetration of the probe into the sample, even with a negligible load on it. This abrupt decrease in the probe position (onset temperature), as illustrated in Figure 1.18, can in most cases be assigned to crystal melting, and the temperature of the break on the curve represents the melting point.

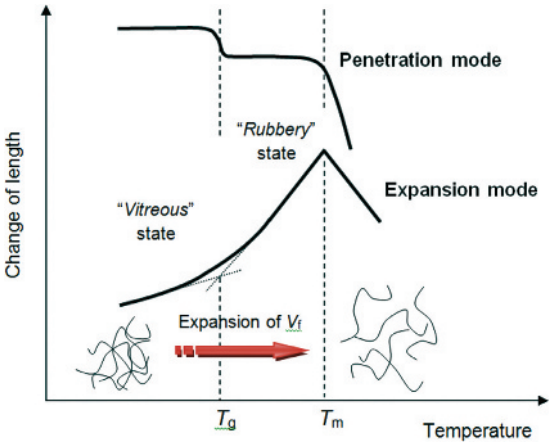

Figure 1.18 Schematic representation of TMA curves for a semicrystalline specimen in expansion or penetration-mode experiments. In the first testing mode, the coefficient of thermal expansion can be determined in certain temperature ranges in the linear parts of the $L-T$ or $V-T$ graph, using Eq. (1.42) for α_L, and Eq. (1.2c) for α, respectively.

Ideally, linear thermal expansion and subsequent contraction of a specimen to its original dimensions are totally reversible phenomena. Nonetheless, if the material softens as it is heated while subjected to a mechanical load it will flow and creep, resulting in a nonreversible dimensional deformation. Moreover, if the material was stretched (oriented) when soft and then cooled before the experiment, residual stresses will remain in the sample (memory effects). Within the conditions of the thermomechanical experiment, stress relaxation on heating will cause irreversible morphological changes (i.e., randomization of the orientation achieved during manufacture) along with shrinkage of the testing material. The length changes typically measured by conventional TMA are thus a convolution of the above effects, unless the specimen is completely isotropic and measurements are made under zero loads. A separation of overlapping thermodynamic and kinetic, reversing and nonreversing, dimensional changes is achieved in modulated temperature TMA (MTTMA) experiments [106]. In this case, the dependent physical quantity measured is the length, with the sample exposed to a sinusoidal temperature modulation superimposed on a linear underlying heating, cooling, or isothermal profile, similar to MTDSC. The modulation conditions are different from MTDSC, since the sample and test fixture and enclosure are larger in the mechanical test, thus requiring longer equilibration (and scan) times.

Several studies demonstrate the usability of TMA as a complementary technique to DSC, DTA, or thermogravimetric analysis studies, in performing structural and thermal characterization of homogeneous polymer systems (e.g., mixtures of poly(vinyl phenyl ketone hydrogenated (PVPhKH) with poly(2-ethyl-2-oxazoline) or poly(styrene-*co*-4-vinylpyridine) (PS4VP) [221]), mixtures showing elevated structural heterogeneity at selected blend compositions (e.g.,

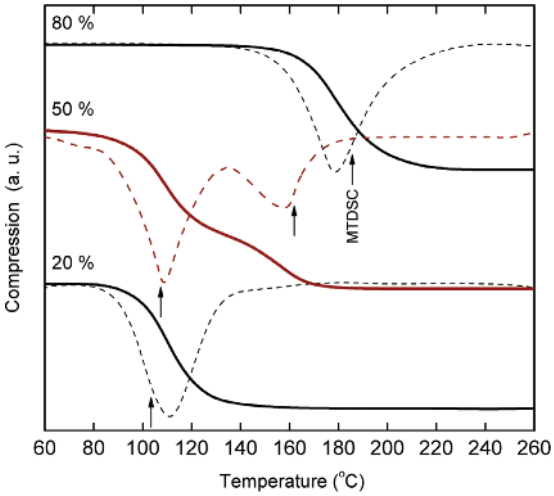

Figure 1.19 The (—) TMA curve and (– –) derivative curve of the sample thickness changes of PVPhKH + PPO blends with 20, 50, and 80 wt. % PPO. Vertical arrows show the location of T_g as determined by MTDSC. Note the double glass-transition signal only in the intermediate blend composition. Replotted data from ref. [222], with permission © 2004 John Wiley & Sons.

PVPhKH + PPO blends, Figure 1.19 [222]), or phase-separated systems (polyurethane + PMMA, PVC + PMMA [223]).

1.4.3 Dynamic Mechanical Analysis (DMA)

There are three fundamental test methods for characterizing the viscoelastic behavior of polymers: stress relaxation, creep, and dynamic mechanical analysis (DMA) [15,107]. DMA methods, in particular, are most popular among thermal analysts for measuring mechanical properties and glass-transition-related relaxation modes, due to their high sensitivity, versatility, and increased resolution of overlapping mechanisms. Successful applications of DMA and related techniques for the study of polymeric solids and liquids are well documented [15,107], with particularly important results extracted in evaluations of orientation processes, of the effects of additives, and structural modifications or phase separation processes in composites. The relatively short measuring times (important when curing, aging, and crystallization processes are of interest), compared to those required in stress relaxation or creep experiments, and the wide range of information extracted for complex materials are noteworthy advantages of DMA.

In dynamic mechanical spectroscopy, one measures the mechanical properties of materials typically by imposing in a sinusoidal fashion a small strain (or, equivalently, stress) on a sample and measuring the resulting stress (strain) response as a function of temperature. For a perfectly elastic material (Hookean

solid), stress and strain are in phase. In an ideal liquid behavior (Newtonian fluid), however, instead of deforming reversibly under load the material will flow; the strain is now proportional to the rate of change of the stress. The phase angle difference of $\delta = 90°$ between sinusoidal stress and strain in liquids is the key for the use of DMA as a tool in the characterization of viscoelastic polymers. Since such materials have properties intermediate between those of an ideal solid and an ideal liquid, they will exhibit a phase lag (δ) somewhere between 0° (ideal solid) and 90° (ideal liquid). Along these lines, an application of a sinusoidal force (strain) to the testing material,

$$\varepsilon(t) = \varepsilon_{\max} \cdot \sin(\omega t), \tag{1.43a}$$

where ω denotes the angular frequency, produces a stress of the form

$$\sigma(t) = \sigma_{\max} \cdot \sin(\omega t + \delta). \tag{1.43b}$$

The relative amplitudes of stress and strain and the phase lag, which reflects the relative degree of viscous character to elastic character, can thus be obtained. DMA data are commonly reported using the complex modulus function

$$E^* = \frac{\sigma(t)}{\varepsilon(t)} = \frac{\sigma_{\max} e^{i(\omega t + \delta)}}{\varepsilon_{\max} e^{i\omega t}} = \left(\frac{\sigma_{\max}}{\varepsilon_{\max}}\right) e^{i\delta} = \frac{\sigma_{\max}}{\varepsilon_{\max}} (\cos(\delta) + i \sin(\delta)) = E' + iE''. \tag{1.44}$$

Its real component, E', is known as the *storage modulus* and is a measure of the elastic character or solid-like nature of the material. The imaginary part, E'', is known as the *loss modulus* and is a measure of the viscous character or liquid-like nature of the material. In a physical sense, the first is related to the stiffness of the material, and the latter reflects the damping capacity of the material. For an ideal elastic solid, E' is simply Young's modulus of the material and E'' is zero, while for an ideal viscous liquid E' is zero and the loss modulus is related to the viscosity of the material. The ratio of the loss modulus to the storage modulus is known as the *damping factor* or *loss tangent*, or, more commonly, as

$$\tan \delta = \frac{E''}{E'}. \tag{1.45}$$

Tan δ ranges from zero for an ideal elastic solid to infinity for an ideal liquid, and represents the ratio of energy dissipated to energy stored per cycle of deformation. Analogous definitions apply for the parameters used in tests under a shear mode of deformation (i.e., the complex shear modulus G^* and $\tan \delta = G''/G'$) and rheological measurements in polymer liquids [107].

The dynamic mechanical data obtained for polymer-based systems convey information on a broad range of relaxation processes, that goes from very local motions (secondary relaxations, generally due to branching chains or side chains) to segmental mobility exhibiting cooperativity (α-relaxation or dynamic glass transition), or even large-scale relaxation processes (Rouse dynamics or reptation) [224]. Thermal analysts usually perform a series of temperature scans at a constant oscillatory frequency, covering a narrow range of frequencies

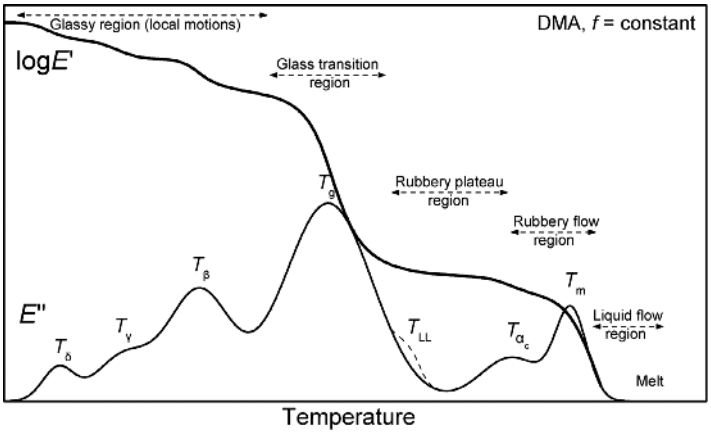

Figure 1.20 An idealized isochronal DMA scan of a partially crystalline polymer, showing the effect of various molecular relaxations on the storage modulus, E', and loss modulus, E'', curves. Peaks ascribed to the various transitions are indicated in the loss modulus spectrum.

(*isochronal* scans) (Figure 1.20). The mechanically active relaxation modes populate the spectrum in a number dependent on the complexity of the system and the magnitude of the temperature window. In amorphous polymers, for example, loss peaks at $T/T_g < 1$ are related to secondary relaxation processes. For semicrystalline polymers, one should also note the presence of the melting peak, and a secondary relaxation (α_c-peak) related to the slippage of the crystallites past each other. The liquid–liquid transition (at T_{LL}) may also be present within the rubbery plateau region.

Identifying the glass transition and how various system modifications affect T_g is a major application of DMA. The glass transition is generally easily detected from isochronal dynamic mechanical data because of the sharp decrease in storage modulus E' (or, equivalently, in shear storage modulus G'), and the corresponding loss dispersion in E'' (or in shear loss modulus G'') or $\tan\delta$, which peak at T_g. Either estimate is valid, but the values attained from each plot are different: the T_g value obtained from the $\tan\delta$ peak is several degrees higher than that from the peak in E'', as shown in Figure 1.21 for PVC [225]. The loss modulus peak more closely denotes the initial drop of E' from the glassy state into the transition. In this respect, the T_g value based on the E'' peak is generally close to the intersection of the two tangents to the log storage modulus curve originating from both the glassy region and the transition region, the so-called onset temperature; it is therefore regarded as the most appropriate value. For most linear amorphous polymers, the glass-transition region is relatively narrow (width < 20 °C) and thus the difference between the E'' and $\tan\delta$ peak temperature is of minor importance. There are cases, however (e.g., partially crystalline polymers, cross-linked thermosets, miscible polyblends, and heterophase polymers), where the transition region is very broad (50–60 °C) and none of the two

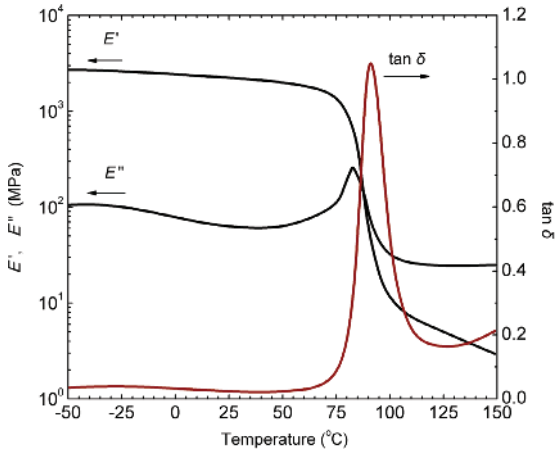

Figure 1.21 Temperature dependence of the storage modulus E', loss modulus E'', and mechanical loss factor $\tan\delta$, of PVC. Runs were conducted at a heating rate of 2 °C min^{-1} at an oscillating strain frequency of 1 Hz. Adapted data from ref. [225], with permission © 2011 John Wiley & Sons.

definitions may be entirely suitable for specifying T_g. Note that the frequency of oscillation needs to be taken into account in T_g determinations using dynamic mechanical (or dielectric) relaxation studies, just as the heating rate intervenes in calorimetric results. The frequency of 1 Hz is usually chosen as a compromise value that provides T_g values comparable to other thermal methods, while allowing collection of mechanical data at a sufficient rate to permit reasonable experimental times. DMA experiments using multiple frequencies deliver additional information (relaxation maps, activation energies, etc.) useful for defining kinetic parameters for the glass transition. The latter permit the prediction of material properties over broader frequency ranges (time-temperature superposition principle), such as those the material could encounter in actual end use.

1.4.4
Dielectric Analysis (DEA)

The application of dielectric analysis (DEA) in the characterization of many different kinds of polar macromolecular materials and polymer-based composites is a steadily growing field of research [213,226]. Related studies have provided detailed insight into the molecular relaxation dynamics at various time and length scales. The properties and phenomena usually investigated by dielectric techniques include transition temperatures, chemical relaxation, cold crystallization and stabilizer effects, influence of space charges, microstructure, plasticization and oxidation phenomena, water–polymer interactions and hydration properties, physical aging, weathering, or effects of gamma and neutron radiation [16]. The remarkable sensitivity of several dielectric techniques to the presence of structural nanoheterogeneities is related to their small probe length

scales (~3 nm), as opposed to conventional DSC that can only sense movements at considerably larger length scales (~20–60 nm). The application of DEA even in apolar substances has become feasible by introducing polar groups in their structure, either by chemical modification (labeling) of the polymer chain (chlorination, oxidation, etc.) or by dissolving of suitable polar probe molecules, which act as dielectric probes of polymer dynamics. In the latter case, strong coupling of the probe molecule fluctuations with the molecular motions in its environment is essential [227]. A successful application of this approach has been presented for binary blends comprising PE, PS, or PP, using low concentrations of the highly soluble and polar probe molecule 4,4′-(*N*,*N*-dibutylamino)-(*E*)-nitrostilbene [228].

High-precision measurements of complex physical quantities, connected with the orientational fluctuations of permanent dipoles or the translational mobility of charges, are now possible at an extremely wide frequency range (10 μHz, . . . , 30 GHz) through a variety of sophisticated experimental methods and measuring techniques; all these are collectively described as DEA techniques [213,226]. In dielectric relaxation spectroscopy (DRS), for example, an alternate current bridge or similar device is typically used to measure the equivalent conductance, *G*, and capacitance, *C*, of a material as a function of frequency *f* (or $\omega = 2\pi f$). All the experimental information regarding electrical relaxation at a given temperature is contained in the functions

$$G(\omega) = \varepsilon''(\omega)\varepsilon_0\omega\frac{A}{d} \tag{1.46a}$$

$$C(\omega) = \varepsilon'(\omega)\varepsilon_0\frac{A}{d}, \tag{1.46b}$$

where *A* and *d* are sample's cross-sectional area and thickness, respectively, and ε_0 is the permittivity of free space. In that way, one obtains the frequency dependence of the components, $\varepsilon'(\omega)$ and $\varepsilon''(\omega)$, of the complex relative permittivity,

$$\varepsilon^*(\omega) = \varepsilon'(\omega) - \mathrm{i}\varepsilon''(\omega), \tag{1.47}$$

and other important dielectric functions [229]. The real part of relative permittivity expresses the ability of the dielectric medium to store energy and consists of the contributions of free space and the real part of the susceptibility of the material itself, while the imaginary component describes the energy losses entirely due to the material medium. The dielectric data (commonly permittivity, but also dielectric loss tangent $\tan\delta = \varepsilon''/\varepsilon'$ or electric modulus $M^* = 1/\varepsilon^*$) are usually presented in *isothermal plots*, that is, as a function of frequency at a constant temperature (Figure 1.22). In the frequency domain, $\varepsilon'(\omega)$ due to dipoles' relaxation exhibits dispersion, falling from ε_r (relaxed) to ε_u (unrelaxed) with increasing frequency. The dielectric loss band $\varepsilon''(\omega)$ of secondary relaxations displays a broad and generally symmetric shape, with a half-width of 3–6 decades (in a logarithmic scale) that usually narrows as temperature rises. The broad shape of the respective bands, compared with the width of the single relaxation time (Debye-type) mechanism (1.14 decades), is usually explained in terms of

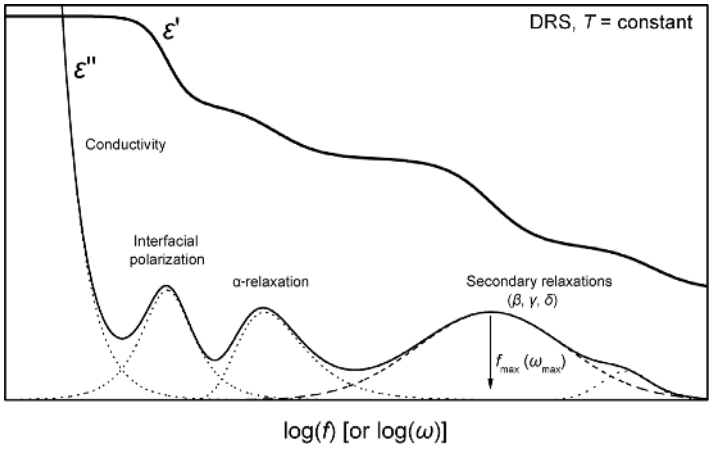

Figure 1.22 Generic behavior of frequency dependence of permittivity components (ε' and ε'') for the typical dielectric relaxation modes in glassy polymers and related composites. Interfacial polarization effects are common in heterogeneous materials (e.g., immiscible or partially miscible polymer blends), while crystalline phases and additives are potential sources of additional relaxations.

a distribution of environments in which the molecular entities relax. The α-relaxation (glass transition) displays a relatively broad but asymmetric shape, with a half-width of 2–5 decades. Permittivity data collected at some temperature are typically analyzed by a superposition of several Havriliak and Negami (HN) functions [230] and a conductivity term,

$$\varepsilon^*_{\text{exp}}(\omega) = \varepsilon_\infty + \sum_i \frac{\Delta\varepsilon_i}{\left[1 + (\text{i}\omega\tau_{\text{HN}})^{1-\alpha_{\text{HN},i}}\right]^{\beta_{\text{HN},i}}} - \text{i}\frac{\sigma_{\text{dc}}}{\varepsilon_0\omega^p}, \tag{1.48}$$

where σ_{dc} is the dc conductivity of the material ($p = 1$ for purely ohmic conductivity). The shape parameters $0 \le \alpha_{\text{HN}} < 1$ and $0 < \beta_{\text{HN}} \le 1$ describe the width and the asymmetry of the loss peak, respectively, and with the addition of the dielectric strength $\Delta\varepsilon = \varepsilon_{\text{r}} - \varepsilon_{\text{u}}$ and τ_{HN} (a parameter directly related to the relaxation time τ) provide a complete description of each relaxation process. The dielectric glass-transition temperature ($T_{\text{g,diel}}$) is defined by the convention $\tau_\alpha(T_{\text{g,diel}}) = 100\,\text{s}$, and corresponds to the temperature at which the maximum of the loss factor band is located at the frequency of $f_{\text{max},\alpha} = 1.6 \times 10^{-3}\,\text{Hz}$. As with DMA, dielectric relaxation data can also be plotted as a function of temperature at a constant frequency (*isochronal plots*). Current-temperature ($I(T)$) spectra, resembling the isochronal $\varepsilon''(T)$ plots, are collected using the thermally stimulated (depolarization) currents (thermally stimulated currents [TSC] or thermally stimulated depolarization currents [TSDC]) technique. The equivalent frequency of this technique is in the range 10^{-4}–$10^{-2}\,\text{Hz}$, depending on the rate used for sample heating [213], and is sufficiently low to permit increased resolution of the complex signals recorded in polymer composites. In both cases, an

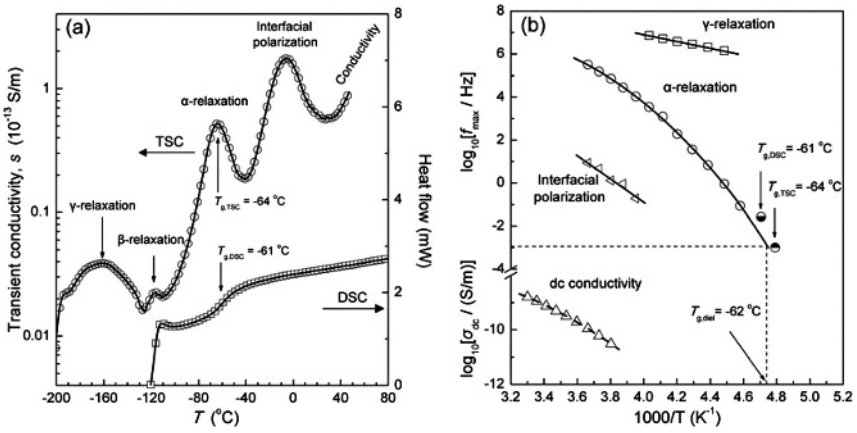

Figure 1.23 (a) TSC (heating rate 5 °C min^{-1}, equivalent frequency ~10^{-3} Hz) and DSC (20 °C min^{-1}, ~2.6 10^{-2} Hz) spectra of a segmented polyurethane. (b) Arrhenius diagram of the various relaxation modes and dc conductivity. The lines correspond to the fittings of the data to the Arrhenius (straight lines) and VFTH (curved lines) equations. Partly based on data appearing in ref. [231], with permission © 2005 Springer.

oscillation frequency (or heating rate) dependent estimate of T_g is readily identified by the position of the peak corresponding to the α-relaxation mechanism.

Dielectric experiments performed at different temperatures allow analytical recording of the temperature dependences of the relaxation times or frequencies (Arrhenius plots). These can be further analyzed to provide, for example, the glass-transition temperature, dynamic estimates of the fragility index, data about the degree of curing and polymerization (by online dielectric monitoring [213]), an insight into the factors controlling polymers' miscibility and morphology, quantitative information about the degree of intermolecular and interface interactions in blends and composites, as well as conductivity percolation thresholds. The information extracted from dielectric studies is complementary to that obtained by DMA, DSC, and sensitive molecular spectroscopies. The data shown in Figure 1.23 for a thermoplastic segmented polyurethane reveal a close proximity for the dielectric and calorimetric estimates for the glass-transition temperature [231]. The limited agreement often found in T_g estimates of different thermoanalytical techniques, even in cases of comparable frequencies, is in part related to the different modes of segmental motion activated by the thermal, electrical, or mechanical stimulus used in each experiment.

1.5
Blend Morphology and Glass Transitions

The most frequent result of mixing of two polymers is an immiscible system that exhibits complete phase separation due to the chemical incompatibility (i.e., the

repulsive interaction) between the components. Compatibilization via chemical, structural, or compositional modifications is often necessary to achieve some level of molecular mixing and better response to selected applications. A miscible binary system, on the other hand, is purportedly homogeneous down to the molecular level, with a domain size comparable to the dimensions of the statistical chain segment. The latter describes a rather limiting situation, since our current perception of miscibility also includes systems with compositional nanoheterogeneities. Poor consideration of the extent and relative strength of inter- and intramolecular interactions and of the impact of excess mixing volume effects often result in rather inaccurate theoretical predictions of the phase diagrams and miscibility windows of several polymer blends, calling for independent experimental validation. Glass-transition temperature determinations currently provide the most popular miscibility test. However, the effectiveness of thermal analyses and of several other relaxational (or vibrational) approaches in determining miscibility or phase behavior in multicomponent systems heavily relies on the nature of the technique and the probe length scale (i.e., the minimal domain size capable of producing experimentally resolvable behavior). Related issues will be critically examined in the following paragraphs.

1.5.1 Miscibility and Phase Boundaries in Polymer Blends

Complete miscibility and phase stability in a binary mixture, of composition φ at fixed temperature and pressure, requires that the following thermodynamic conditions,

$$\Delta G_{\text{mix}} = \Delta H_{\text{mix}} - T\Delta S_{\text{mix}} < 0 \tag{1.49a}$$

$$\left(\frac{\partial^2 \Delta G_{\text{mix}}}{\partial \varphi_i^2}\right)_{P,T} > 0, \tag{1.49b}$$

are satisfied [4]. If the latter condition is fulfilled merely in a limited range of compositions, then the blend is partially miscible, with stable one-phase mixtures expected only at the ends. At a given temperature, the sign of Gibb's free energy of mixing function, ΔG_{mix}, almost exclusively depends on the value of the enthalpy (heat) of mixing ΔH_{mix}, since $T\Delta S_{\text{mix}}$ attains always positive values due to the increase in entropy on mixing. The chemical nature of the polymers and their molecular mass are the main characteristics that affect miscibility. The former determines the strength of the cohesive forces between the components, with the most favorable conditions attained in the presence of strong specific interactions (e.g., hydrogen bonds; Section 1.7.1), while the molecular mass influences ΔG_{mix} in two different ways. If the mixing is endothermic ($\Delta H_{\text{mix}} > 0$), then the higher the molecular mass the lower is the entropy change, rendering miscibility less probable. The opposite happens if ΔH_{mix} is negative, since the number of intermolecular interactions increases by increasing the molecular mass, even if these interactions imply a reduction of ΔS_{mix}.

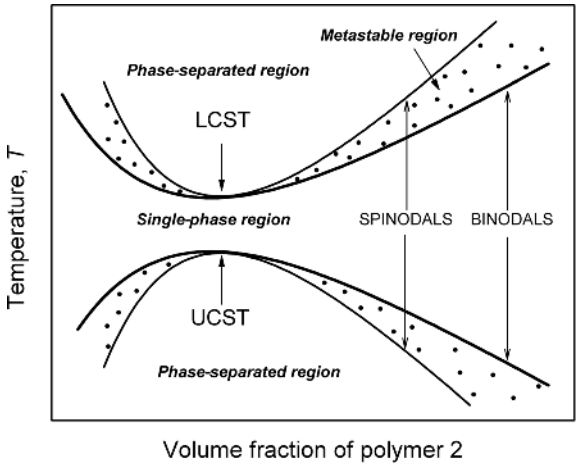

Figure 1.24 Phase diagram showing the LCST and UCST, respectively, behavior of polymer blends. Nonsymmetric phase diagrams are common in binary blends of polymers with large differences in their molecular masses.

For a given combination of polymers, blend composition and temperature have substantial bearing on system's morphology. Figure 1.24 shows a schematic phase diagram of a binary system, with the three regions of different degree of miscibility: the single-phase miscible region between the two binodals, the four fragmented metastable regions between binodals and spinodals, and the two phase-separated regions of immiscibility, bordered by the spinodals. The binodal curve is related to the equilibrium phase boundary between miscible (one-phase) and metastable regions. In general, the binodal is defined by the condition at which the component chemical potentials are equal, and is determined by the points of common tangent to the free energy curve (Figure 1.25a). The spinodal curve separates metastable and unstable (unconditionally two-phase) regions, where the curvature of the free energy versus composition graph changes from positive to negative and the second derivative of ΔG_{mix} is zero. The point of intersection of these curves is denoted as the critical point. Phase separation takes place when a single-phase system suffers a change of composition, temperature, or pressure that forces it to enter either the metastable or the spinodal region (e.g., a shift from the single-phase system at T_{A} to a phase-separated one at T_{B}, Figure 1.25b). When the binary system enters from the single-phase region into the metastable region, the phase separation occurs by a mechanism resembling crystallization – slow nucleation, followed by the growth of phase-separated domains. Inside the spinodal, the system is unstable to all concentration fluctuations and the blend spontaneously separates into coexisting phases via the mechanism known as spinodal decomposition. Given sufficient time for the process, structure rearrangement will eventually lead to very large regions of the two coexisting phases; however, the spinodal structure can be frozen-in by rapidly cooling the mixture below its glass-transition temperature or by triggering

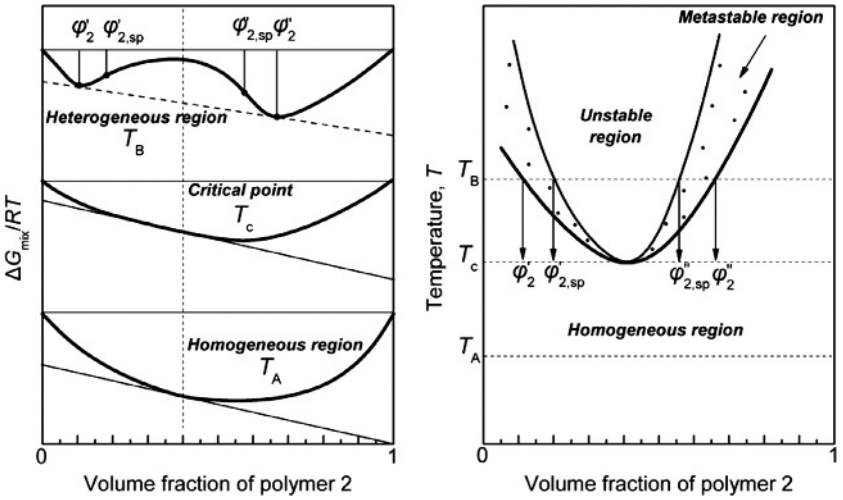

Figure 1.25 Generalized behavior of $\Delta G_{mix}/RT$ versus volume fraction of polymer 2 (φ_2) plot (Figure 1.25a), for various positions on the phase diagram (Figure 1.25b) of a binary polymer blend with LCST behavior. The dashed line on the upper site of Figure 1.25a is the common tangent that connects the binodal points.

a chemical reaction between the components. The diagram also shows two critical solution temperatures, the lower, lower critical solution temperature (LCST) (at a higher temperature), and the upper, upper critical solution temperature (UCST) (at a lower temperature). Phase diagrams with two critical points are typical for mixtures of low molar mass components [232], whereas polymer blends usually display only one of them (e.g., LCST [233–238] or UCST [239–241]). An LCST is common in enthalpically driven demonstrations of polymers' miscibility, as is the case of mixtures of poly(vinyl methyl ether) (PVME) with PS [233] or poly(2-chloro styrene) (P2CS) [234]. Here, favorable enthalpic interactions promote mixing of phases at the molecular level, while immiscibility at higher temperatures is entropically driven, with the unfavorable component of entropy of mixing emerging from either equation-of-state effects (e.g., differences in free volume) or the collapse of existing interassociations (e.g., strong intercomponent hydrogen bonding). In several cases, such as in blends of PS with polyisoprene (PI) [239], polybutadiene (PB) [240], or poly(α-methyl styrene) (PαMS) [241], entropics provide a stabilizing contribution strong enough to offset destabilizing enthalpic interactions; these systems exhibit an UCST behavior, with a phase separation observed on cooling driven by unfavorable energetics [104].

Theoretical assessments of miscibility windows are commonly based on the compositional dependence of $\Delta G_{mix}/RT$ (e.g., see Figure 1.25). The lattice theory for the enthalpy of mixing in polymer solutions, developed by Flory [113] and Huggins [114], finds frequent application for modeling the free energy of binary polymer mixtures. The assumption of random mixing of the two polymers and

volume additivity ($\Delta V_{mix} = 0$) leads to the well-known expression for the combinatorial entropy of mixing,

$$\Delta S_{mix} = -R\left[\frac{\varphi_1}{N_1}\ln\varphi_1 + \frac{\varphi_2}{N_2}\ln\varphi_2\right], \tag{1.50}$$

where φ_i and N_i are the volume fraction and the number of segments of the ith polymer, respectively, and R is the gas constant. Applying the concept of regular solutions and assuming all pair interactions within the framework of mean-field theory yield for the enthalpy of mixing the approximate relation [3]

$$\Delta H_{mix} = BV\varphi_1\varphi_2 = \chi_{12}RT\varphi_1\varphi_2, \tag{1.51}$$

where V is the total volume of the mixture, B is the interaction energy density, and χ_{12} is the so-called Flory–Huggins binary interaction parameter. The term "parameter" is widely used to describe χ_{12} but it is definitively better characterized by the term "function," given its dependence on quantities such as temperature, composition, pressure, molar mass, and related distribution, and even on model parameters such as the coordination number of the lattice and the length of the segment. For incompressible binary systems, the free energy of mixing can thus be expressed as

$$\frac{\Delta G_{mix}}{RT} = \frac{\varphi_1}{N_1}\ln\varphi_1 + \frac{\varphi_2}{N_2}\ln\varphi_2 + \chi_{12}\varphi_1\varphi_2. \tag{1.52}$$

It can be seen that the combinatorial entropy of mixing decreases with increasing molar mass (N_i is proportional to the degree of polymerization) and practically vanishes for high molar mass polymers. The state of mixing is thus highly dependent on the nature and magnitude of the contribution of the enthalpic term. Positive values of χ_{12} necessarily lead to immiscibility for mixtures of polymers with high molecular weight. Specific interactions, such as ionic or hydrogen bonds, are implicitly eliminated from the Flory–Huggins model, as ΔH_{mix} is derived only for the Van der Waals interactions. However, experimentally determined χ_{12} values can include specific interactions, with negative interaction parameters often obtained from melting point depression or inverse gas chromatography studies. Note that depending on the functional form of the temperature dependence of χ_{12} a wide variety of phase diagrams is possible. For example, the UCST behavior is well accounted for by the Flory–Huggins theory, with $\chi_{12} = C_1 + C_2/T$, but the theory fails to predict LCST.

In the association model approach, Painter and Coleman [242] suggested adding to the simple Flory–Huggins expression an additional term, $\Delta G_H/RT$, to account for the free-energy changes corresponding to specific interactions, most commonly – but not necessarily – hydrogen bonds. The equation, also modified to account for same-chain contacts and screening effects, takes the form

$$\frac{\Delta G_{mix}}{RT} = \frac{\varphi_1}{N_1}\ln\varphi_1 + \frac{\varphi_2}{N_2}\ln\varphi_2 + (1-\gamma_{ii})\chi_{12}\varphi_1\varphi_2 + \frac{\Delta G_H}{RT}, \tag{1.53}$$

where γ_{ii} is an intramolecular screening parameter, defined as the fraction of same-chain contacts. Ordinary screening effects in mixtures containing linear

polymer structures lead to γ_{ii} values between 0.25 and 0.35, while higher values are obtained when hyperbranched components are used (dendrimer-like polymers, polymers with chain-end or side-chain tethered polyhedral oligomeric silsesquioxanes, etc.) [243]. The association model considers χ_{12} to represent only unfavorable "physical" forces (dispersion and weak polar forces), which provide a positive contribution to ΔG_{mix}. It is therefore determined using the non-hydrogen-bonded Hildebrand solubility parameters (δ_i, defined as the square root of the cohesion energy function), through the relation

$$\chi_{12} = \frac{V_{ref}}{RT}(\delta_1 - \delta_2)^2, \tag{1.54}$$

with V_{ref} denoting a reference volume. The association model quantitatively determines $\Delta G_H/RT$ and the compositional dependence of blend T_g for selected hydrogen-bonded blend systems (see Section 1.6.2.3). The only necessary parameters to be known are the molar volumes of the individual segments, the relevant enthalpies of hydrogen bond formation, and the equilibrium constants that describe self- and interassociation. These parameters are readily obtained from group contributions and infrared spectroscopy studies.

1.5.2
State of Dispersion and the Glass Transition

The approaches mentioned above bear some major limitations (e.g., by neglecting changes in free volume on mixing) that reduce the effectiveness of related theoretical predictions of polymer–polymer miscibility. It is therefore a common practice to locate the compositional window and the relevant length scale of phase homogeneity by experimental means. Polymer blends are generally assigned as miscible (single phase) or immiscible (multiphase) based on the result of some convenient physical test. Nevertheless, the evaluations are highly dependent on the nature and resolution of the probing technique. The classical turbidity (or haze) measurement, for example, which is used to appraise phase homogeneity based on the turbidity of systems comprising phases with significant differences in their refractive indices, is characterized by a level of resolution on the micrometer's scale (1–100 μm). This is also the threshold of the light-scattering techniques typically used in miscibility evaluations. Related techniques seem to be of limited practical importance for the majority of polymer blends, since their structural heterogeneities have smaller domain sizes (within the range 50 nm to 5 μm). Short-wavelength radiation scattering, such as scattering of X-rays and thermal neutrons with wavelengths in the range of 0.1–0.3 nm, permits much finer structures to be resolved. Phase separation in domain sizes down to 5 and 20 nm can be easily identified with small-angle scattering techniques such as small-angle X-ray scattering (SAXS) and small-angle neutron scattering (SANS), respectively. SAXS has been mainly used in morphological studies of semicrystalline blends, in the determination of spinodal and binodal temperatures in binary polymer systems, as well as to measure χ_{12}. SANS, on

the other hand, has been extensively used to study conformation and morphology in single- or multicomponent macromolecular systems, in the molten or liquid states. Among other molecular spectroscopy techniques, ESR spectroscopy and solid-state NMR measurements of the spin-lattice relaxation times are capable of distinguishing motional traces and structural or dynamic heterogeneities at domain sizes down to 2–4 nm. Wide-angle X-ray scattering (WAXS) offers much higher resolution, permitting the identification of structural heterogeneities down to true molecular levels, with scattering phase dimensions in the range 0.1–1 nm. Apparently, the assessment of phase homogeneity by a particular method or technique does not necessarily mean that the assertion is readily extendible to lower length scales.

Without a doubt, glass-transition temperature determinations currently provide the most popular test for miscibility evaluations. Depending on the chemical nature and the morphology of the system, several DSC studies indicate that multiple glass-transition signals are expected to appear at a level of heterogeneity characterized by domain sizes within the range of 15–20 nm; contributions from considerably lower domain sizes are detected using thermal techniques of higher sensitivity and resolving power (Section 1.4). Still, several complications exist that frequently cast doubt on the interpretation of related results. Problems arise from the fact that the glass-transition behavior of any glassy system encompasses the slowly dissipating memories of its preparation procedure, and the effects of any special treatment applied to the material prior to testing. The above factors, in combination with potential differences in the rate at which the system has been brought to the conditions of measurement, affect in a usually poorly predictable way its morphological characteristics and preclude direct comparisons of data obtained for the same material from different laboratories or using different experimental protocols. In view of that, several studies [2,244] clearly demonstrate that a reliable direct relationship between miscibility and the glass-transition phenomenon can be anticipated only in cases where the blend has achieved its equilibrium morphology before the evaluation, and the behavior of the glass-transition signal is unaffected by the experimental method.

On the condition that all abovementioned requirements are fulfilled, the number of transitions and the compositional dependence of the respective glass-transition temperatures offer reliable "indicators" of miscibility, partial miscibility (compatibility), or immiscibility between blend components. Figure 1.26 demonstrates schematically the expected compositional variation of the glass-transition temperatures, and the temperature variation of typical dispersion signals in dynamic mechanical or dielectric relaxation experiments (see Table 1.3), in each of these cases. A classic and simple experimental criterion for determining miscibility is based on the measurement of a single glass-transition signal for all blend compositions, located in between the glass-transition temperatures of the components and consistent with the composition of the blend (Figure 1.26a). The single glass-transition temperature recorded is also frequently referred to as the "blend-average T_g"; its position depends on the type and extent of the interactions between the components, as well as on mixing-induced variations in the free

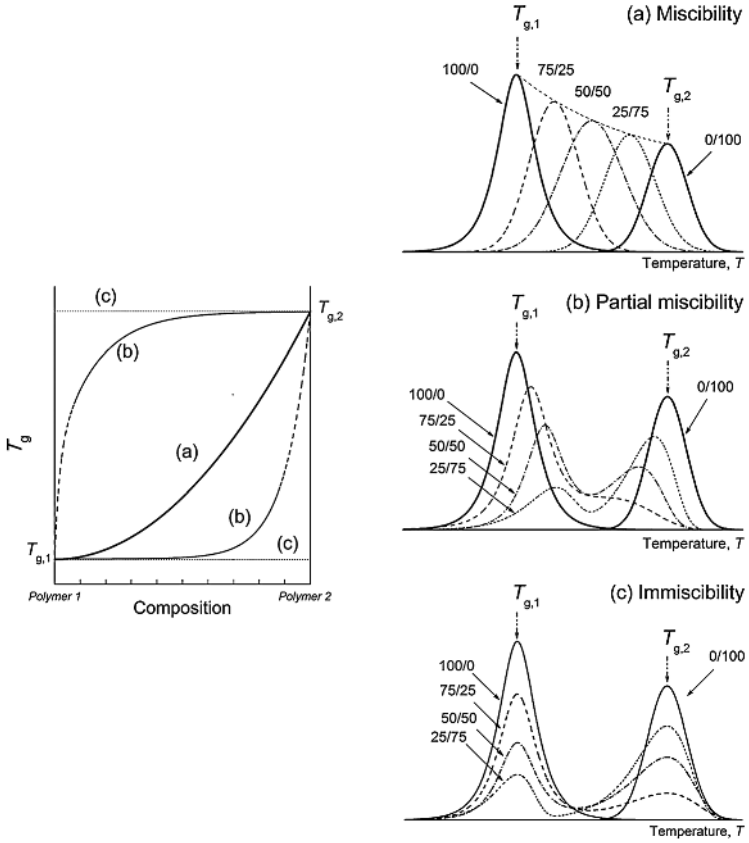

Figure 1.26 Schematic plot of the expected shifts of glass-transition signals of binary polymer mixtures, in the case where miscible (a), partially miscible (b), or immiscible (c) blends are formed. A behavior analogous to that shown in plot (b) is likely to appear in dynamically heterogeneous miscible blends (see Section 1.6.2.5).

volume (see Section 1.6). In the case of partially miscible (or compatible) polymer blends, the glass transitions of both components are recorded (Figure 1.26b): convergence of the glass-transition temperatures of the two phases is observed, along with a change in the width and the strength of the signals. Completely immiscible polymer blends clearly demonstrate two glass-transition regions for all blend compositions, but in this case peak positions are nearly composition independent (Figure 1.26c).

In the ordinary immiscible polymer blends and related commercial materials, an asymmetric *interface* exists, which may remain indefinitely [1]. Depending on the statistical segment length and the binary interaction parameter of the two polymers, interpenetration at the interface may extent to a depth of a few to several nanometers. The term *interphase* or *interphase region* is used to describe the interpenetration zone, which may have physical properties distinctly

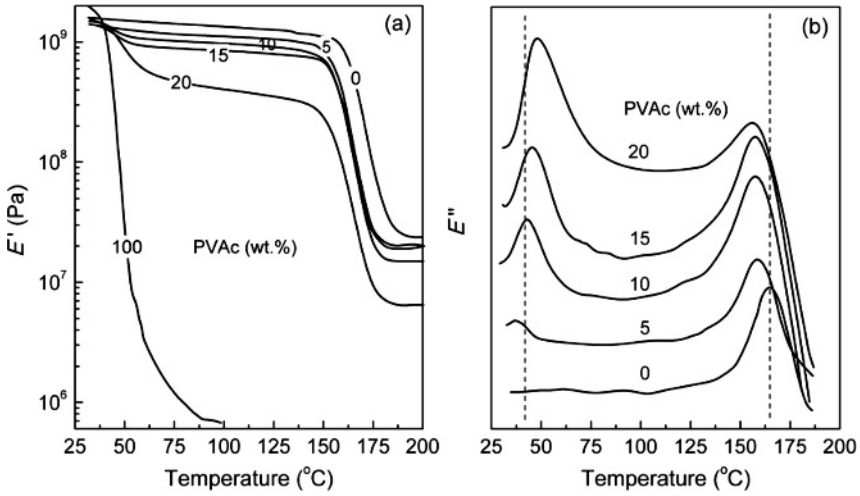

Figure 1.27 Storage modulus $E'(T)$ (a) and loss modulus $E''(T)$ (b) isochrones (1 Hz) for PVAc + epoxy thermosets with different PVAc contents. After ref. [245], with permission © 2010 Springer.

different from either polymer. The interphase regions in several polymer blends, like those containing a dispersed phase of a low-T_g rubber, provide great toughness and/or impact resistance to the final products. Segmental motions activating within the interphase are likely to produce minor shifts and/or asymmetric broadening in the apparent glass-transition signals of the constituting polymers. Along these lines, the transition temperatures of each component in a phase-separated blend may vary within a window with a width less than one-tenth of the T_g contrast (e.g., see the response of the immiscible PVAc + epoxy resin blends depicted in Figure 1.27) [245]. Such minor changes are frequently reported to arise from morphology changes, physical interactions, mismatch between the thermal expansion coefficients of the components (negative pressure effect), or dilution effects. Note that when chains in the interphase are chemically (as in block or graft copolymers) or physically bonded (e.g., at most, through hydrogen bonding of alike chains) a strengthened interphase is formed, providing a tougher material and much stronger perturbations in the glass transitions of the system.

The immiscible binary blends formed by PP, PE, or PS offer an illustrative example of the relation between the compositional variations of morphology and changes of the glass-transition temperature [228,246]. Figure 1.28 shows cross-sectional views of PP + PS samples prepared by melt blending in a single screw extruder. Fine micron-scale morphologies consisting of PS dispersed throughout a PP matrix, ranging from 0.5 to 20 μm, appear when PS is a minority phase. A co-continuous structure is observed at equal mass fractions (a phase inversion point near $w_{PS} = 0.50$), illustrating a configuration in which both phases surround each other, while a PP dispersed in PS structure appears at

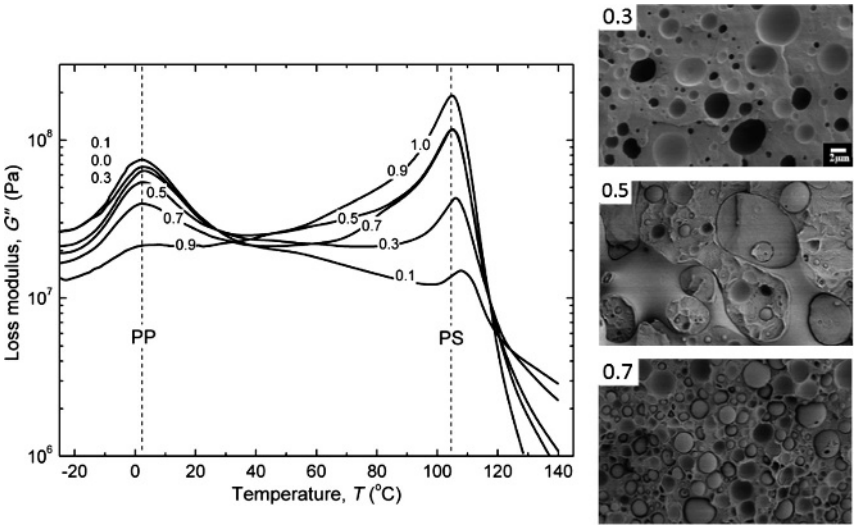

Figure 1.28 DMA loss modulus curves, showing the glass transitions of PP and PS in immiscible PP + PS blends. Numbers indicate the mass fraction of PS in the blends, and the vertical lines indicate the T_gs of neat PP and PS. Insets show scanning electron microscopy (SEM) micrographs of selected blends ($w_{PS} = 0.30$, 0.50, and 0.70). The PS domain morphology in the first image ($w_{PS} = 0.30$) is represented by the dark etched (PS removed) regions. Replotted and adapted from ref. [246], with permission © 2006 Elsevier.

higher PS loadings. Immiscibility is evident in MTDSC and rheological measurements of the glass transitions in all blend compositions. The DMA spectra shown in Figure 1.28 reveal a tendency of the glass-transition temperature of PS to increase as its loading decreases below 50 wt.%, representing a shift opposite to that expected if parts of the constituent polymers were miscible. The gradual upshift is restricted to compositions in which the PP phase surrounds the PS phase either partially or completely. Thirtha *et al.* [246] explained this behavior taking into account the compressive pressure exerted on the amorphous PS domains due to differential shrinkage between the amorphous PS and crystallizing PP. Furthermore, the glass-transition temperature of PP (~3 °C) does not change with composition, suggesting that the phase interactions are weak physical, not chemical, and are dependent on changes in morphology that accompany changes in composition.

The compatibilization of inherently immiscible polymers proffers significant modifications in both the relaxational and glass-transition behavior of the components, as well as in the morphology of the resultant materials. Epoxy resin, for example, appears to be an efficient reactive compatibilizer for immiscible poly (trimethylene terephthalate) (PTT) + polycarbonate (PC) blends [247]. With reference to Figure 1.29, when epoxy content reaches 2.7 phr, or more, the blends cease to exhibit a distinct two-phase morphology, indicating stronger interfacial adhesion of the blend; etched cavities are absent at the fracture surface, and the

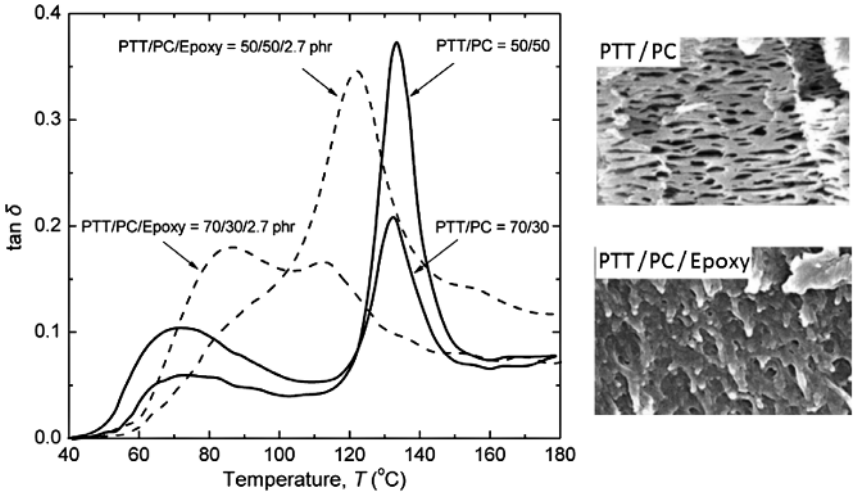

Figure 1.29 DMA damping factor versus temperature curves, showing the glass transitions of immiscible and compatibilized (with epoxy resin) PTT + PC blends, melt-mixed at 250 °C for 10 min. SEM micrographs compare the morphologies of selected blends (PTT/PC = 50/50 and PTT/PC/epoxy = 50/50/2.7 phr). The PC-rich phase domain in PTT + PC is represented by the dark etched (PC removed) regions with stalactitic morphology. Replotted and adapted from ref. [247], with permission © 2005 Taylor & Francis.

scraggy surface reveals clear miscibility among microdomains, consistent with the changes in the glass transformation range observed in the damping factor versus temperature spectrum.

Miscible polymer blends still have heterogeneity in the segmental length scale because of the chain connectivity (that results in the self-concentration of the segments of respective chains) as well as the dynamic fluctuation over various length scales. As a result, in several cases the blend components feel different dynamic environments that may translate into different temperature dependences of their segmental relaxation rates. This type of dynamic heterogeneity often results in a wide glass transformation range, a broad distribution of the segmental relaxation modes, and the thermorheological complexity of this distribution. Two separate glass transitions may even appear, as has been clearly demonstrated using techniques of increased resolving power in several miscible polymer mixtures with components showing a strong dynamic contrast (ΔT_g exceeding ~100°) and weak intermolecular interactions (see Section 1.6.2.5). The weakly intermolecularly hydrogen-bonded PMMA + poly(vinyl phenol) (PVPh) blends, for instance, appear homogeneous (fully miscible) when inspected at a domain-size scale exceeding ~20–30 nm, taking into account the single composition-dependent glass transition reported for all blend compositions by conventional DSC (Figure 1.30a [248]). Nevertheless, the binary mixtures appear heterogeneous at lower probing length scales (~2–15 nm), after considering the pair of transitions found in melt-mixed blends by DMA, or

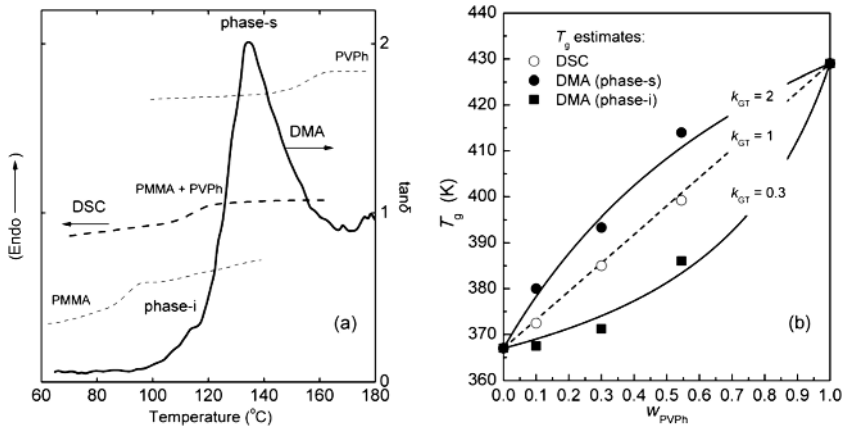

Figure 1.30 (a) Comparison of the DSC (heating rate 20 °C min^{-1}) and DMA (oscillating frequency of 10 Hz) spectra of a representative PMMA + PVPh blend ($w_{PVPh} = 0.3$). The DSC spectra of the two homopolymers are also shown. (b) Compositional variation of the glass-transition temperatures. DMA estimates are downshifted by 16°. Lines represent data fits based on the GT equation (Section 1.6.2.1). Replotted and adapted from ref. [248], with permission © 1996 American Chemical Society.

observing the proton spin-lattice relaxation time in the rotating frame [$T_{1\rho}$(H)] in tetrahydrofuran (THF) cast blends by solid-state NMR spectroscopy [249]. With reference to the thermograms shown in Figure 1.30a, Li and Brisson [248] related the major DMA peak to a blend rich in syndiotactic-like PMMA segments (phase-s) and the minor peak (lower strength and T_g) to a blend rich in isotactic-like PMMA segments (phase-i), with diffuse boundaries between them and distinctly different compositional dependences of the respective transition temperatures (Figure 1.30b).

Several complications in miscibility evaluations also arise in the case of melt-miscible partially crystalline blends, where multiple glass-transition-like transitions may appear (e.g., contributions from intermediate rigid-amorphous phases with T_gs below, at, or above T_m [156]) although the polymers themselves are miscible. Bearing in mind the above findings, the "single-T_g" miscibility criterion undoubtedly constitutes an oversimplification of the actual picture, as the validity of related assessments is critically dependent on the preparation process and the experimental technique used for the evaluation. As indicated by Utracki, the presence or absence of a single glass transition in a polymer blend practically provides a means for evaluating "technological miscibility," that is, to distinguish systems that are so well homogenized so that their phase domains will remain unaffected by conventional processing conditions (e.g., mixing methods and subsequent heating–cooling cycles). Homogeneity on the single-segment level is probably unattainable (due to the constraints of chain flexibility), so a characteristic domain size will be present in all blends; this can range from several repeat units (nominally miscible) to several microns (unambiguously immiscible).

Accordingly, blends displaying a single glass transition (one T_g) should be deemed miscible only on a scale at or above the total number of segments cooperatively relaxing at the glass transition, and after considering the spatial resolution limit of the employed experimental technique.

1.6 Analyzing Glass Transitions in Single-Phase Systems

Information on the state of mixing and intercomponent interactions in a binary polymer system can be extracted by analyzing the aspects of the experimental glass-transition behavior, with important quantitative results usually obtained for single-phase and compatibilized materials. The main procedures adopted in related studies involve monitoring of changes in the shape (breadth and asymmetry of the respective signal), the strength, and particularly the location (apparent T_g) of the glass transformation range, as a function of composition (Section 1.6.1). Without a doubt, when polymers are combined it is essential to understand how the properties of the resulting materials will change with compositional variations. A key objective of the application research is to develop mixing rules for the desired properties, with the glass-transition temperature getting significant attention. Mixing rules are hardly ever linear. They may be synergetic, which means the desired property increases strongly with the mass (w), volume (φ), or molar (x) fraction of the minor component, or nonsynergetic when the property deteriorates. For single-phase materials, the typical mixing rule includes the contributions from each component as well as additional interaction terms, while, for partially miscible or immiscible blends, mixing rules can be extremely complex due to the different morphologies that may develop. The following paragraphs (Section 1.6.2) present established theoretical or empirical mixing rules for the glass-transition temperature, in addition to the interpretations of common experimentally observed dependences, with illustrative examples extracted from the available literature on miscible polymer blends, small-molecule + polymer mixtures and interpenetrating polymer networks.

1.6.1 Shape Characteristics and Strength of the Transition

The breadth of the glass transition provides information about the homogeneity of the system, as it reflects the width of the distribution of relaxation times connected to the transition mechanism. The broadness of a transition signal is defined in DSC studies as the difference between the onset and endset temperatures of the ΔC_p step at T_g. In dynamic experiments (DMA and DEA studies), the broadness of the segmental α-relaxation mode is commonly represented by the width at half-height of the respective loss modulus, dielectric loss, or loss tangent ($\tan\delta$) peaks; the derivative of a DSC curve (dC_p/dT versus T plot) in the glass transformation range may be used in the same way. In binary mixtures of

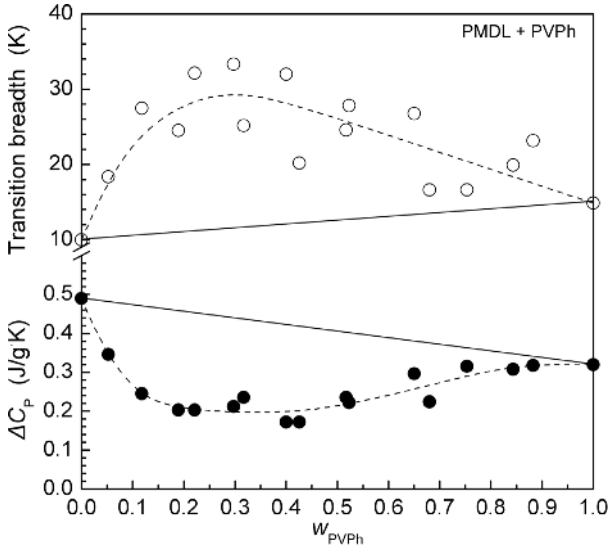

Figure 1.31 Composition dependence of the heat capacity difference at T_g and of the breadth of the glass transition region of *miscible* poly(*N*-methyldodecano-12-lactam) (PMDL) + PVPh blends. In each plot, linear dependences are depicted by solid lines, while the dashed curves are guides for the eye. After ref. [251], with permission © 2011 John Wiley & Sons.

low-molecular-mass glass formers (e.g., solvent + solvent mixtures), the transition width is approximately composition independent [250], indicating equivalent distributions of local environments. In contrast, in most miscible binary polymer systems, the observation of a single glass transition is accompanied by a *moderate-to-strong* signal broadening, compared with the width of the transitions recorded in the neat components (Figure 1.31) [251,252]. An intermediate behavior is more likely in several small-molecule + polymer mixtures. Most homopolymers typically exhibit glass transition widths of 10–15 °C, while in polymer blends, cross-linked polymers, and other polymer-based composites, the width can be greater by a factor of 3–4. In carefully conducted experiments, this broadening may even translate into a *bimodal pattern* [250]. The latter is usually qualitatively interpreted based on the existence of structural heterogeneities on segmental level, and concentration fluctuations within a local distribution of volumes associated with specific intercomponent interactions [250,253], which may pass undetected in evaluations relying on typical light-scattering techniques.

The intensity of the transition signal is directly related to the mobility of the chains and the fraction of amorphous chains in a partially crystalline blend, excluding the RAF near crystallite faces (see Section 1.7.2). Depending on the type of the probe method, a number of parameters can be used as quantitative measures of the intensity of the process, such as the heat capacity change at T_g (ΔC_p in DSC) or the strength of the dielectric α-transition signals ($\Delta\varepsilon_\alpha$ in DEA).

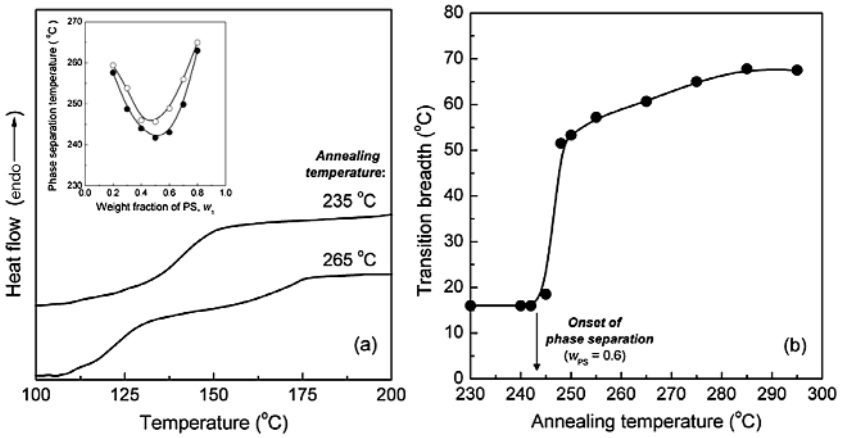

Figure 1.32 (a) DSC thermograms of a PS + TMPC blend ($w_{PS} = 0.50$) after annealing at 235 °C or 265 °C, below and above, respectively, the respective phase separation temperature (~245 °C). The inset shows the phase separation temperatures obtained by DSC (filled circles) and light transmission (open circles). (a) Change of the transition breadth for a PS + TMPC blend ($w_{PS} = 0.60$) as a function of annealing temperature. In all cases, annealing time was 5 min. After ref. [238], with permission © 1992 Elsevier.

Early studies indicate that the $\Delta C_p(w)$ and $T_g(w)$ dependences show a nonlinear and somewhat reversed behavior in blends that exhibit specific interactions (Figure 1.31), while a linear behavior is expected in systems with noninteracting components [254]. Along these lines a decrease in the strength is usually associated with the formation of more ordered structures, with enhanced restrictions for the segmental motions occurring within the blend environment, as a result of intense specific interactions among functional groups along the chains and a concomitant reduction in free volume.

The phase boundary curve of a binary blend can be determined by studying, as a function of annealing temperature and time, the development of the two phases that form when the miscibility gap is entered [236,255]. The usability of transition breadths in determining phase behavior is illustrated in Figure 1.32, using the calorimetric analysis of the thermally induced phase separation process occurring in PS + tetramethyl bisphenol-A PC blends [238]. Solution-cast samples of the above mixture demonstrate a single-T_g behavior, at all blend compositions. On heating, the blends turn cloudy due to phase separation and the onset temperature of the phase separation can be readily identified by optical methods (e.g., light transmission; open circles in the inset of Figure 1.32a), but also from the glass-transition behavior after heat treatment. The simple experimental procedure employed involves heating the blend at a progressively increasing high annealing temperature for a short period of time, followed by rapid cooling (quenching). In that way, the phase structure at the annealing point is frozen and the nonequilibrium morphology can be explored by subsequent study of thermal events. The glass-transition region recorded by DSC may

be either single or bimodal, depending on whether the annealing temperature is below or above, respectively, the phase separation temperature. An LCST-type phase boundary can thus be determined by identifying, for each blend composition, the lowest annealing temperature (cloud point) at which the breadth of the calorimetric glass-transition signal shows a drastic increase (Figure 1.32b). Good agreement between the experimental pattern obtained by DSC and the predicted spinodal curve is often demonstrated [236].

1.6.2 Description and Interpretation of T_g versus Composition Behaviors

What holds for the glass-transition temperatures generally holds for several other properties of binary blends. Mechanical properties, resistance to chemicals, radiation, or heat, they all generally plot the same way as the T_g does with respect to the relative amounts of each polymer in the blend. For that reason, an extensive theoretical and experimental effort has been devoted in attempts to establish relations for the compositional dependence of the glass-transition temperature of amorphous blends. The usability of the ensuing functions is primarily judged by their ability to describe real experimental patterns without resorting to the use of adjustable parameters. In several purely phenomenological approaches, however, a number of heuristic parameters have been introduced to achieve better correlation of models to experimental data, inevitably, at the expense of their predictive power. In view of that, frequently emerges the need to provide a posteriori plausible physical meaning to important empirical parameters, or establish classification schemes for the blend behaviors. Given the multiplicity of approaches and the complexity of the ensuing data interpretations, an overview of the origins and the limits of applicability of selected equations will be discussed in some detail in the following sections.

1.6.2.1 Specific Volumes or Flexible Bonds Additivity Models

Most of the $T_g(w)$ expressions proposed hitherto for binary systems can be represented as variations of the *general* mathematical form:

$$T_g = \frac{w_1 T_{g,1} + k w_2 T_{g,2}}{w_1 + k w_2}, \tag{1.55}$$

with parameter k representing a model-specific constant, which is usually assumed temperature independent. A relation of this form has been proposed by Gordon and Taylor (GT) [256], based on the assumption of *volume additivity* (i.e., ideal volume of mixing) and the existence of a linear change in volume with temperature. Their constant, k_{GT}, is given by

$$k_{GT} = \rho_1 \Delta\alpha_2 / \rho_2 \Delta\alpha_1,$$

where ρ_i represents the densities, and $\Delta\alpha_i = (\alpha_{liquid} - \alpha_{glass})_i$ is the change in expansivities at the glass transition of the homopolymers. The GT relation was initially derived for copolymers, and subsequently extensively used in studies of

binary mixtures. Equation (1.55) is also analogous to the relation proposed for copolymers by Wood [257], as well as to the Kelley–Bueche [258] relation for the volume fraction dependence of the glass-transition temperatures observed in diluent + polymer systems. In another approach, DiMarzio extended the Gibbs–DiMarzio entropy theory of the glass transition for polymer blends [259,260], assuming that additivity of the flexible bonds is responsible for conformational changes. This treatment provided a description of the change of T_g as a function of the fractions of flexible bonds (B_i, with $i = 1, 2$),

$$T_g = B_1 T_{g,1} + B_2 T_{g,2}. \tag{1.56}$$

By relating the bond fraction to the weight fraction via

$$w_1 = m_1 B_1 \gamma_1 / (m_1 B_1 \gamma_2 + m_2 B_2 \gamma_1),$$

with $w_1 + w_2 = 1$, where γ_i is the number of flexible bonds per repeating unit, and m_i is the mass of the monomer unit, the DiMarzio equation becomes identical in form with Eq. (1.55), with its constant written as

$$k_{DM} = m_1 \gamma_2 / m_2 \gamma_1.$$

The GT equation leads to the simple Fox equation [261]

$$\frac{1}{T_g} = \frac{w_1}{T_{g,1}} + \frac{w_2}{T_{g,2}} \tag{1.57}$$

by invoking the Simha–Boyer rule, $\Delta\alpha_i T_{g,i} = 0.113$ [110], and assuming similar specific volume for the two components ($\rho_1 \approx \rho_2$). In the limiting case, where $k_{GT} = 1$, the GT equation also reduces to the expression for the linear combination (mass additivity)

$$T_g = w_1 T_{g,1} + w_2 T_{g,2}. \tag{1.58}$$

This provides the simplest estimate of the glass-transition temperature of binary mixtures. The routine application of the above equations in miscible binary systems produces smooth, monotonic, theoretical $T_g(w)$ dependences that frequently either substantially *underestimate* (Figure 1.33) or *overestimate* (Figure 1.34) the experimental patterns [10,262,263]. In view of that, their application for predictive purposes should be considered with cautiousness.

1.6.2.2 Additivity of Free Volumes

Several years ago careful analyses of literature data indicated that a singular point, or cusp, may be present in the glass-transition temperatures versus composition curves of some binary mixtures [266–269]. Such a behavior was demonstrated and quantitatively described by Kovacs [266] in the framework of the free-volume theory, assuming a negligible excess volume between the two polymers on mixing. Based on the free-volume approach, if the difference $\Delta T_g = T_{g,2} - T_{g,1}$ between the two homopolymers involved becomes large, the free volume of the high-T_g polymer becomes zero at a critical temperature T_{crit}. As a result, equations deriving from the free-volume theory become invalid below

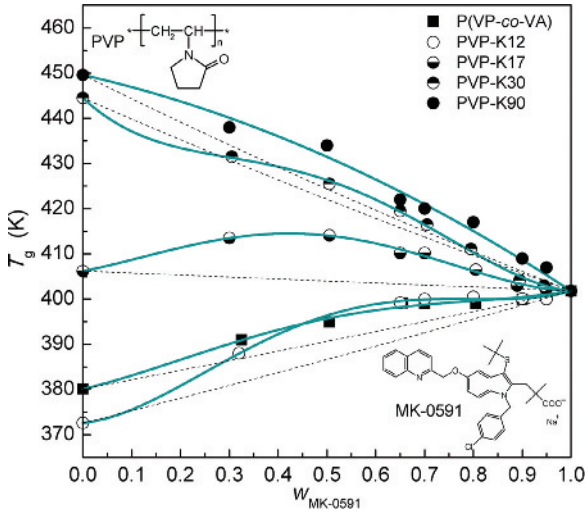

Figure 1.33 Compositional variation of the T_g of solid dispersions of the model hydrophobic drug MK-0591 with different pharmaceutical grades of PVP [with T_g (°C) = 175 − 9685/K^2], or P(VP-*co*-VA) [264]. Solid lines are fits to the BCKV model equation, while dashed lines are theoretical predictions based on the Fox equation. After ref. [10], with permission © 2011 Elsevier.

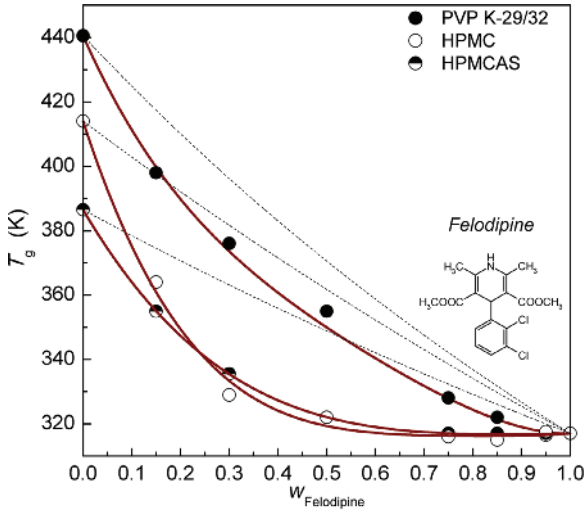

Figure 1.34 T_g versus composition patterns of miscible solid dispersions of amorphous felodipine in PVP K-29/32, hydroxypropyl methylcellulose (HPMC), or hydroxypropyl methylcellulose acetate succinate (HPMCAS) [265]. Solid lines are fits to the BCKV model equation, while dashed lines are theoretical predictions based on the GT equation. After ref. [10], with permission © 2011 Elsevier.

that point, since in a different case one would stumble on the physically unrealistic situation of a negative free volume. This critical temperature and the corresponding critical volume fraction φ_{crit} (relative to polymer 1) were calculated by Kovacs as

$$T_{crit} = T_{g,2} - \frac{f_{g,2}}{\Delta\alpha_2} \tag{1.59a}$$

and

$$\varphi_{crit} = \frac{f_{g,2}}{[\Delta\alpha_1(T_{g,2} - T_{g,1}) + f_{g,2}(1 - \Delta\alpha_1/\Delta\alpha_2)]}, \tag{1.59b}$$

respectively, where $f_{g,2}$ is the free-volume fraction of polymer 2 at its respective transition temperature. Kovacs showed that below T_{crit} the glass-transition temperature of the mixture is given by

$$T_g = T_{g,1} + \frac{f_{g,2}}{\Delta\alpha_1}\left(\frac{\varphi_2}{\varphi_1}\right). \tag{1.60}$$

According to this equation, T_g depends uniquely on the parameters of polymer 1 ($T_{g,1}$, $\Delta\alpha_1$, and φ_1), if $f_{g,2}$ is given by the universal value of 0.025. Data in the range $T > T_{crit}$ can be described using the classical equations [e.g., Eqs. (1.55), (1.57), or (1.58)]; however, a judicious selection of a particular functional form has to be made given the usually limited width of the pertinent concentration range.

In cases where the excess mixing volume is not negligible, Braun and Kovacs [267] proposed a modified form of Eq. (1.60)

$$T_g = T_{g,1} + \frac{\varphi_2 f_{g,2} + g\varphi_1\varphi_2}{\varphi_1\Delta\alpha_1}, \tag{1.61a}$$

which is again valid below T_{crit}. In this equation, g is an interaction term which is defined by

$$g = \frac{V_{ex}}{V}\frac{1}{\varphi_1\varphi_2}, \tag{1.61b}$$

where V_{ex} is the excess volume due to specific interactions. V_{ex} and g are positive if the interactions between the components are stronger than or at least equal to the average interactions between molecules of the same species, and negative otherwise. Typical values of g found in the literature range from −0.020 to +0.020. The parameter g can be incorporated into the GT equation to provide the relation [267]

$$T_g = \frac{\varphi_1 T_{g,1} + k\varphi_2 T_{g,2} + g\varphi_1\varphi_2}{\varphi_1 + k\varphi_2}, \tag{1.62}$$

where volume fractions are used instead of weight fractions, and $k = \Delta\alpha_2/\Delta\alpha_1$. Equation (1.62) can also be used to fit the data above T_{crit} provided a sufficient number of points is available.

The above treatments give a singular point, or cusp, in the T_g-composition curve of miscible polymer blends when $T_{crit} > T_{g,l}$. Typical examples of this

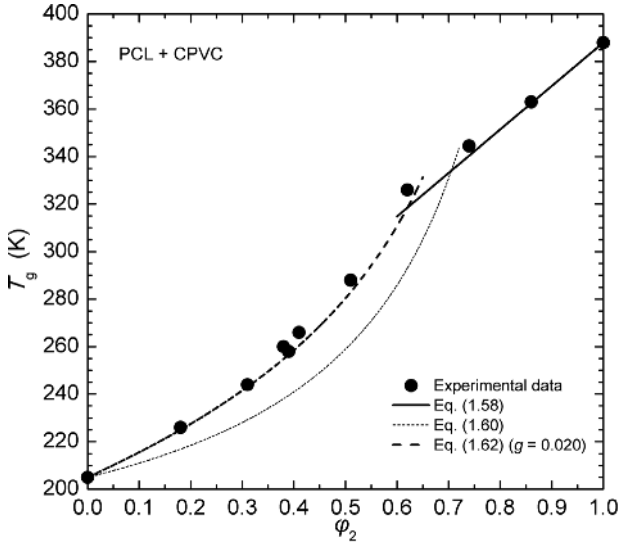

Figure 1.35 Glass-transition temperature of PCL + chlorinated PVC (CPVC) blends as a function of volume fraction, φ_2, of CPVC in the amorphous phase (data from ref. [268], with permission © 1988 John Wiley & Sons). Using the iso-free-volume theory predictions of $f_{g,2} = 0.025$ and $\Delta\alpha_2 = 0.00\,048\,K^{-1}$, T_{crit} is estimated to be $T_{crit} = T_{g,2} - 52\,K = 336\,K$ and $\varphi_{crit} = 0.28$ (relative to polymer 1).

behavior can be found in blends of poly(ε-caprolactone) (PCL) with several chlorinated polymers [267,268] (e.g., chlorinated PVC; Figure 1.35), PVAc with aliphatic polyesters [270], PEO + PVPh [271], PVME + PVPh [271,272], poly(vinyl ethyl ether) (PVEE) + PVPh [273], and several other binary mixtures [269,270,274]. As a rule of thumb, Aubin and Prud'homme [268] indicate that a cusp is likely to appear if the difference ΔT_g is greater than 52 K, in practice higher than at least 70°–80°, and $\Delta\alpha_2$ is sufficiently large.

1.6.2.3 Predictions Based on Thermodynamic Considerations

Couchman and Karasz [275] and Couchman [276,277] followed a classical thermodynamic treatment of the glass transition that provided several relations for the compositional dependence of the apparent glass-transition temperature in various single-phased solid solutions. The approach is based on the supposition of continuity of the thermodynamic entropy [275] or enthalpy [276] functions at T_g, and equality of the respective excess functions of mixing of the liquid (melt) and glass states. In the entropy model used by Couchman and Karasz, the components of a miscible binary polymer blend were considered to have pure-component molar entropies denoted as S_1 and S_2, and respective mole fractions x_1 and x_2. The molar entropy of the mixed system is expressed as

$$S = x_1 S_1 + x_2 S_2 + \Delta S_{mix}, \tag{1.63}$$

where ΔS_{mix} incorporates all excess entropy changes (conformational, thermal, etc.) associated with mixing. By considering as S_1^o and S_2^o the pure-component molar entropies at the respective glass-transition temperatures, the mixed system total molar entropy takes the form

$$S = x_1\left(S_1^o + \int_{T_{\mathrm{g},1}}^{T} C_{\mathrm{p},1}\mathrm{d}\ln T\right) + x_2\left(S_2^o + \int_{T_{\mathrm{g},2}}^{T} C_{\mathrm{p},2}\mathrm{d}\ln T\right) + \Delta S_{\mathrm{mix}}, \tag{1.64}$$

where $C_{\mathrm{p,l}}$ and $C_{\mathrm{p},2}$ are the molar heat capacities of the components. Relations of the above form apply for both the total molar entropies of the glassy (S^{G}) and the liquid (S^{L}) states. At a fixed pressure, the glass transition of the mixture is defined by the continuity condition $S^{\mathrm{G}}(T_{\mathrm{g}}) = S^{\mathrm{L}}(T_{\mathrm{g}})$, which leads to the relation:

$$\begin{aligned} &x_1^G\left(S_1^{o,G} + \int_{T_{\mathrm{g},1}}^{T_{\mathrm{g}}} C_{\mathrm{p},1}^G\mathrm{d}\ln T\right) + x_2^G\left(S_2^{o,G} + \int_{T_{\mathrm{g},2}}^{T_{\mathrm{g}}} C_{\mathrm{p},2}^G\mathrm{d}\ln T\right) + \Delta S_{\mathrm{mix}}^G \\ &\quad = x_1^L\left(S_1^{o,L} + \int_{T_{\mathrm{g},1}}^{T_{\mathrm{g}}} C_{\mathrm{p},1}^L\mathrm{d}\ln T\right) + x_2^L\left(S_2^{o,L} + \int_{T_{\mathrm{g},2}}^{T_{\mathrm{g}}} C_{\mathrm{p},2}^L\mathrm{d}\ln T\right) + \Delta S_{\mathrm{mix}}^L \end{aligned}. \tag{1.65}$$

Considering that the excess entropy of mixing is continuous during the glass transition (i.e., $\Delta S_{\mathrm{mix}}^G = \Delta S_{\mathrm{mix}}^L$), and using the (zeroth order) approximation that the transition isobaric capacity increments,

$$\Delta C_{\mathrm{p},i} = C_{\mathrm{p},i}^L - C_{\mathrm{p},i}^G\,(i = 1, 2),$$

are temperature independent, Eq. (1.65) provides the expression

$$\ln T_{\mathrm{g}} = \frac{x_1\Delta C_{\mathrm{p},1}\ln T_{\mathrm{g},1} + x_2\Delta C_{\mathrm{p},2}\ln T_{\mathrm{g},2}}{x_1\Delta C_{\mathrm{p},1} + x_2\Delta C_{\mathrm{p},2}}. \tag{1.66}$$

The above equation can be equivalently expressed in terms of mass (weight) fractions, instead of the molar fractions,

$$\ln T_{\mathrm{g}} = \frac{w_1\Delta C_{\mathrm{p},1}\ln T_{\mathrm{g},1} + w_2\Delta C_{\mathrm{p},2}\ln T_{\mathrm{g},2}}{w_1\Delta C_{\mathrm{p},1} + w_2\Delta C_{\mathrm{p},2}}, \tag{1.67}$$

with $\Delta C_{\mathrm{p},i}$ denoting the heat capacity change per unit mass. This equation reduces to several other common equations, following a certain number of simplifying assumptions. By setting $k = \Delta C_{\mathrm{p},2}/\Delta C_{\mathrm{p},1}$, one obtains the logarithmic GT-like expression

$$\ln T_{\mathrm{g}} = \frac{w_1\ln T_{\mathrm{g},1} + kw_2\ln T_{\mathrm{g},2}}{w_1 + kw_2}, \tag{1.68a}$$

a relation initially proposed by Utracki [244]. Furthermore, if it is assumed that $\Delta C_{p,1} = \Delta C_{p,2}$ (a rather crude approximation), then the relation of Pochan *et al.* [278] is derived as

$$\ln T_g = w_1 \ln T_{g,1} + w_2 \ln T_{g,2}. \tag{1.68b}$$

Making use of the expansions of the form $\ln(1+y) = y$, for small y, Eq. (1.67) can be written as

$$T_g = \frac{w_1 \Delta C_{p,1} T_{g,1} + w_2 \Delta C_{p,2} T_{g,2}}{w_1 \Delta C_{p,1} + w_2 \Delta C_{p,2}}, \tag{1.69}$$

which corresponds to the general form of $T_g(w)$ equation (Eq. (1.55)), using

$$k_{CK} = \Delta C_{p,2} / \Delta C_{p,1}$$

as a parameter. Assuming that $\Delta C_{p,i} T_{g,i} = \text{constant}$ (Boyer criterion: $\Delta C_p T_g = 115\,\text{J g}^{-1}$), Eq. (1.69) finally transforms to the Fox equation.

As in the case of the GT function, the applicability of Eq. (1.69) remains low even if its so-called *constant* is used as free fitting parameter, with satisfactory results obtained only for random mixtures (e.g., the commercialized miscible blend of PS and PPO, with weakly interacting components [279]). It has been suggested that the entropy of mixing as well as molecular interactions may be contributing factors for the frequently observed inconsistencies among the theoretical predictions and actual experimental behaviors. Elaborate modifications of the Couchman–Karasz function have been proposed to increase its accuracy [280] and extend its applicability to nonrandom systems [277]. To account, for example, for the effect of the entropy of mixing on the glass-transition temperature, Pinal [280] presented an entropic analysis that extended Eq. (1.66) in the form of

$$\ln T_g = \frac{x_1 \Delta C_{p,1} \ln T_{g,1} + x_2 \Delta C_{p,2} \ln T_{g,2}}{x_1 \Delta C_{p,1} + x_2 \Delta C_{p,2}} - \frac{\Delta S_{c,mix}}{\Delta C_{p,m}}. \tag{1.70}$$

Here, $\Delta C_{p,m}$ is the heat capacity difference between the liquid and the crystalline forms of the material, and $\Delta S_{c,mix}$ is the configurational entropy of mixing that is accessible to the liquid within the timescale of the experiment.

The fitting parameter free method developed by Painter *et al.* [281] to predict the composition dependence of the glass-transition temperature of strongly interacting systems derived an equation,

$$\left[w_1 \Delta C_{p,1}(T_g - T_{g,1}) + w_2 \Delta C_{p,2}(T_g - T_{g,2})\right] + w_2 \left[\left(H_B^{H,L}\right)_{T_g} - \left(H_B^{H,L}\right)_{T_{g,2}}\right] + \Delta H_{mix}^{H,L} = 0, \tag{1.71}$$

separated into three components: a nonspecific interaction term, a term that accounts for that part of the temperature dependence of the specific heat that is due to self-association, and a heat of mixing in the liquid state term. In this relation, $(H_B^{H,L})_{T_g}$ stands for the pure state enthalpy of the self-associating polymer at T_g, while $\Delta H_{mix}^{H,L}$ is the heat of mixing determined at blend's T_g. The thermodynamic Painter–Coleman association model has been found to predict well

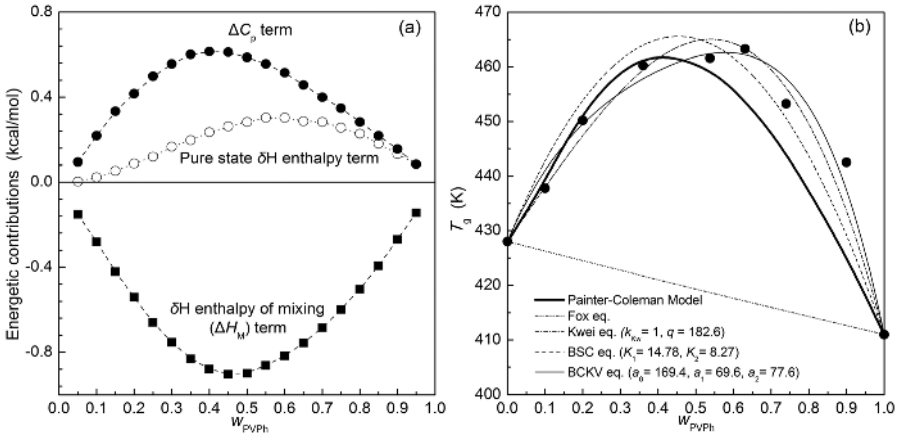

Figure 1.36 (a) Energetic contributions to the T_g equation, and (b) the predicted blend T_g for mixtures of PVPy with the self-associating PVPh. The prediction of the Fox equation (no specific interactions considered) and the results of various polynomial fitting functions (see Section 1.6.2.4) are included for comparison. After refs [263,281], with permission © 1991 American Chemical Society.

polymer–polymer miscibility and the glass-transition behavior of most hydrogen-bonded polymer blends, and particularly of mixtures characterized by a strongly negative heat of mixing. An illustrative example of this type provides the blends of self-associating PVPh and non-self-associating poly(vinyl pyridine) (PVPy) [281] (Figure 1.36), where strong intercomponent interactions are promoted by the presence of the pyridine group in PVPy, capable of accepting the hydrogen-bonding proton of PVPh. Other examples include mixtures of PVPh with poly(ethyl methacrylate-*co*-methyl methacrylate) [282], PVAc, PVME, P2VP or poly(4-vinyl pyridine) (P4VP) [283], poly(styrene-*co*-vinylphenol) + poly (tert-butyl acrylate) blends [281], PS4VP (15 mol% of 4-vinylpyridine) + poly (styrene-*co*-acrylic acid) (PSAA, 14 mol% acrylic acid) blends [284], poly(styrene-*co*-*N*,*N*-dimethylacrylamide) (PSAD, 17 or 25 mol% *N*,*N*-dimethylacrylamide) + PSAA (14, 18, 27, or 32 mol% acrylic acid) blends [284], poly(p-(hexafluoro-2-hydroxyl-2-propyl)styrene) with PVAc or poly(ethylene-*co*-vinyl acetate) [285], and PS4VP + poly(styrene-*co*-methacrylic acid) (PSMA, 15 mol% of methacrylic acid) blends [286]. Different types of $T_g(w)$ patterns reported for hydrogen-bonding miscible blends [287] are typically discussed in terms of entropy or enthalpy changes induced by the relative amount of intramolecular (self-association) and intermolecular hydrogen bonding. The Painter–Coleman association model can also produce – with moderate success, however – negative or even sigmoidal deviations of blend T_gs from the simple rule of mixtures [287], which may appear depending on the relative strength and the type of the compositional dependence of the energetic terms of Eq. (1.71) [281]. As a result of the relation among fragility and intermolecular interactions, the association model has been successfully applied to also predict blend compositions with maximal fragility [285].

Several other entropy-related models that feature adjustable parameters have also been considered [288,289] to account for interchain interactions that bring on strong entropy of mixing effects on the glass transition (i.e., negative excess mixing volumes) and produce structured mixtures. Kim and coworkers [288], for example, using configurational entropy and the Flory–Huggins theory derived the equation

$$T_g = \exp\left[\frac{z'R}{M_1\Delta C_{p,1}}\left(1-\gamma\ln\left(\frac{z'-1}{e}\right)\right)\left(\frac{\varphi_1}{r_1}\ln\varphi_1+\frac{\varphi_2}{r_2}\ln\varphi_2\right)+\left(\varphi_1\ln T_{g,1}+\varphi_2\ln T_{g,2}\right)\right], \tag{1.72}$$

with z' being the lattice coordination number. In Eq. (1.72,) $r_1 = v_1/v_0$ and $r_2 = v_2/v_0$, where v_i are the molar volumes of components 1 and 2, respectively, and v_0 is the unit lattice volume (normally set for convenience as $v_0 = 1$). In addition, γ is a proportionally constant, an adjustable parameter, representing the specific interaction between two polymers. Still, for routine applications the usability of the above relation is hampered by the poor knowledge of the required parameters. In another thermodynamic approach, by Lu and Weiss [289], the enthalpy of mixing is represented by a van Laar relationship (Eq. (1.51)), resulting in the relation

$$T_g = \frac{w_1T_{g,1}+kw_2T_{g,2}}{w_1+kw_2}+\frac{Aw_1w_2}{(w_1+kw_2)(w_1+bw_2)(w_1+cw_2)^2}, \tag{1.73}$$

where $A = \chi_{12}R(T_{g,2}-T_{g,1})c/M_1\Delta C_{p,1}$, $k \approx \Delta C_{p,2}/\Delta C_{p,1}$, $b = M_2/M_1$ (ratio of molecular mass of the repeat units of each polymer), and $c = \rho_1/\rho_2$. Reliable experimental estimates of the Flory–Huggins binary interaction parameter are usually difficult to obtain. Therefore, rather than predicting the $T_g(w)$ dependence for a given miscible polymer blend, this relation probably offers only a mean to calculate χ_{12} for a limited number of systems from their experimental $T_g(w)$ patterns. An example provides the results for poly(ether ketone ketone) (PEKK) + thermoplastic polyimide (TPI) blends (Figure 1.37). The values of χ_{12}, calculated from Eq. (1.73) for the three PEKK + TPI blends are −0.1, −1.0, and −2.4, respectively. The negative χ_{12} indicates an attractive interaction between PEKK and TPI, and its decreasing trend (i.e., more negative value) with increasing TPI concentration suggests miscibility improvement as the thermoplastic component increases [290].

1.6.2.4 Empirical Concentration Power T_g (w) Equations and Systems' Complexity

Given the complexity of the structures attained and the frequent lack of information from independent studies (e.g., data on the enthalpies of hydrogen-bond formation and the equilibrium constants used in the Painter–Coleman association model), it is often difficult to achieve predictions of blends' behavior based on fixed properties of the starting materials. The inclusion of several fitting parameters is thus considered inevitable in an attempt to alleviate the shortcomings of the established theoretical $T_g(w)$ equations. In the early 1950s, Jenckel

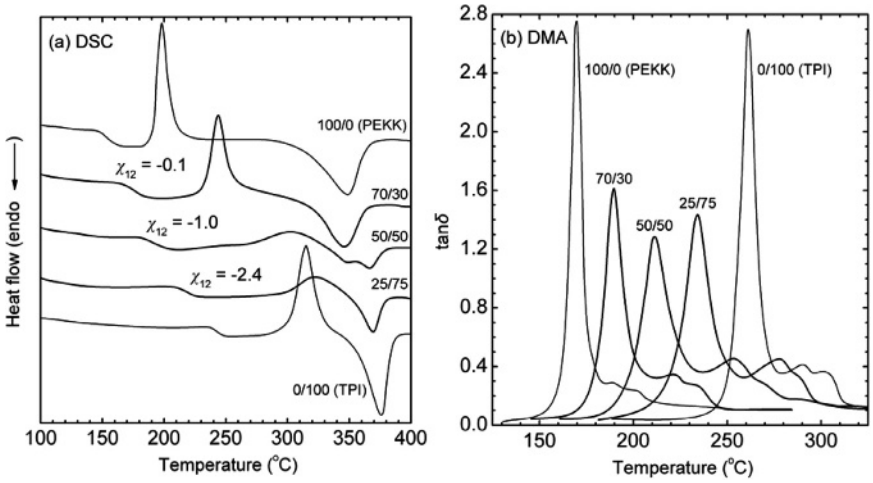

Figure 1.37 DSC (heating scans at 20 °C min^{-1}) and DMA (oscillating frequency 1 Hz, heating rate 2 °C min^{-1}) spectra for PEKK, TPI, and selected miscible blends. Both methods provide similar $T_g(w)$ dependences, which can be used in χ_{12} determinations based on the thermodynamic approach of Lu and Weiss. Replotted and adapted from ref. [290], with permission © 2004 John Wiley & Sons.

and Heusch [291] proposed for plasticized polymer blends an empirical concentration second-order power equation of the form

$$T_g = w_1 T_{g,1} + w_2 T_{g,2} + k_{JH}(T_{g,2} - T_{g,1}) w_1 w_2, \tag{1.74}$$

with a parameter, k_{JH}, used to characterize the solvent "quality" of the plasticizer molecules [291]. This relation can effectively describe strong, but only monotonic (all positive or all negative) and smooth, deviations from the linear mixing rule. Concentration second-order power equations for the compositional dependence of the blend T_g have also been proposed by Kanig [292], who related the changes in the interaction energies to the respective Gibbs energies for generating one mole of holes in the equilibrium polymer melt, and by DiMarzio [260], who assumed – beside flexible bond additivity – the effect of volume changes due to the different specific volumes of the blend components at T_g. In another widely applied approach, Kwei [293] extended the GT equation to a concentration second-order power equation by introducing a quadratic term, qw_1w_2, to read

$$T_g = \frac{w_1 T_{g,1} + k_{Kw} w_2 T_{g,2}}{w_1 + k_{Kw} w_2} + q w_1 w_2. \tag{1.75}$$

The physical meaning of the empirical Kwei parameters, k_{Kw} and q, has been the subject of subsequent interpretations based on the strength of specific interactions in the blend and the balance between the breaking of self-association interactions and the formation of interassociation interactions. By this equation, sigmoidal curves can be explained, but only with positive deviations from

additivity in the low-T_g range and negative deviations in the high-T_g range; to reproduce data showing the reversed behavior or more complicated dependences, additional correction terms are required. One of the most effective equations in describing complex $T_g(w)$ patterns is the phenomenological virial-like concentration third power function proposed by Brekner, Schneider, and Cantow (BSC equation) [294,295]

$$T_g = T_{g,1} + (T_{g,2} - T_{g,1})[(1 + K_1)w_{2c} - (K_1 + K_2)w_{2c}^2 + K_2 w_{2c}^3]. \qquad (1.76)$$

The variable $w_{2,c}$ is the expansivity-corrected mass fraction of the GT expression $w_{2,c} = kw_2/(w_1 + kw_2)$, with $k \approx T_{g,1}/T_{g,2}$. This functional form results directly from the assumption that both the free-volume distribution and the conformational mobility in polymer mixtures are dependent on the specific intercomponent interactions. It has been pointed out that parameter K_1 mainly accounts for the differences between the interaction energies of the binary heterointeractions (between different components) and homointeractions (between molecules of the same component), while parameter K_2 depends on contributions resulting from conformational entropy changes. Depending on the values of the fitting parameters of Eq. (1.76), K_1 and K_2, and of their difference, $K_1 - K_2$, it has become possible to categorize the glass-transition behavior of various binary systems into general classes [295].

Interestingly, even the two-parameter empirical equations fall short in describing very complex $T_g(w)$ behaviors that come into sight, when, for instance, at least one of the components partly crystallizes in the blend environment (Figure 1.38) [296], entropic or enthalpic factors prevail at different compositional ranges [251], or the neat components have almost identical segmental mobilities ($\Delta T_g \approx 0$, Figure 1.39). Tentative explanations of these discrepancies are often based on molecular size effects, the diminishing (or enhanced) free volume of one component in the presence of the other or composition-dependent excess mixing volume effects. As an example, the patterns of poly(epichlorohydrine) (PECH) + PVME [297] and PαMS + poly (cyclohexyl methacrylate) (PCHMA) [298] blends can be explained only by bearing in mind the combined effect of heterocontact formation on interchain orientation and the corresponding conformational entropy changes. A negative excess mixing volume – which signifies less space for molecular and macromolecular chain relaxation – is highly probable in the case of PECH + PVME. Here, according to the IR and ^{13}C NMR data of Alegría *et al.* [297], the heterocontacts between PECH (with —Cl as electron-acceptor moieties) and PVME (with —OCH_3 as electron-donating moieties) are merely slightly favored. Specific volume determinations corroborate an analogous interpretation for the case of the PαMS + PCHMA mixtures: in the intermediate composition ($w_1 = 0.5$), the specific volume calculated for the blend assuming volume additivity is $V_g = 0.966\ mL\ g^{-1}$, while the experimental value is only $0.958\ mL\ g^{-1}$ [298].

If the effects of the enthalpic and entropic changes are not symmetrical, then irregular patterns with maxima and/or minima deviating from the midpoint of

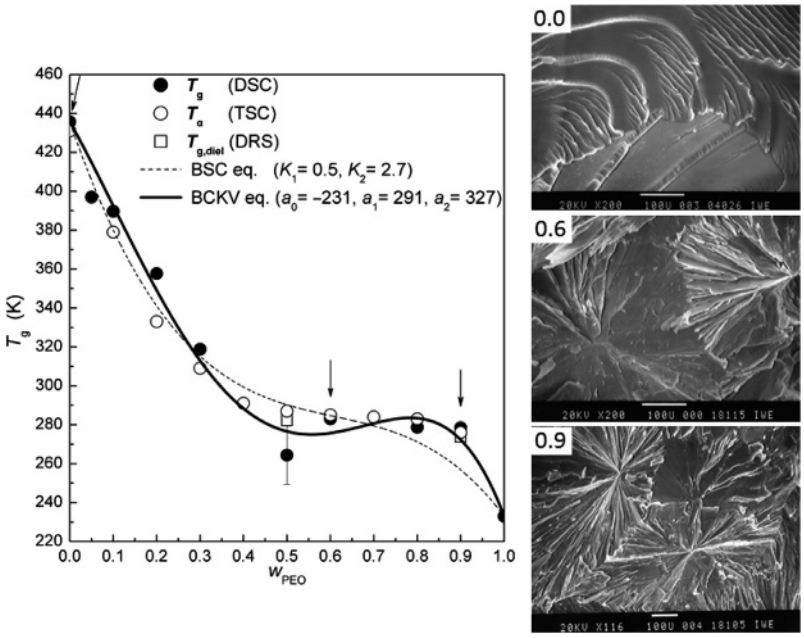

Figure 1.38 Plots of glass-transition temperatures as a function of blend composition for thermosetting networks prepared with PEO ($M_w = 4.0 \times 10^3$ g mol^{-1}). SEM images demonstrate the presence of spherulitic formations of crystalline PEO at $w_{PEO} \geq 0.5$. Fitting lines to the calorimetric data, based on the BSC and BCKV equations, are shown. Data taken from ref. [296], with permissions © 2007 American Chemical Society.

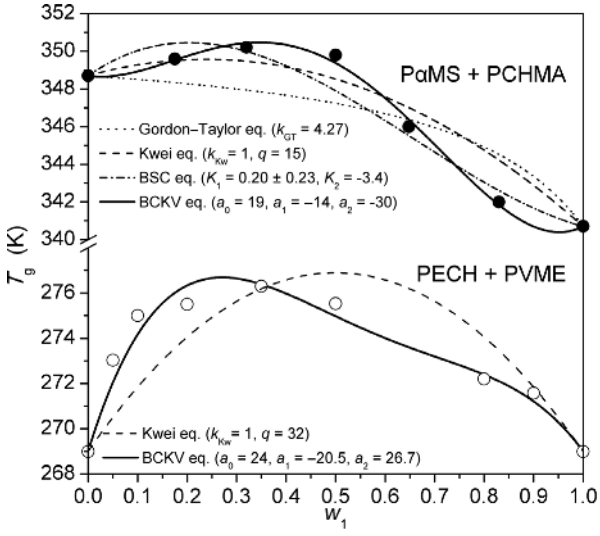

Figure 1.39 $T_g(w)$ plots of miscible blends of polymers with low T_g-contrast: PECH + PVME (dielectric loss peak at 1 kHz, $\Delta T_g \approx 0$) [297], PαMS + PCHMA (DSC data, $\Delta T_g = 8°$) [298]. From ref. [263], with permission © 2010 Elsevier.

the composition ($2w_1 - 1 = 0$) are usually observed. In view of that, an empirical three-parameter equation has been proposed by Brostow, Chiu, Kalogeras, and Vassilikou-Dova (BCKV equation) [299]

$$T_g = w_1 T_{g,1} + w_2 T_{g,2} + w_1 w_2 \left[a_0 + a_1 (2w_1 - 1) + a_2 (2w_1 - 1)^2 \right] \qquad (1.77)$$

and successfully tested in binary polymer mixtures, interpenetrating polymer networks, interpolymer complexes, and oligomeric organic + polymer blends [10,262,263]. The quadratic polynomial on the right-hand side of Eq. (1.77), centered around $2w_1 - 1 = 0$, is defined to represent deviations from linearity; that is, with $a_0 = a_1 = a_2 = 0$ the equation leads to the simple rule of mixtures. The number and magnitude of the adjustable parameters required to represent an experimental $T_g(w)$ pattern have been postulated to provide quantitative measures of system's complexity [10]. Based on detailed comparisons between the results obtained for a number of binary systems (Figure 1.40), using established equations and the BCKV function, the empirical parameter a_0 and its normalized form, $a_0/\Delta T_g$, have been shown to reflect mainly differences between the strengths of inter- and intracomponent interactions. The magnitude and sign of the higher order parameters are in part related to asymmetric (composition-dependent) energetic contributions of heterocontacts, entropic effects, and structural nanoheterogeneities (e.g., crystalline inclusions) observed in some blend compositions.

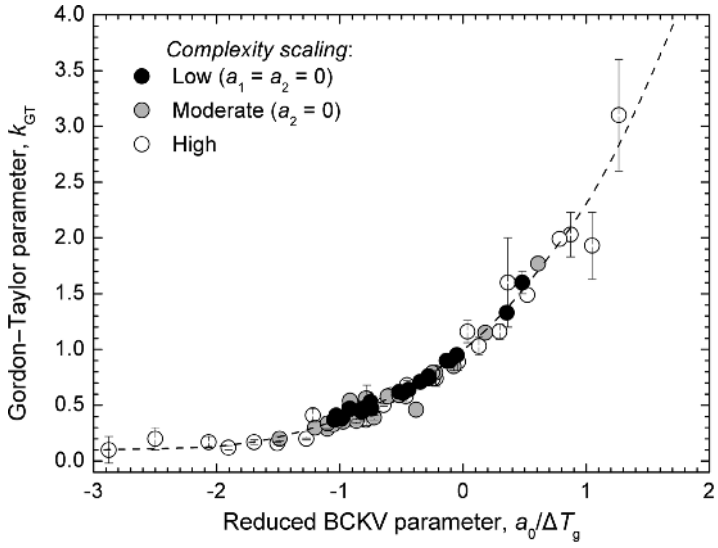

Figure 1.40 Dependence between the fitting estimates of the parameter of the GT equation (k_{GT}) and the reduced principal parameter of the BCKV equation ($a_0/\Delta T_g$). Data for over 80 binary polymer [262,263] and drug + polymer [10] (with permission © 2011 Elsevier) miscible systems are included. The dashed line is a guide for the eye.

1.6.2.5 Dynamically Heterogeneous Miscible Blends

In most miscible polymer mixtures, the calorimetric glass transitions are unusually broad (e.g., with asymmetrically broadened derivative peaks) and this feature is frequently accompanied by several well-known anomalies, such as the failure of the time-temperature superposition principle [300]. Display of two concentration-dependent glass transitions – a phenomenon long considered an indication of partial miscibility and large-scale spatial heterogeneities – has been proven to exist in several "dynamically heterogeneous" blends that are miscible on the molecular level. Dynamic heterogeneity is connected with the observation of distinct relaxation (dynamic) behavior for each component in a mixture, despite the existence of phase homogeneity. Traces of this behavior are already known from the late 1960s, as a result of the application of sensitive thermal analysis techniques (e.g., DMA data on PS + PPO blends), with the first report of bimodal calorimetric glass-transition signals in PS + PαMS blends dating back to 1982 [301]. Since then, bimodal transitions have been theoretically justified [302] and experimentally demonstrated (e.g., Figure 1.41) in a large number of molecularly mixed binary systems [252,303–314].

Both in the cases of the partially miscible and the dynamically heterogeneous miscible blends, a number of glass transitions are likely to be seen only in carefully conducted experiments with techniques of higher signal-resolving power, higher sensitivity (i.e., detection of much lower concentrations of relaxing segments of some type), and probes of sufficiently small length scale [300,304]. In studies of the relaxation behavior of PVME + PS blends, for example, Lorthioir

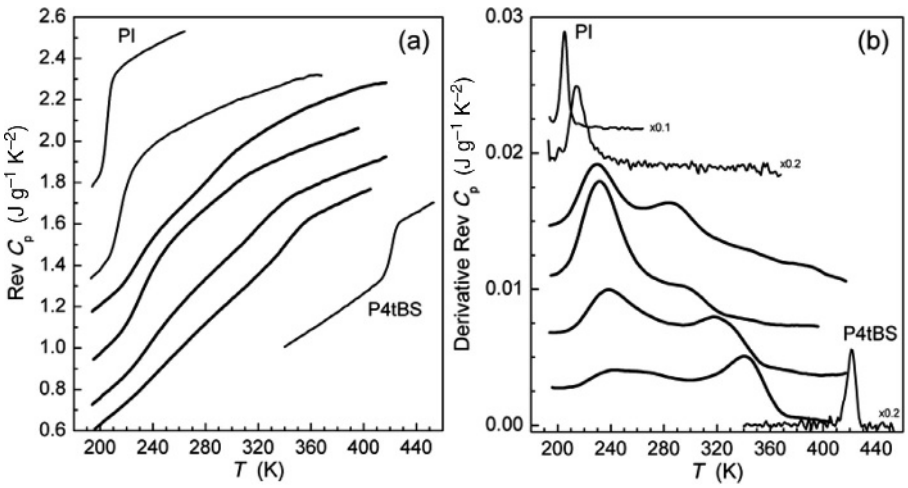

Figure 1.41 MTDSC thermograms of miscible PI + P4tBS blends: (a) reversible C_p curves, and (b) temperature derivative curves. From pure PI to pure P4tBS, the curves represent blends with PI mass fraction of $w_{PI} = 0.75$, 0.50, 0.40, 0.33, and 0.25, respectively, with two distinct glass transitions recorded at intermediate blend compositions. Vertical shifts and reduced scales (plot (b)) have been used for clarity. From ref. [303], with permission © 2009 American Chemical Society.

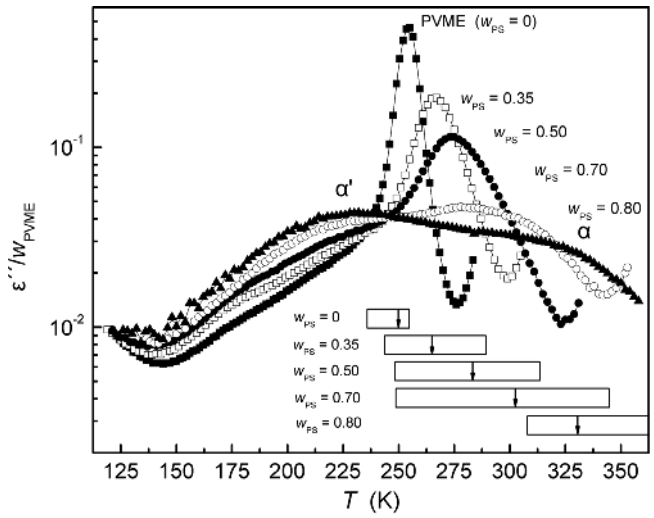

Figure 1.42 Isochronal $\varepsilon''(T)$ spectra obtained at $f = 1$ Hz on pure PVME and various PVME + PS blends. For each sample, ε'' values have been divided by the PVME weight fraction (w_{PVME}). The boxes below the curves indicate the breadth of the single calorimetric transitions recorded for each system, while vertical arrows indicate the midpoint T_g value. Adapted from ref. [304], with permission © 2003 American Physical Society.

et al. [304] observed a single glass-transition region in each blend composition by conventional DSC (Figure 1.42), while a bimodal dielectric relaxation signal is readily discernible in several mixtures. With reference to Figure 1.42, in the blend with $w_{PS} = 0.80$ the typical glass-transition mode (α-relaxation) appears near blend's calorimetric T_g (at 332 K), while a second glass-transition signal (α′-relaxation) forms at a much lower temperature (225 K) and relates to motions of polar PVME chain segments confined in a nonpolar matrix created by frozen PS chains. Note that near the calorimetric glass-transition temperature of the blend the relaxation rate of PVME is over three decades faster compared to that of PS segments.

Several approaches explore the origins of dynamic heterogeneity in polymer blends considering either differences in the intrinsic mobility of the components, thermal concentration fluctuations, the effect of chain connectivity, or combinations of them [304–311]. One approach extends the CM, in which cooperativity between neighboring molecules leads to a broad distribution of local environments (i.e., relaxation times) for each component. In terms of the free-volume theories, one may consider that a distribution of free volumes around component segments is responsible for a wide distribution of T_g values. Another approach highlights the contribution of thermodynamically driven local concentration fluctuations in generating and controlling the unique local environment experienced by each component [308,309]. These fluctuations are manipulated by component molecular masses and the binary interaction parameter χ_{12}.

Related models consider further the local concentration fluctuations to be quasi-stationary near the glass transition, since their average relaxation time is much longer than that of segmental dynamics in the same range of temperatures [308]. This approach has been successfully applied in a limited number of blends, indicating that the relevant length scale is roughly 10 nm near T_g.

The methodology developed by Lodge and McLeish (LM model) [311] puts forward an analysis of dynamic heterogeneity and the ensuing pair of effective glass transitions for each blend component ($T_{g,i}^{\text{eff}}(\varphi)$, with $i = 1, 2$) considering the "self-concentration" effect. As a consequence of chain connectivity, the average number of nearest neighbors of a given segment that belong to the same component is larger than the number of neighboring segments of the other component. Accordingly, in a region of volume V centered on the basic structural unit of each polymer in the miscible blend, the effective concentration sensed by each polymer segment will be larger than the macroscopic one (i.e., $\varphi_{\text{eff},i} > \varphi_i$). If the typical length scale associated with a relaxational process, as the glass transition, is such that $\varphi_{\text{eff},i}$ is larger than φ_i, the dynamics will be intermediate between that of the pure polymer and the average dynamics of the blend. In a different perspective, if the length scale of the probe is low enough to effectively sample and resolve segmental motions within such small volumes, then two glass-transition signals will be an immediate result. Based on the LM model, the effective local composition, that is, the local composition of the blend in a volume $V \sim l^3$ around the segment i, is described by the relation

$$\varphi_{\text{eff},i} = \varphi_{\text{self},i} + (1 - \varphi_{\text{self},i})\varphi_i, \tag{1.78}$$

where $\varphi_{\text{self},i}$ is the self-concentration of the pertinent polymer segment and φ_i the nominal (average) concentration of the same blend component. These local compositions might be quite different from that of the bulk as the flexibility of the polymer chain decreases. The length scale related to the monomeric friction factor is regarded of the same order as the Kuhn length, l_k (the length scale beyond which the conformation of the chain becomes Gaussian), defined as $C_\infty l_b$, where C_∞ is the characteristic ratio, and l_b is the length of the average backbone bond. The relaxation of the Kuhn segment is influenced by the concentration of monomers within a volume $V \approx l_k^3$. The self-concentration for each component is thus calculated as the volume fraction occupied by the Kuhn length's worth of monomers inside V, using the relation

$$\varphi_{\text{self}} = \frac{C_\infty M_0}{\rho k_b N_A V}, \tag{1.79}$$

where k_b is the amount of backbone bonds per repeat unit. In the framework of the LM model, each blend component experiences a distinct effective glass-transition temperature that depends on φ_{eff}. Estimates of the self-concentration (between 0.1 and 0.6 based on calculations using Eq. (1.79)) are initially used to determine the effective local concentrations. With the assumption that $T_{g,i}^{\text{eff}}(\varphi) = T_g(\varphi)\big|_{\varphi=\varphi_{\text{eff},i}}$, the effective glass-transition temperature of each component can be obtained using the Fox equation, and confronted to the experimental

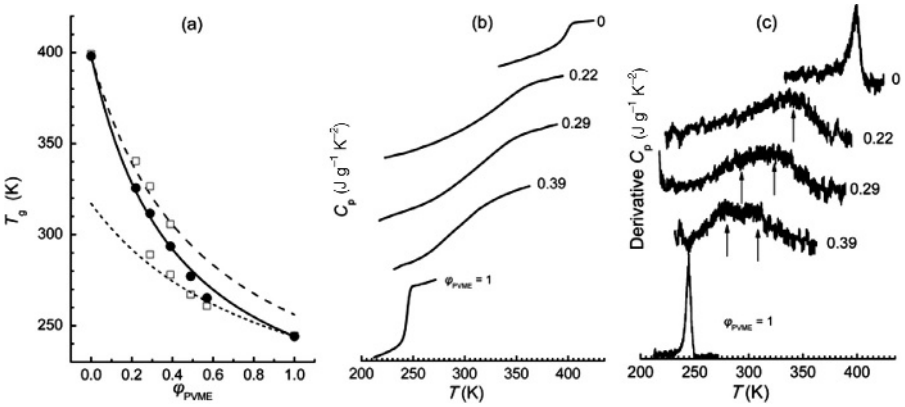

Figure 1.43 (a) $T_{g,av}$ (circles) and $T_{g,1}$ and $T_{g,2}$ (squares) of PVME + PoCS blends against φ_{PVME}. Dashed and dotted curves are $T_{g,eff}$ values for the PoCS and PVME components, respectively, calculated by the LM model. The solid curve is determined by the GT equation with $k_{GT} = 0.3$. (b) C_p curves. (c) Derivative C_p curves. $T_{g,1}$ and $T_{g,2}$ are assigned with arrows [306], with permission © 2005 American Chemical Society.

patterns [311–313,315]. Alternatively, the self-concentration can be incorporated as parameter in a suitable $T_{g,av}(\varphi)$ or $T_g^{eff}(\varphi)$ equation, to be indirectly obtained by subsequent fitting of experimental data [262,304–306,312]. In this manner, self-concentration quantifies the extent to which a component has its dynamics perturbed by the blend partner. The upper limit of $\varphi_{self} = 1$ denotes a component showing its pure or neat component dynamics, while $\varphi_{self} = 0$ corresponds to a component whose dynamics are slaved to those of the blend partner. An example of the application of the LM model analysis for miscible PVME + poly(*o*-chlorostyrene) (PoCS) blends is shown in Figure 1.43 [306].

Several papers provide comparisons of the LM model predictions to either calorimetric data or dynamic results (Table 1.4). The model is generally successful in predicting component dynamics in athermal polymer blends, though this success usually relies on using φ_{self} as a fitting parameter rather than using its theoretic estimate. In the case of PI + poly(vinylethylene) (PVE), for example, the theoretical value of $\varphi_{self,2}$ is very low to account for the observed behavior [316], suggesting that the self-concentration effect predicted by the LM model is not strong enough to account for the tracer dynamics of PVE in a PI matrix. Data evaluations are usually consistent with the model prediction of a smaller self-concentration for the slower component (i.e., $\varphi_{self,1}/\varphi_{self,2} > 1$), which is expected to arise from its stiffer backbone and larger Kuhn length (higher persistence length) [311]. Nevertheless, wide differences often appear between model predictions and experimental derivations of the self-concentration. Typically, theoretical predictions are based on the assumption that $V = l_k^3$, despite the fact that even within the assumptions of the LM model a length scale that is of the order of Kuhn's length, and not necessarily equal to it, is anticipated. Ample experimental evidence suggests that φ_{self}, for a given polymer, is matrix dependent,

Table 1.4 Examples of miscible binary polymer systems exhibiting distinct segmental dynamics for the components in the blend environment and results from their analysis in terms of the LM model.

System	ΔT_g (°C)	Experimental technique	$\varphi_{self,1}$	$\varphi_{self,2}$	Reference
PVAc + PMMA	44	Fluorescence spectroscopy	0.80[a)]	0.66[a)]	[314]
PI + PVE	60–65	DSC, NMR, DRS	0.45[b)]	0.25[b)]	[311,318]
				0.20[b)]	[319]
				0.50[a)]	[320]
PCHA + PCHMA	75	ESR, DSC	0.21[b)]	0.41[b)]	[305]
PEO + PVAc	96	DSC	0.26[b)]	0.23[b)]	[311]
			0.64[a)]	0.16[a)]	[313]
			0.40[a)]	0.08[a)]	[300]
PEO + PLA	110	DSC	0.37[a)]	0.19[a)]	[313]
PI + PS	130	^{13}C and ^{2}H NMR	0.45[b)]	0.27[b)]	[321]
			0.33[a)]	0.42[a)]	[321]
PVME + PS	130	MTDSC, DRS, TSC	0.25[c)]	0.27	[304,306]
	50–130	DEA, DSC[d)]			[239,322]
PVME + P2CS	150	DSC, DRS, SAXS	0.25[b)]		[240]
			0.62[a)]	0.24[a)]	[323]
PVME + PoCS	154	MTDSC, DRS, TSC	0.25[b)]	0.22[b)]	[304,311]
			0.15[c)]	0.20[c)]	[262]
PαMS (5-mer) + PαMS	180	DSC	0.22	0.22	[324]
			0.051[c)]	0.087[c)]	[324]
PCL + PSMAn(14)	190	TSC, DSC, WAXS	0.33[b)]	0.27	[325]
PEO + PMMA	200	DSC	0.23[b)]	0.25[b)]	[302]
			0.55[a)]	0.60[a)]	[302]
PCL + PC	206	DSC, DMA, TSC, WAXS	0.33[b)]	0.05[b)]	[312]
			0.47[a)]	0.19[a)]	[312]
			0.20[c)]	0.49[c)]	[312]
PI + P4tBS	215	MTDSC, DSC	0.45[b)]	0.2[b)]	[303]
			0.63[a)]	0.03[a)]	[303]

a) Result of fitting using the Fox equation.
b) Model prediction using Eq. (1.79) and $V = l_k^3$.
c) Result of fitting using complex $T_g(\varphi)$ equations.
d) In contrast to DEA, early DSC studies indicate only a single calorimetric signal.

and thus the addition of a geometric factor may be required [300,313,317]. The LM model ignores confinement effects, which may become important below the glass-transition temperature of the blend when the high-T_g component becomes glassy and confines the more mobile low-T_g component. In PI + poly

(4-*tert*-butylstyrene) (P4tBS) [303] and PEO + PMMA [302], for instance, the results reveal enhanced dynamics for the fast component in a miscible blend at temperatures beneath the glass-transition temperature of the slowest component (nonequilibrium or confinement effect). The model disregards concentration fluctuations or strong intermolecular interactions, which can influence both the mean relaxation time and the breadth of the distribution [300,304].

Several instances of borderline miscibility have been reported by examining the glass-transition behavior of binary systems of very weakly interacting polymers, such as PVAc with poly(methyl acrylate) (PMA) [254], PMMA [316], or PEO [313]. Miscibility or immiscibility has been reported for PVAc + PMMA blends, depending on the nature of the solvent [232,316,326], the conditions of mixing, and the type of thermal treatment [327]. It has been suggested that in solution the conformational changes resulting from hydrogen bond interactions between the two chemically similar polymers and the solvent molecules (chloroform) may be liable for miscibility [326]. The extremely weak enthalpic interaction among PEO and PMMA chains and the slightly negative Flory–Huggins interaction parameter are responsible for the marginal miscibility detected for PEO + PMMA blends, based on the single glass-transition temperature following a Fox-type compositional dependence [328]. The strong dynamic heterogeneity of the system (Table 1.4) is reflected in the complex compositional and temperature dependence of component relaxation times, which indicate that each component in the blend retains a separate rheological identity [328]. There are, in fact, frequent reports of two T_gs and complicated blend morphologies for compositions with PMMA as a majority component ($w_{PMMA} \geq 0.6$) [329]. Strong intermolecular hydrogen bonding, on the other hand, produces a coupling of the segmental dynamics of the components in blends of polymers with even very large intrinsic mobility differences. As a consequence, suppressed dynamic heterogeneity has been demonstrated in PVME + PVPh (for $w_{PVME} \leq 0.5$) [330], PVEE + PVPh (for $w_{PVEE} \leq 0.4$) [273,331], and poly(ethyl methacrylate) (PEMA) + PVPh [332] mixtures, while the time-temperature superposition principle has been reported to hold for PVEE + PVPh, or the strongly interassociated mixtures of PVPh with P2VP, P4VP, or PVAc [283], for which the Painter–Coleman model is also successfully applied.

1.7
Case Studies

1.7.1
Miscibility Achievement via Chemical Modification

In the absence of specific intermolecular interactions, the Gibbs free energy of mixing is usually positive for polymer blends, due to the small combinatorial entropy of mixing and the positive enthalpy of mixing. Consequently, to exhibit thermodynamic miscibility of the blend, in general, there needs to be some

degree of intermolecular interactions (e.g., hydrogen bonding, ion–dipole, π–π, and charge-transfer interactions) that will provide a favorable heat of mixing. Hydrogen bonding is a particularly important mechanism to expand the range of miscible polymer pairs since if no favorable interactions are present miscibility is very rare and is only found when solubility parameters match each other ($\Delta\delta_{crit} \leq 0.1$ $(MPa)^{1/2}$). If favorable weak interactions are present (e.g., dipole–dipole forces), miscibility can be found even if the difference in solubility parameters approach $\Delta\delta_{crit} = 1.0\,(MPa)^{1/2}$, but when hydrogen bonds are established it can go up to ~6.0 $(MPa)^{1/2}$ [3].

Over the past few decades, there has been considerable interest in enhancing the miscibility of polymer blends, either by adding a third component as a compatibilizing agent or by introducing specific functional groups into the polymers to promote exothermic interactions between them. Many novel and useful polymer blends have been produced in this manner, with the styrene-based polymers constituting an important category (Table 1.5). In the absence of specific interactions between segments of PS and PMMA, for example, their blends exhibit a

Table 1.5 Type of the deviation from the linear mixing rule and description of the T_g (w) patterns in selected miscible binary blends containing styrene-type units (DSC data).

Polymer 1[a)]	Polymer 2[a)]	ΔT_g (°C)	$T_g(w)$ patterns		Ref.
			Deviation	Comments	
PαMS	PCHMA	8	Positive	Complexity: BSC ($K_1 = 0.20$, $K_2 = -3.4$), BCKV ($\alpha_0 = 19$, $\alpha_1 = -14$, $\alpha_2 = -30$). Solvent: chloroform	[258,263]
SAN (17.3)	PMMA	8	Positive	BCKV ($\alpha_0 = 12$, $\alpha_1 = -8$, $\alpha_2 = 0$). Solvent: chloroform	[254,263]
PSCA(15)	P4VP (16.6)	13	Positive	Kwei ($q = 50$, $k_{Kw} = 1$). Hydrogen bonding and partial protonation of the pyridine units (FTIR). Solvent: DMF	[337]
PS4VP (5–50)	PSMA(20)	16. . .33	Positive	Kwei ($q = 20$. . .60, $k_{Kw} = 1$). Hydrogen bonding (FTIR). Solvent: chloroform	[338]
PS4VP (15)	PSAA(14)	15	Positive	Painter–Coleman model. BCKV ($\alpha_0 = 21$, $\alpha_1 = 5.6$, $\alpha_2 = 2.4$). Solvent: THF	[284]
PSAD(17)	PSAA(18)	17	Positive	BCKV ($\alpha_0 = 21.6$, $\alpha_1 = 0.1$, $\alpha_2 = 17$). Solvent: THF	[263,339]
PSAD(17)	PSAA(27)	20	Negative	BCKV ($\alpha_0 = -4.9$, $\alpha_1 = 2.6$, $\alpha_2 = -6.2$). Solvent: THF	[263,340]
PSAD(25)	PSAA(14)	21	Negative	Painter-Coleman model. BCKV ($\alpha_0 = -38.8$, $\alpha_1 = -6.13$, $\alpha_2 = 67.46$). Solvent: THF	[284]
PSAD(17)	PSAA(32)	26	Negative	BCKV ($\alpha_0 = -64.9$, $\alpha_1 = 36$, $\alpha_2 = -4.5$). Solvent: THF	[263,340]

PS	PPE	24 . . . 122	Negative	BCKV: $\alpha_0/\Delta T_g = -1.04 \ldots -0.20$. Solvent: benzene	[262,341]
PVPhKH	PS4VP	30	Positive	GT ($k_{GT} = 2.03$). Hydrogen bonding (FTIR). Solvent: chloroform	[221]
PSCA(15)	PS4VP(17)	31	Positive	Kwei ($q = 22$, $k_{Kw} = 1$). Hydrogen bonding (FTIR). Solvent: DMF	[342]
PS4VP (15)	PSMA(15)	33	Positive	Painter–Coleman model. BCKV ($\alpha_0 = 77.46$, $\alpha_1 = 0.18$, $\alpha_2 = -63.33$). Hydrogen bonding and partial protonation of the pyridine units (FTIR). Solvent: THF	[286]
PIBM4VP (20)	PSMA(12)	39	Positive	Kwei ($q = 12.81$, $k_{Kw} = 1$). BCKV ($\alpha_0 = 13.8$, $\alpha_1 = \alpha_2 = 0$). Solvent: heptane	[263,343]
PIBM4VP (10)	PSMA(12)	49	Negative	BCKV ($\alpha_0 = -64.8$, $\alpha_1 = 74$, $\alpha_2 = -12.6$). Solvent: heptane	[263,343]
PSHS(28)	PNB	43	Negative	GT ($k_{GT} = 0.33$). Hydrogen bonding (FTIR). Solvent: anisole	[344]
PSHS(5)	PNB	64	Negative	GT ($k_{GT} = 0.37$). Hydrogen bonding (FTIR). Solvent: anisole	[344]
PIBM4VP (20)	PSMA(29)	76	Positive	Kwei ($q = 38.6$, $k_{Kw} = 1$). BCKV ($\alpha_0 = 39.6$, $\alpha_1 = -25$, $\alpha_2 = -58$). Solvent: heptane	[263,343]
PA-6	MnSPS	81	Positive	Lu–Weiss. $-2 < \chi_{12} < -1.5$. Specific interactions among MnS and amide groups (FTIR). Solvent: *m*-cresol	[289]
PS	TMPC	93	Negative	Solvent: THF	[236]
PS	PPO	107 . . . 205	Negative	BCKV: $\alpha_0/\Delta T_g = -0.28 \ldots -0.74$. Solvent: benzene	[263,279]
PVME	PS	50 . . . 135	Negative	BCKV: $\alpha_0/\Delta T_g = -0.22 \ldots -0.66$. Solvent: toluene	[263,295]
PVME	PS	123	Negative	BCKV ($\alpha_0 = -142$, $\alpha_1 = 33$, $\alpha_2 = 0$). Dynamically heterogeneous (van der Waals interactions). Solvent: toluene	[262,345]
PVME	P2CS	154	Negative	BCKV ($\alpha_0 = -150$, $\alpha_1 = 81$, $\alpha_2 = 0$). Dynamically heterogeneous (dipole–dipole interactions). Solvent: toluene	[234,262]

a) Numbers in parentheses denote the molar percentage of the second monomer in each copolymer, with the exception of SAN for which the number refers to weight percentage.

distinct phase-separated morphology. Miscibility with PMMA is only achieved by chemical modification of the molecules, such as by incorporation of hydrogen-bonding capable functional groups along the chains of PS. The copolymer poly(styrene-*co*-acrylonitrile) (SAN), with 17–24 wt.% acrylonitrile, provides an interesting case [333]. Given the small T_g contrast of the components ($\Delta T_g \leq 10°$), conventional DSC data appear insufficient to differentiate among miscible SAN + PMMA blends and their immiscible physical mixture. In the latter

case, the bimodal structure of the glass-transition signal (two T_gs) becomes apparent only in differential heat capacity spectra obtained using MTDSC and for systems with ΔT_g exceeding ~5°. Styrene-hydroxy styrene copolymers (PSHS) also form miscible blends with various polymers, such as a homologous series of poly(alkyl methacrylate)s [334], PCL [335], poly(acrylic acid) [336], and polyethers [271]. Hydrogen bonding between the carbonyl ester groups and the hydroxyl groups in hydroxystyrene units inserted into PS chains provides the driving force for miscibility. Similarly, a number of studies suggest improved miscibility of PS with P4VP, or PS4VP, by incorporating proton-donor monomers (acrylic acid, *p*-vinyl phenol, cinnamic acid, maleic acid, or methacrylic acid, etc.) into PS, to utilize the proton acceptor nature of 4-vinylpyridine.

For the systems included in Table 1.5, a tendency appears to develop for positive departures of the $T_g(w)$ patterns from the linear mixing rule (mass additivity) for low ΔT_g's (<20°) and negative deviation for blends with intense dynamic asymmetry. The type of the $T_g(w)$ dependences and metric properties of these patterns depend on the interplay of entropic (free volume) and enthalpic (relative strength and extend of intercomponent interactions) factors. The relative significance of each factor bears influences from a number of parameters, such as the molecular mass [279,295,341] and flexibility of the polymer chains, the type and accessibility of the functional groups, and the conditions of blend preparation (melt mixing or solvent cast). As an example, the compositional variation reported for the T_gs of the miscible binary blends formed by the weakly interacting PS and PPO ($\chi_{12} = -0.06$) shows a decreasing departure from linearity with increasing molecular mass of PS (Figure 1.44a) [279]. In addition,

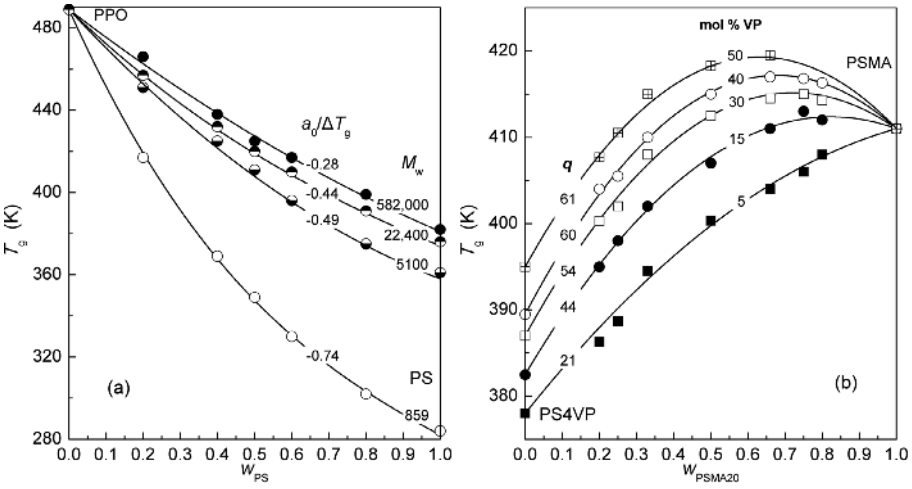

Figure 1.44 Compositional variation of the glass-transition temperatures recorded for (a) PS + PPO blends, with PSs of different molecular masses: $M_w = 859$, 5100, 22 400, and 582 000 g mol^{-1} [263,279] (with permission © 2010 Elsevier), and (b) PS4VP + PSMA20 blends, with PS4VP of different 4-vinylpyridine loadings: 5, 15, 30, 40, or 50 mol% [338], with permission © 2011 John Wiley & Sons.

depending on the nature of the interacting species, their densities within the polymer chains, and the nature of the solvent [344,346], miscible polymer blends, or interpolymer complexes can be prepared [338,342,343]. Benabdelghani and Etxeberria [338], for example, reported a gradually intensified elevation of the $T_g(w)$ pattern (Figure 1.44b), accompanied by higher thermal stability for the blends and a stronger intercomponent hydrogen-bonding interaction, with an increasing amount of 4-vinylpyridine units in PS4VP + PSMA blends. Conversely, in PSAD + PSAA blends, Djadoun and coworkers [339,340] observed a shift to an increasingly negative deviation as the density of the carboxylic groups within PSAA increases (e.g., by using copolymers with 18, 27, or 32 mol% acrylic acid), due to the occurrence of higher amounts of self-associated carboxyl groups and the corresponding reduction in heterocontacts.

A fair amount of research activity has been devoted particularly to miscible systems comprising PVPh – otherwise referred to as poly(4-vinyl phenol), poly(*p*-hydroxystyrene), poly(4-hydroxystyrene) (P4HS), or poly(*p*-vinyl phenol) – and its copolymers, since the hydroxyl group at para position of the pendent phenyl ring is capable of hydrogen bonding with proton-accepting functional groups (carbonyl, ether) found in several other amorphous (Table 1.6) or partially crystalline (Table 1.7) polymers [347–369]. Thermal analysis studies of the glass transformation range clearly demonstrate miscibility of PVPh with polymers such as poly(vinyl pyrrolidone) (PVP) [347], *polyacrylates* (e.g., PMA and PEA), and *polymethacrylates* (e.g., PMMA, PEMA, and poly(*n*-propyl methacrylate) [P*n*PMA]) [249,352], *polyethers* (e.g., PEO) [348]), *poly(vinyl alkyl ethers)* (e.g., PVME [271,283,330] and PVEE), and *polyketones* (poly(vinyl methyl ketone)). In addition, PVPh can also form miscible blends with PVAc and its random copolymers, a number of *aliphatic polyesters*, such as PCL [271], poly(butylene succinate) (PBSuc) [349], poly(ethylene succinate) (PESuc) [350], poly(*β*-hydroxybutyrate) (PHB) [351], poly(hydroxyvalerate) (PHV) [353], poly(ethylene adipate) (PEA), and poly(butylene adipate) (PBA) [353], poly(L-lactide) (PLLA), poly(D,L-lactide) (PDLLA) [355,356], as well as some *aromatic polyesters* (e.g., PET, poly(butylene terephthalate) (PBT) [354] and PTT [357]). An early review of the glass-transition behavior and miscibility of PVPh with a number of classes of polymers, including polyamides, polyimides, polyurethanes, polyesters, and PCs, has been published by Landry and coworkers [369].

Blends that are prepared by solvent casting often do not represent an equilibrium structure due to varying solvent–polymer interactions among their constituents. This is particularly true for strongly intermolecularly interacting systems, with the limiting case corresponding to solvent-induced phase separation when solvent molecules interact more strongly with one of the blend components. In view of that, several reports indicate that the nature of the solvent has a noticeable effect on the shape of the composition dependence of the glass-transition temperatures. The glass-transition and segmental relaxation dynamics of PVPh + PMMA blends, for instance, have been studied by a number of techniques, which indicate that PMMA and PVPh are miscible at all compositions and over a wide temperature range, due to strong intercomponent hydrogen

Table 1.6 Type of the deviation from the linear mixing rule and description of the T_g (w) patterns in selected miscible binary blends of PVPh with amorphous polymers (DSC, MTDSC, or DRS data).

Second component	ΔT_g (°C)	$T_g(w)$ patterns		Ref.
		Deviation	Description and comments	
PVPy	17	Positive	Kwei ($q = 183$, $k_{Kw} = 1$)	[281]
PATM	21	Positive	Kwei ($q = 86$, $k_{Kw} = 1$), BCKV ($\alpha_0 = 11.5$, $\alpha_1 = 0$, $\alpha_2 = -33$). Solvent: THF	[358]
PVP	25	Positive	Kwei ($q = 140$, $k_{Kw} = 1$). Solvent: DMF	[347]
P4VP	27	Positive	Kwei ($q = 96$, $k_{Kw} = 1$), $\chi_{12} = -18.2$, $\Delta\nu = 410\,cm^{-1}$. Solvent: MEK	[283]
PAA	50	Negative	Solvent: DMF	[359]
Phenoxy	55	Negative	Entropy changes due to a decrease in the density of hydrogen bonding. Solvent: THF	[360]
PMMA	66	s-Shaped	BCKV ($\alpha_0 = 2.3$, $\alpha_1 = 55$, $\alpha_2 = 46$). Solvent: MEK	[249]
PTHFMA	72	Positive	Kwei ($q = 30.3$, $k_{Kw} = 1.38$), BCKV ($\alpha_0 = 64.1$, $\alpha_1 = -14.9$, $\alpha_2 = -71.2$). Solvent: THF	[361]
PEMA	76	Positive	BCKV ($\alpha_0 = 35.1$, $\alpha_1 = 7.3$, $\alpha_2 = 6.8$). Solvent: MEK	[282]
P2VP	83	Positive	Kwei ($q = 58$, $k_{Kw} = 1$), $\chi_{12} = 2.9$, $\Delta\nu = 395\,cm^{-1}$. Solvent: THF[a)]	[283]
Phenolic	84	Negative	Deviation result of an entropy change corresponding to a decrease in the density of hydrogen bonding. Solvent: THF	[360]
P*n*PMA	85	Positive	Kwei ($q = 10$, $k_{Kw} = 1.17$), BCKV ($\alpha_0 = 19.5$, $\alpha_1 = 57.4$, $\alpha_2 = -7.6$). Solvent: 2-butanone	[361]
PMTMA	118	Positive	Kwei ($q = 86$, $k_{Kw} = 1$), BCKV ($\alpha_0 = 67.9$, $\alpha_1 = 54.4$, $\alpha_2 = 95.7$). Solvent: THF	[358]
PMA	143	Negative	BSC ($K_1 = -0.36$, $K_2 = -0.90$). Solvent: acetone	[346]
PVAc	152	Negative	Kwei ($q = -84$, $k_{Kw} = 1$), $\chi_{12} = -2.67$, $\Delta\nu = 72\,cm^{-1}$. Solvent: MEK	[283]
PEEMA	160	s-Shaped	Kwei ($q = -144$, $k_{Kw} = 3.2$), BCKV ($\alpha_0 = 34.5$, $\alpha_1 = 101.3$, $\alpha_2 = 0$). Solvent: acetone	[362]
PEA	172	Negative	BSC ($K_1 = 0.19$, $K_2 = -0.62$). Solvent: acetone	[346]
PVEE	186	s-Shaped	BCKV ($\alpha_0 = 2.3$, $\alpha_1 = 55.0$, $\alpha_2 = 45.6$). Solvent: MEK	[249,273]
PVME	178	Negative	Kovacs ($g = -0.011$, $\varphi_{2c} = 0.49$, $T_{crit} = 344\,K$). Solvent: THF	[271]
	188	Positive	GT ($k_{GT} = 1.1$), independent of the solvent used (THF, acetone)	[363]
	200	Negative	Kwei ($q = -152$, $k_{Kw} = 1$), $\chi_{12} = -0.45$, $\Delta\nu = 210\,cm^{-1}$. Solvent: MEK	[283]

a) $\Delta\nu$ = difference between the vibrational frequencies of free and hydrogen-bonded (OH $\cdots$ O=C) hydroxyls.

Table 1.7 Type of the deviation from the linear mixing rule and description of the T_g (w) patterns in selected miscible binary blends of amorphous PVPh with semicrystalline polymers (DSC data). The reported parameters of the Kwei and BCKV equations are assessed from curve fitting of as-received $T_g(w)$ data, without correction for the real composition of the amorphous phase.

Second component	ΔT_g (°C)	$T_g(w)$ patterns		Ref.
		Deviation	Description and comments	
PBN	81	None	Kwei ($q = 0$, $k_{Kw} = 1$), $\chi_{12} < 0$. Solvent: *n*-hexane	[364]
PTT	105	None	$B = -7.8$ cal cm^{-3}, $\chi_{12} = -0.74$. Melt blending	[357]
PLLA	118	Negative	Kwei ($q = -78$, $k_{Kw} = 1$), $B = -8.8$ cal cm^{-3}, $\chi_{12} = -0.42$. Solvent: dioxane	[355]
PDLLA	120	Negative	Kwei ($q = -87$, $k_{Kw} = 1$), $B(w) \leq -11.8$ cal cm^{-3}. Solvent: THF	[356]
PHB	141	Negative	Complexity: amorphous PVPh squeezed into the interlamellar region of PHB (BCKV: $\alpha_0 = -70$, $\alpha_1 = -11$, $\alpha_2 = 50$). $\chi_{12} = -1.4$, $B = -12.5$ cal cm^{-3}. Solvent: THF + chloroform (1:1)	[351]
PHV	157	Negative	Kwei ($q = -38$, $k_{Kw} = 0.45$), $\chi_{12} = -1.2$. Solvent: THF	[353]
P(3HB-*co*-3HH)	168	Negative	Complexity: BCKV ($\alpha_0 = -143$, $\alpha_1 = 18$, $\alpha_2 = 75$). GT ($k_{GT} = 0.45$). Blends prepared with 20 mol% 3-HH. Strong intermolecular δH (FTIR). Solvent: acetone	[365]
P(BA-*co*-BT)	181	Negative	Kwei ($q = -82$, $k_{Kw} = 1$), $\Delta\nu = 101$ cm^{-1}. Melt blending	[354]
PBT	183	None	Kwei ($q = 5$, $k_{Kw} = 1$), $\Delta\nu = 103$ cm^{-1}. Melt blending	[354]
PESuc	191	Negative	Complexity: BCKV ($\alpha_0 = -287$, $\alpha_1 = 262$, $\alpha_2 = -201$). Solvent: DMF	[350]
PMDL	206	s-Shaped	Complexity: BCKV ($\alpha_0 = 28$, $\alpha_1 = -60$, $\alpha_2 = -95$). Miscibility dictated by enthalpic (δH at $w_{PVPh} \geq 0.28$) or entropic (random mixing at $w_{PVPh} < 0.28$) factors. Solvent: THF (and precipitation in hexane)	[251]
PBSuc	208	Negative	Complexity: BCKV ($\alpha_0 = -281$, $\alpha_1 = 175$, $\alpha_2 = -57$), $\chi_{12}(w) = -1.03 \ldots -2.57$. Solvent: DMF	[349]
PCL	210	Negative	Kwei ($q = -85$, $k_{Kw} = 1$), B = −9.82 cal cm^{-3}, $\Delta\nu = 85$ cm^{-1}, $\Delta\nu* = -65$ cm^{-1}. Solvent: THF[b)]	[335]
PBA	211	Negative	Kwei ($q = -225$, $k_{Kw} = 1$), $\Delta\nu = 95$ cm^{-1}. Solvent: THF	[354]
PBSA	215	Negative	Kwei ($q = -160$, $k_{Kw} = 1$), $\chi_{12} = -0.82$. Solvent: THF	[366]
PEO	217	Negative	Kovacs ($g = -0.020$, $\varphi_{2c} = 0.62$, $T_{crit} = 348$ K). $\chi_{12} = -1.5$. Solvent: THF	[271,348,367]
PESeb	229	Negative	Kwei ($q = -125$, $k_{Kw} = 1$). δH interactions (FTIR). $\chi_{12} = -1.3$, B = −4.7 cal cm^{-3}. Solvent: MEK	[368]

a) All blends prepared by the solvent-casting method except from PBT or P(BA-co-BT) + PVPh that were prepared by melt blending, and miscible PLLA or PDLLA + PVPh prepared by solution precipitation.

b) $\Delta\nu*$ = difference between the vibrational frequencies of self-associated (OH···OH) and interassociated (OH···O=C) hydrogen-bonded hydroxyls.

bonding. In the miscible blends obtained by solution casting from methyl ethyl ketone (MEK) solution, the breadths of the glass-transition regions in the blends are only slightly broader (15°–20°) compared to those found in neat PMMA or PVPh (~10°) [249]. In contrast, the same polymers are trapped in a phase-separated state when THF is used as solvent [346], since their solubility in this liquid is significantly different and PMMA precipitates first during the solvent evaporation process [370]. The ^{1}H spin-lattice relaxation times of PMMA and PVPh show no change in the blend environment [371], a result also advocating immiscibility of the polymers at the length scale of the ^{13}C cross-polarization/magic angle sample spinning NMR study. An analogous behavior is found in several other systems, including blends of poly(acrylic acid) (PAA) with PVPh, solvent-cast from *N*,*N*-dimethylformamide (DMF) (miscible, at a molecular length scale 2–3 nm, as evidenced by NMR data and the single-T_g criterion) or ethanol (immiscible, two composition-independent T_gs) [359].

Generally speaking, the irregular $T_g(w)$ patterns observed for several binary mixtures point toward the existence of a complex system, in the sense that at least one important property (e.g., the degree of polymers' mixing, the relative balancing between hetero- and homocontacts or between enthalpic and entropic contributions, and the tendency for crystallization) has a distinctive compositional dependence [263]. Inspecting the data presented in Tables 1.5–1.7, the question that emerges is why both positive and negative deviations in T_g – or, even, both miscibility and immiscibility – occur in systems featuring intermolecular hydrogen bonding. Undoubtedly, factors such as the length of the repeating unit and the degree of polymerization, the mobility of the side chains, and the number (density) and accessibility of the hydrogen-bonding functional groups in each polymer have a drastic effect – in a not always predictable way – on the phase behavior. An example provides the combined DSC and FTIR studies of Lee and Han [364] in blends of PVPh with poly(*n*-alkylene 2,6-naphthalate)s containing alkylene units of different lengths. The number of methylene units in the polyester affects chains' mobility and the accessibility of the ester carbonyl functional groups toward the hydroxyl groups of PVPh, which in turn impact glass-transition behavior and miscibility. Accordingly, blends of poly(ethylene 2,6-naphthalate) or poly(trimethylene 2,6-naphthalate) with PVPh demonstrate partial or complete immiscibility, while poly(butylene 2,6-naphthalate) (PBN) appears miscible with PVPh over the whole range of compositions in the amorphous state. Disregarding possible effects from the use of different solvents, the $T_g(w)$ patterns of the various polymethacrylates included in Table 1.6 also indicate a tendency for stronger positive deviation from additivity with increasing number of proton accepting groups in the side chain of the thermoplastic component. In accordance with this, the reduced prime BCKV parameter increases from $\alpha_0/\Delta T_g = 0.035$ in PMMA (one carbonyl group per side chain) to 0.590 in poly(methylthiomethyl methacrylate) (PMTMA) (two proton acceptor groups per side chain) and goes up to 0.890 in poly(tetrahydrofurfuryl methacrylate) (PTHFMA) (three different groups per side chain). For PVPh + PMTMA, in particular, FTIR studies indicate strong hydrogen-bonding

interactions between the thioether sulfur atoms of PMTMA and hydroxyl groups of PVPh, while NMR reveals structural homogeneity extending down to ~3 nm.

A number of studies also provide information on differences in the degree and strength of intercomponent hydrogen-bonding interactions present in polymer blends and the corresponding copolymers, and their effect on the glass-transition behavior [287,372,373]. According to the Painter–Coleman association model, the interassociation equilibrium constant of PEMA-*co*-PVPh ($K_A = 67.4$) is higher than the interassociation equilibrium constant of PEMA + PVPh ($K_A = 37.4$), indicating that the experimental T_g's for copolymers and blends of the same composition should be different. This situation has been experimentally verified by Coleman and coworkers, who demonstrated a higher T_g in copolymer's case [272]. A plausible explanation of the observation considers the different degrees of rotational freedom that arise from intermolecular screening and spacing effects. Furthermore, spectroscopic studies reveal that the number of hydrogen bonds formed between hydroxyl and ester groups in PEMA + PVPh blends is significantly smaller than in random PEMA-*co*-PVPh copolymers containing the same segments. Similar behavior is found in PVP-*co*-PVPh copolymers and the corresponding PVP + PVPh blends [287], or PMMA + poly(methyl acrylic acid) (PMAA) and PMMA-*co*-PMAA (Figure 1.45 [373]), but not in non–hydrogen-bonding systems, such as those comprising isoprene and vinyl ethylene units (PI-*block*-PVE copolymers and PI + PVE blends [372]).

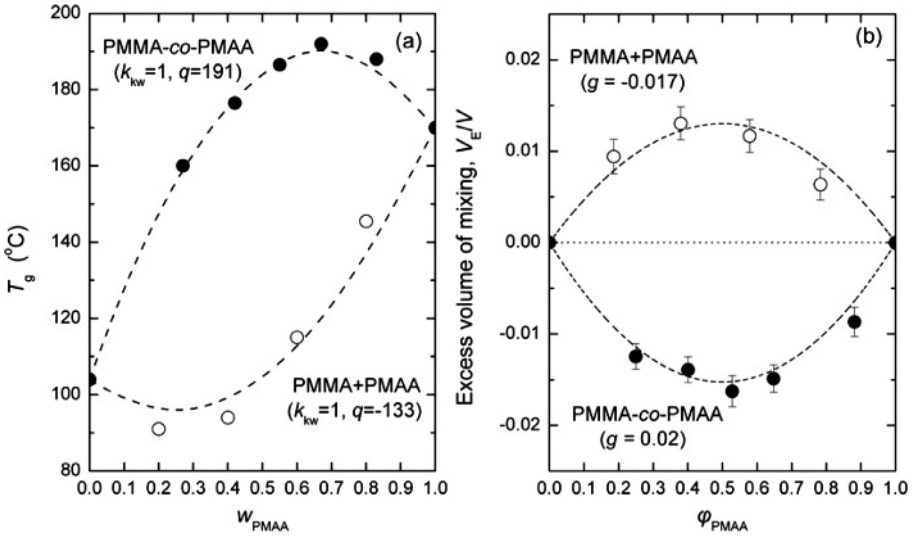

Figure 1.45 Comparison of the composition dependences of T_g (a) and the excess mixing volume (b) for PMMA + PMAA blends and PMMA-*co*-PMAA copolymers. The dashed lines show the fitting results of the Kwei equation (plot a), and the excess mixing volume predictions of the Kovacs' free-volume theory (plot b). Replotted data from ref. [373], with permission © 2003 Elsevier.

1.7.2 Microstructure of the Amorphous Phase in Semicrystalline Blends

Blending of crystalline with amorphous polymers is a convenient way for the development of amorphous–crystalline interfaces and various morphological patterns, which may result in an improvement of several physical properties (e.g., toughness, ductility, and impact strength). Although the miscibility window and structural morphologies of related systems have been methodically described in time course, intense research activity is still engaged in studies of aspects of the segregation between the crystalline/amorphous interface and of the possible relationships between intercomponent interactions and domain size of the separated phases. Detection of a single glass transformation range is typical of the nonrigid (bulk-like) miscible amorphous phase, formed by the amorphous fraction of the crystalline polymer and the amorphous component, with miscibility achievement generally interpreted as a result of specific (hydrogen bonding [335]) or nonspecific interchain interactions, or by simply invoking the matched polarity of the blend components [374].

The aliphatic polyester PCL provides an illustrative paradigm of technologically important semicrystalline polymers, offering a potential replacement for conventional polymers due to its biodegradability and low-temperature adhesiveness. PCL is known for its ability to provide miscible blends with polymers, such as chlorinated polyethylenes [375], PVC [376], PC [377], SAN (with 8–28 wt.% acrylonitrile) [378,379], poly(styrene-*co*-maleic anhydride) (PSMAn, with 14 mol% maleic anhydride) [325], poly(styrene-*co*-vinylphenol) (with >13 mol% of VPh in the copolymer) [380], poly(benzyl methacrylate) (PBzMA), and poly(phenyl methacrylate) (PPhMA) [374], PVME, phenolic, phenoxy, and PVPh [335,381–383] (Table 1.8). Several studies reveal interrelations among the extent of partial crystallization and the glass-transition temperature of the amorphous phase. Rim and Runt [380], for example, observed that the greater the SAN concentration in PCL + SAN blends, the higher the T_g and the lower the tendency for PCL crystallization. FTIR spectroscopy provides links between thermophysical properties (T_g and T_m) and the structural organization of phases in crystalline-amorphous blends exhibiting specific interactions. The stretching vibrations of the carbonyl group of PCL and proton donating (e.g., hydroxyl) groups in several amorphous counterparts provide excellent probes of intermolecular interactions. For instance, based on estimates of the Kwei parameter, q, the average strengths of the intermolecular interactions in blends of PCL with phenolic, PVPh, and phenoxy are weaker than the corresponding self-association for the homopolymers: $q = -10$ (phenolic) > -85 (PVPh) > -100 (phenoxy) (Kwei fits for $k_{Kw} = 1$) [335]. From a thermodynamic viewpoint, the strength of the specific interaction in a blend can also be described by its interaction energy density parameter, B, which is obtained from the depression in the equilibrium melting point based on the Nishi–Wang equation. The negative values of B (-12.51, -9.82, and $-7.55\ \mathrm{cal\,cm^{-3}}$ for blends with phenolic, PVPh, and phenoxy, respectively) and the single glass-transition signals obtained are indicative

Table 1.8 Type of the deviation from the linear mixing rule and description of the T_g (w) patterns in selected miscible binary blends comprising semicrystalline PCL (DSC data).

Second component	ΔT_g (°C)	$T_g(w)$ patterns		Ref.
		Deviation	Comments	
PECl (30 . . . 48% Cl)	50 . . . 67	Negative	GT ($k_{GT} = 0.26$ and 0.35, for 36 wt.% and 48 wt.% Cl, respectively). Melt mixing	[375]
Phenolic	125	Negative	Kwei ($q = -10$, $k_{Kw} = 1$), B = −12.51 cal cm^{-3}, $\Delta\nu = 95$ cm^{-1}, $\Delta\nu* = -30$ cm^{-1}. Solvent: THF	[335]
PBzMA	126	Negative	GT ($k_{GT} = 0.25$), nonspecific interactions; miscibility due to matched polarity. Solvent: THF	[374]
PVC (56% Cl)	143	Negative	GT ($k_{GT} = 0.56$), $\chi_{12} = -0.33$. Solvent: THF	[376]
Phenoxy	159	Negative	Kwei ($q = -100$, $k_{Kw} = 1$), B = −7.55 cal cm^{-3}, $\Delta\nu = 45$ cm^{-1}, $\Delta\nu* = -105$ cm^{-1}. Solvent: THF	[335]
SAN (27.5% AN)	160	Negative	GT ($k_{GT} = 0.47$). Solvent: THF	[379]
SAN (25% AN)	173	Negative	GT ($k_{GT} = 0.63$), $\chi_{12} = -0.52$. Solvent: 1,2-dichloroethane	[378]
CPVC (63% Cl)	170	Negative	GT ($k_{GT} = 0.69$), $\chi_{12} = -0.35$. Solvent: THF	[376]
CPVC (67% Cl)	181	Negative	GT ($k_{GT} = 0.76$), $\chi_{12} = -0.38$. Solvent: THF	[376]
PPhMA	180	Negative	Nonspecific interactions; miscibility due to matched polarity. Solvent: THF	[374]
PVPh	206	Negative	Kovacs ($g = -0.014$; positive excess mixing volume)	[382]
	210	Negative	Kwei ($q = -85$, $k_{Kw} = 1$), B = −9.82 cal cm^{-3}, $\Delta\nu = 85$ cm^{-1}, $\Delta\nu* = -65$ cm^{-1}. Solvent: THF	[335]
	217	Negative	GT ($k_{GT} = 0.24$). Solvent: THF	[383]
PC	210	Negative	Kovacs ($g = -0.0227$, $\varphi_{2c} = 0.72$, $T_{crit} = 372$ K). Solvent: CH_3Cl (and precipitation in methanol)	[377]
P4HS	197	Negative	Kovacs ($g = -0.01$, $\varphi_{2c} = 0.58$, $T_{crit} = 375$ K). Solvent: THF[a)]	[384]
P4HSBr	213	Negative	Kovacs ($g = 0.02$, $\varphi_{2c} = 0.51$, $T_{crit} = 387$ K). Solvent: THF[a)]	[384]

a) Analysis performed on $T_g(w)$ data with correction for the real composition of the amorphous phase.

of miscibility, with the relative strength of hydrogen bonding increasing for lower values of B. The frequency difference ($\Delta\nu$) between the hydrogen-bonded hydroxyl absorption and free hydroxyl absorption bands in FTIR spectra provides an independent verification of the above behavior, by demonstrating that the average strength of the intermolecular hydrogen-bonding interaction decreases in the same order: $\Delta\nu = 95$ cm^{-1} (phenolic) > 85 cm^{-1} (PVPh) > 45 cm^{-1} (phenoxy) [381].

Observations of strong elevations in the experimental glass-transition temperatures, with respect to the T_g versus composition patterns of their wholly amorphous mixtures [337,384], are common in blends with some amount of crystallinity. The discrepancy may, to a certain extent, be corrected if the

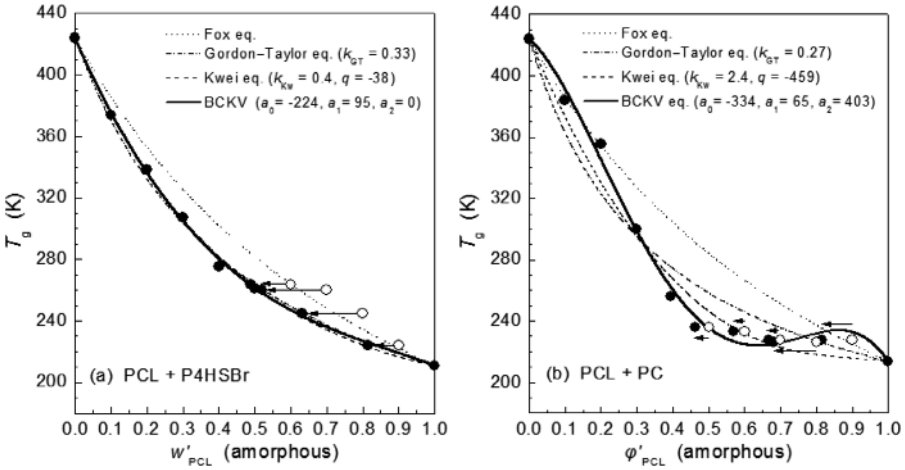

Figure 1.46 Blend T_g versus amorphous phase composition (w', φ') dependences reported for (a) PCL + P4HSBr [384], and (b) PCL + PC [377]. Open symbols refer to the actual experimental data, plotted as a function of the overall weight (w_1) or volume (φ_1) content of PCL in the blend, which were subsequently corrected for blend crystallinity (filled symbols denoted by arrows). From ref. [262], with permission

experimental data are plotted not as a function of the overall weight fraction of the component but in dependence of its real weight fraction in the amorphous phase in the blend (e.g., see Figure 1.46a for PCL + poly(4-hydroxystyrene) brominated (P4HSBr) [384]). In several cases, however, the unusual nonmonotonic T_g versus composition variation persists, even after the necessary corrections for the actual weight fractions of each component in the amorphous phase of the mixture (e.g., see Figure 1.46b for PCL + PC [377]). In terms of microstructure, such rather atypical variations may be – in part – attributed to the formation of complex rigid amorphous phases and different types of segregation of the amorphous polymer. Because of the highly entangled nature of polymer systems, on crystallization and cooling below T_g amorphous layers that are unable to crystallize themselves become entwined with crystalline regions and are constrained in loops and chains connected to the crystal surface (Figure 1.47); this fraction is described as the rigid amorphous phase (or "rigid amorphous fraction"). The physical tethering of amorphous chains progressively diminishes as one moves away from the crystal surface, giving to these chains an increasingly greater degree of mobility. The remaining MAF relates to the unconstrained bulk-like amorphous phase, which exhibits the strong glass transition (at T_g) as described earlier. In order of increasing degree of segregation, one may find in partially crystalline materials: interlamellar segregation (the amorphous fraction resides in the interlamellar region within the lamellar stack), interfibrillar segregation (the amorphous chains are placed outside the lamellar stacks of the crystalline component(s), but are still located within the spherulite), and/or interspherulitic segregation (the amorphous phase is expelled from the lamellar stacks and

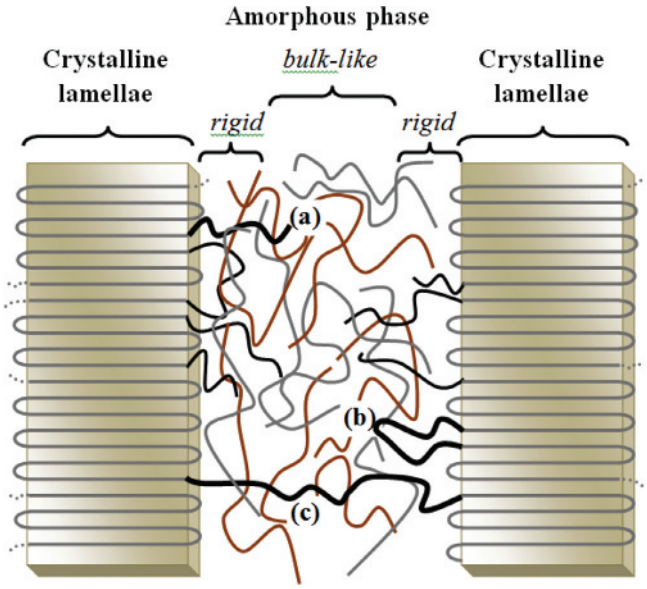

Figure 1.47 Scheme showing a small section of the well-ordered lattice of crystalline lamellae within a spherulite in a binary polymer blend with a semicrystalline component and the amorphous interlamellar links composed of chains from both polymers. The different zones where a rigid amorphous phase is present or a bulk-like glass transition behavior is likely to appear are shown. Cilia (a), loose loops (b), and tie molecules (c) in the interlamellar region are also indicated.

resides between neighboring spherulites). The structural complexity encountered in many crystalline–amorphous systems is likely to generate highly complicated $T_g(w)$ dependences, which are often only described by heuristic multiparametric mixing rules. In the case of the PCL + PC mixture, in which both components are partially crystalline, one may observe a cusp at a critical composition, above which the Braun–Kovacs equation can be successfully implemented [377]. Similar arguments also apply for the blends of PEO with cellulose acetate butyrate (CAB) [274]. In the latter system, complementary optical microscopy and SAXS experiments verified the complexity of the blend revealing that at low CAB contents the chains of the amorphous component are incorporated into interlamellar regions and commence to segregate to the interfibrillar region with an increase of its weight fraction.

1.7.3
Ternary Polymer Blends: Phase Behavior and Glass Transitions

With the increasing application of multicomponent systems, much interest has been directed toward ternary polymer blends [357,360,385–400]. The thermodynamic phase relationships for ternary mixtures, where one component is

solvent and the other two polymers, were described in the early studies of Scott [386] and Tompa [387] based on the Flory–Huggins lattice model. Since then, the majority of miscibility studies on ternary polymer blends remain focused on the hypothesis that any polymer miscible with any of two other polymers can "compatibilize" their immiscible binary pair. Examples illustrative of the above behavior provide poly(vinylidene fluoride) (PVDF) [387], PVPh [388], and SAN [389], which independently act as compatibilizers of the immiscible PEMA + PMMA mixture. Miscibility evaluations and phase diagram assessments heavily rely on optical microscopy and calorimetric studies. However, the single-T_g miscibility criterion for ternary blends is far from being considered unequivocal, with uncertainties particularly severe for blend compositions rich in one of the components or for systems comprising components of neighboring T_gs. Questionable assessments are often reported particularly in the case of conventional DSC studies, due to the lack of resolution of this method. For example, the thermal analysis studies of Ponoit and Prud'homme [391] on melt-mixed PECH + PVAc + PMMA ternary blends have demonstrated that PECH effectively compatibilizes the immiscible PVAc + PMMA blends only at PECH loadings exceeding 70 wt.%. The higher resolution of DMA has permitted the identification of structural heterogeneities (immiscibility) – on the basis of system's glass-transition behavior – for several mixtures that would otherwise be deemed miscible based merely on typical DSC scans (Figure 1.48). Zhang and coworkers [385] have furthermore demonstrated instances where, after careful enthalpy relaxation studies, the rather broad glass transformation range recorded

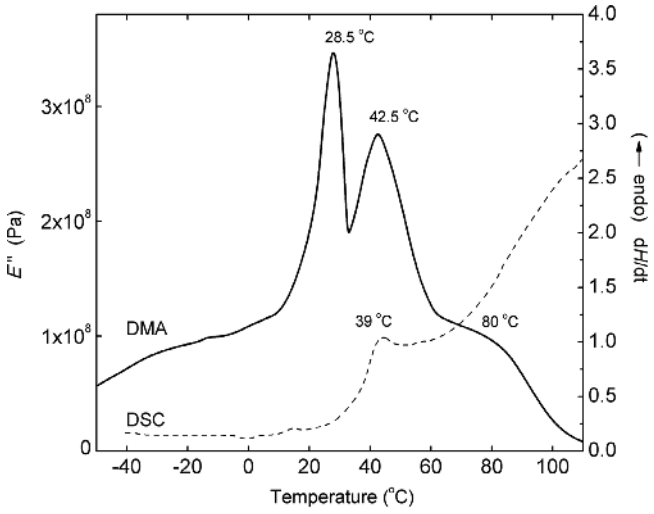

Figure 1.48 DMA (loss modulus E'' at an oscillating strain frequency of 10 Hz) and DSC curves of a PECH + PVAc + PMMA (8.5/23.5/68) blend. Numbers indicate the glass-transition temperatures determined from each thermal technique. Indications of complex blend morphology are only present in the dynamic mechanical spectrum. Replotted data from ref. [391], with permission © 2002 Elsevier.

for particular ternary blend compositions transforms to a multipart signal. Despite the apparent limitations of the glass-transition approach, related studies remain at the frontline of miscibility evaluations of ternary blends. In such cases, however, it seems appropriate to consider the effect of the compatibilizer to involve a reduction of the size of the heterogeneous domains to a value comparable to the probe size of the particular measuring technique.

When all three binary pairs are miscible, completely homogeneous ternary blends or close immiscibility loop phase diagrams are possible. In general, in the absence of strong specific interactions between the components, the ternary phase behavior of polymer blend systems is primarily governed by differences in the physical interaction among the components, which is expressed by the magnitude of the binary interaction parameters, χ_{ij} (or equivalent solubility parameters, δ_i). If just one of the binary interaction parameters is significantly larger than a critical value [385], a large portion of the ternary phase diagram is predicted to be heterogeneous. In addition, a strong driving force toward phase separation exists if there are significant differences in the solubility or interaction parameter values (i.e., $\chi_{ij} - \chi_{ik} \neq 0$), which produces the so-called "$\Delta\chi$ effect". In terms of the Painter–Coleman association model, the effect of strong specific interactions (hydrogen bonds) on the phase behavior is considered to be controlled by the magnitudes of the equilibrium constants describing self- and interassociation, and the difference between the effective interassociation equilibrium constants of the binary systems (ΔK). The latter is usually called the "ΔK effect" and reflects the difference in the "chemical" interaction between the self-associating polymer and the other polymers in the mixture; a strong ΔK effect is responsible for phase separation. Bearing in mind the above restrictions, only very few ternary polymer blends are expected to be homogeneous over their entire range of compositions. These "totally" miscible, ternary blends – including PVDF + PVAc + PMMA [390], PECH + PMMA + PEO [392], PHB + PEO + PECH [393], poly(ether diphenyl ether ketone) + poly(ether ether ketone) + PEI [394], PEI + PET + PBT [395], and PCL + PPhMA + PBzMA [396] – all possess low $\Delta\chi$ effects and no hydrogen-bonding interactions between their segments (i.e., the ΔK effect can be neglected).

Addition of a polymeric component capable of forming strong hydrogen-bonding interactions (i.e., a proton donor) may potentially act as a mutual common link for the other polymers (containing proton-accepting functional groups), leading to a "bridging effect" and the formation of a more homogeneous ternary mixture. For this to happen, however, it is essential that the interassociation equilibrium constants of the two miscible hydrogen-bonding binaries are comparable. Thermal analyses, for example, have provided compelling evidence of phase homogeneity for all blend compositions in ternary blends of PVPh with PVAc and PMA [385], or with pairs of homologous aryl polyesters (PET, PTT, or PBT) [357]. In all these ternary systems, ultimate miscibility is accredited to negligible differences in the level of the physical interactions among their components (no $\Delta\chi$ effect), and the sensitive balancing of the hydrogen-bonding interactions in the ternary blends between PVPh and either

one of the proton accepting polymers (weak ΔK effect). In the case of the phenoxy + phenolic + PCL [400] and phenoxy + phenolic + PVPh [360] ternary blends, where all binaries interassociate through hydrogen bonds, complete miscibility in the amorphous phase has been ascribed to intermolecular hydrogen bonds that exist within the individual binary blends and create a network-like structure.

Several calorimetric studies of the glass-transition behavior of ternary blends demonstrate a closed loop of a phase-separated region in the phase diagram. Examples provide the ternary blends of PEO + phenolic + PCL [389], PVAc + PVPh + PEO [385], PMMA + phenoxy + PEO [397], PMMA + PVPh + poly(vinyl cinnamate) [398], and PS + poly(cyclohexyl acrylate) (PCHA) + P2CS [399], all consisting of three miscible binaries. In the case of the PEO + phenolic + PCL ternary blend (Figure 1.49), for example, the observed interassociation equilibrium constant between the hydroxyl group of phenolic and the ether group of PEO ($K_A = 264.7$) is found substantially higher than the interassociation equilibrium constant between the hydroxyl of phenolic and carbonyl of PCL ($K_C = 116.8$) and the self-association equilibrium constant of hydroxyl multimer formation ($K_B = 52.3$). This result implies that the tendency toward forming the hydrogen bonding between phenolic and PEO dominates over the interassociation of the phenolic with PCL and the self-association by forming the intramolecular hydrogen bonding of the pure phenolic resin. The fact that the phenolic resin interacts more favorably with PEO than that with PCL ($K_A \gg K_C$) produces a strong ΔK effect, which provides the driving force for the closed-loop region of immiscibility.

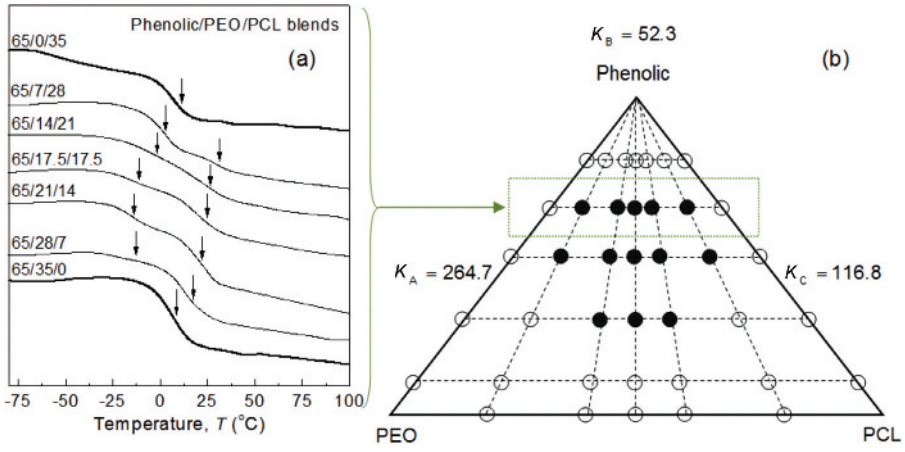

Figure 1.49 (a) Second-run DSC thermograms and (b) closed-loop immiscibility phase diagram at room temperature of PEO + phenolic + PCL blends. All ternary blends containing 65 wt.% phenolic display two glass transitions, implying that they are immiscible in the amorphous phase. Open and filled circles in the phase diagram denote miscible and immiscible blends, respectively. Replotted from ref. [389], with permission © 2002 American Chemical Society.

1.8 Concluding Remarks

The reversible transformation of amorphous materials from a devitrified or viscoelastic (rubber-like) state into the fairly brittle state of solid glass constitutes one of the most puzzling phenomena in materials science. The distinct kinetic and thermodynamic aspects of the glass transition and the diverse experimental responses recorded hitherto for polymers under different molecular environments and geometric constrictions hamper a unified theoretical interpretation of the event. Regardless of the practically imperceptible structural changes during the transition, numerous experimental techniques employing thermal, mechanical, electrical, or electromagnetic excitation of specific molecular motions have provided compelling evidence of the drastic changes in segmental mobility and molecular bonding that occur in the glass transformation range. Thermal analysis techniques are particularly effective in determining characteristics of the cooperative molecular motions activating in the glass transformation range, with numerous studies indicating that the location and width of the respective transitions are regulated by inherent properties of the material (chemical structure, chain architecture, free volume, etc.), in addition to a number of externally controlled factors (pressure, additives, level of confinement, etc.).

The variability of motional probes and the ensuing differences in the probing length scale of the various measuring techniques, the broadly different oscillation frequencies used in popular isochronal dynamic experiments, along with the different (often inappropriate) procedures adopted for conditioning the testing materials, may become sources of misperception – rather than power tools – in the hands of the novice experimentalist. Notwithstanding the above complications, the glass-transition phenomenon and its defining marker, the glass-transition temperature, have for long been explored and used to evaluate the success of polymers' mixing. The resulting materials exhibit properties intermediate or even superior to those of their pure components, offering a means to improve the poor performances of existing polymers without sacrificing any excellent characteristic. The paradigms illustrated in this chapter make evident that the number of transitions and the compositional dependence of the respective glass-transition temperatures offer indicators of miscibility, partial miscibility (compatibility), or immiscibility between blend components. The conventional – although somewhat misused – experimental criterion for determining miscibility in polymer blends is based on the measurement of a single glass-transition signal for all blend compositions, usually located in between the glass-transition temperatures of the components and consistent with the composition of the blend. For miscible binary polymer systems, in particular, the various theoretical or phenomenological approaches critically examined in this chapter have formulated different analytical $T_g(w)$ functions, endorsing as a minimum qualitative correlations of their parameters with miscibility-controlling

factors, such as the type and strength of intercomponent interactions, the relative balancing between inter- and intramolecular interactions, conformational entropy changes, or the magnitude and partition of the excess mixing volume in the system. In the case of the partially miscible or compatibilized polymer blends, the glass transitions of both components are recorded. Convergence of the glass-transition temperatures of the two phases is typically observed, along with a change in the width and the strength of the signals. Interestingly, an analogous behavior often emerges in dynamically heterogeneous blends of weakly interacting components, with the level of homogeneity approaching the segmental length scale. Moreover, dynamic studies of partially mixed systems reveal shifts in the glass-transition temperatures and changes in the width of the transition signals, which provide a measure of the extent of molecular mixing. In contrast, complete segregation of phases (immiscibility) is evidenced by separate glass transitions for all blend compositions, with nearly composition-independent transition temperatures.

The reproducibility and appropriate resolution of the complex glass transition data obtained in several polymer-based composites is prerequisite for achieving unambiguous experimental determinations of structural homogeneity or of the state of dispersion in multiphase systems. The cases discussed in this chapter emphasize the need for testing materials that have attained equilibrium conditions prior to the experiment; that is, the thermal, mechanical or electrical history (memory effects) has to be erased, following standard pretreatments. Moreover, optimal mixing conditions, which include appropriately selected type and amount of solvent(s), temperature of mixing, and method of preparation (i.e., solvent evaporation, coprecipitation or hot-melt extrusion), are essential. Experimental attempts to establish the miscibility window of any pair of polymers via their glass-transition behavior have to consider also the nature, sensitivity, and resolution of the probing technique, the latter being directly related to the limiting domain size with distinguishable thermal response. Along these lines, blends displaying a single glass transition may be deemed miscible only on a scale at or above the total number of segments cooperatively relaxing at the glass transition (i.e., determined level of homogeneity no less than the probe length scale of the particular technique). The issues presented in several sections of this chapter reveal that proper identification of glass transitions entails rigorous separation of the pertinent signals from neighboring transitions (e.g., melting peaks, liquid–liquid transitions), relaxational phenomena (secondary relaxations, interfacial polarizations, enthalpy, or volume relaxation, etc.), or other signals (e.g., noise, background), and subsequent analysis following appropriate models. Unfortunately, despite the advent of modulated temperature techniques in many fields of thermal analysis along with the introduction of novel commercial experimental systems with remarkable accuracy and signal-resolving power, proper consideration of the above issues is often lacking in routine experiments. This situation may cast doubts in several evaluations and precludes straightforward comparisons among seemingly complementary studies of glass formation and polymer dynamics in complex systems.

Abbreviations

BCKV	Brostow–Chiu–Kalogeras–VassilikouDova (equation)
BSC	Brekner–Schneider–Cantow (equation)
CM	Coupling model
CPM	Configuron percolation model
CRR	Cooperatively rearranging region
DEA	Dielectric analysis
DMA	Dynamic mechanical analysis
DRS	Dielectric relaxation spectroscopy
DSC	Differential scanning calorimetry
DTA	Differential thermal analysis
ESR	Electron spin resonance
FLDs	Frustration-limited domains (theory)
FTIR	Fourier transform infrared
GT	Gordon–Taylor (equation)
HN	Havriliak–Negami (equation)
JG	Johari–Goldstein (model)
LCST	Lower critical solution temperature
LM	Lodge–McLeish (model)
MAF	Mobile amorphous fraction
MCT	Mode-coupling theory
MTDSC	Modulated temperature DSC
MTTMA	Modulated temperature TMA
NMR	Nuclear magnetic resonance
PALS	Positron annihilation lifetime spectroscopy
PEL	Potential energy landscape
QSPR	Quantitative structure–property relationships (model)
RAF	Rigid amorphous fraction
RFOT	Random first-order transition (theory)
SANS	Small-angle neutron scattering
SAXS	Small-angle X-ray scattering
TD	Thermodilatometry
TGA	Thermogravimetric analysis
TMA	Thermomechanical analysis
TSC	Thermally stimulated currents
TSDC	Thermally stimulated depolarization currents
UCST	Upper critical solution temperature
VFTH	Vogel–Fulcher–Tammann–Hesse (equation)
WAXS	Wide-angle X-ray scattering
WLF	Williams–Landel–Ferry (equation)
ABS	Acrylonitrile/butadiene/styrene
CAB	Cellulose acetate butyrate
DMF	*N*,*N*-dimethylformamide
HPMC	Hydroxypropyl methylcellulose

HPMCAS	Hydroxypropyl methylcellulose acetate succinate
MnSPS	Manganese sulfonated PS (10.1 mol% of MnS in PS)
PαMS	Poly(α-methyl styrene)
P(3HB-*co*-3HH)	Poly(3-hydroxybutyrate-*co*-3-hydroxyhexanoate)
P(BA-*co*-BT)	Poly(butylene adipate-*co*-butylene terephthalate))
P(VP-*co*-VA)	Poly(vinyl pyrrolidone-*co*-vinyl acetate)
P2CS	Poly(2-chloro styrene)
P2VP	Poly(2-vinyl pyridine)
P4HS	Poly(4-hydroxystyrene)
P4HSBr	Poly(4-hydroxystyrene) brominated
P4tBS	Poly(4-*tert*-butylstyrene)
P4VP	Poly(4-vinyl pyridine)
PA-6	Polyamide-6
PATM	Poly(*N*-acryloylthiomorpholine)
PB	Polybutadiene
PBA	Poly(butylene adipate)
PBN	Poly(butylene 2,6-naphthalate)
PBSA	Poly(butylene succinate-*co*-butylene adipate)
PBSuc	Poly(butylene succinate)
PBT	Poly(butylene terephthalate)
PBzMA	Poly(benzyl methacrylate)
PC	Polycarbonate
PCHA	Poly(cyclohexyl acrylate)
PCHMA	Poly(cyclohexyl methacrylate)
PCL	Poly(*ε*-caprolactone)
PDLLA	Poly(D,L-lactide)
PE	Polyethylene
PEA	Poly(ethylene adipate)
PECH	Poly(epichlorohydrine)
PECl	Chlorinated polyethylene
PEEMA	Poly(2-ethoxyethyl methacrylate)
PEKK	Poly(ether ketone ketone)
PEMA	Poly(ethyl methacrylate)
PEO	Polyethylene oxide
PESeb	Poly(ethylene sebacate)
PESuc	Poly(ethylene succinate)
PET	Poly(ethylene terephthalate)
PHB	Poly(*β*-hydroxybutyrate)
Phenolic	Phenolic resin
Phenoxy	Poly(hydroxylether of bisphenol A)
PHV	Poly(hydroxyvalerate)
PI	Polyisoprene
PLLA	Poly(L-lactide)
PMA	Poly(methyl acrylate)
PMDL	Poly(*N*-methyldodecano-12-lactam)

PMAA	Poly(methyl acrylic acid)
PMMA	Poly(methyl methacrylate)
PMTMA	Poly(methylthiomethyl methacrylate)
PNB	Polynorbornene
PnPMA	Poly(n-propyl methacrylate)
PoCS	Poly(*o*-chlorostyrene)
PP	Polypropylene
PPE	Poly(2,6-dimethylphenylene ether)
PPhMA	Poly(phenyl methacrylate)
PPO	Poly(2,6-dimethyl-1,4-phenylene oxide)
PS	Polystyrene
PS4VP	Poly(styrene-*co*-4-vinylpyridine)
PSAA	Poly(styrene-*co*-acrylic acid)
PSAD	poly(styrene-*co*-*N*,*N*-dimethylacrylamide)
PSCA	Poly(styrene-*co*-cinnamic acid)
PSHS	Poly(styrene-*co*-hydroxystyrene)
PSMA	Poly(styrene-*co*-methacrylic acid)
PSMAn	Poly(styrene-*co*-maleic anhydride)
PTHFMA	Poly(tetrahydrofurfuryl methacrylate)
PTT	Poly(trimethylene terephthalate)
PVAc	Poly(vinyl acetate)
PVC	Poly(vinyl chloride)
PVDF	Poly(vinylidene fluoride)
PVE	Poly(vinylethylene)
PVEE	Poly(vinyl ethyl ether)
PVK	Poly(*N*-vinyl carbazole)
PVME	Poly(vinyl methyl ether)
PVP	Poly(vinyl pyrrolidone)
PVPh	Poly(vinyl phenol)
PVPhKH	Poly(vinyl phenyl ketone hydrogenated)
PVPy	Poly(vinyl pyridine)
SAN	Poly(styrene-*co*-acrylonitrile)
THF	Tetrahydrofuran
TMPC	Tetramethyl polycarbonate
TPI	Thermoplastic polyimide

Symbols

$< \ldots >$	Average value
A, B	Material or model-specific constants
a_0, a_1, a_2	Parameters of the BCKV equation
B	Interaction energy density
B_i	Fraction of flexible bonds of the ith polymer
A_T	Amplitude of temperature modulation
C, C_1, C_2	Model-specific constants

c_i	Model-specific parameters ($i = 1, 2, \ldots$)
C_{app}	Apparent heat capacity
C_p	Heat capacity
D	Thickness
d	Dimension of space
$E*$	Complex modulus ($E^* = E' + iE''$)
E	Energy
F	Free energy; acting force
f	Free-volume fraction; scanning frequency
f_g	Free-volume fraction at T_g
f_{max}	Peak frequency of the dynamic glass transition (α-relaxation)
E, E_{act}	Energy; activation energy
G	Gibbs free energy
$G*$	Shear complex modulus ($G^* = G' + iG''$)
g	Interaction term (Kovacs' model)
H	Enthalpy
I	Current
K, K^*, k_1, k_2, k_3	Material specific constants
K_A, K_C	Interassociation equilibrium constants
K_B	Self-association equilibrium constant
K_1, K_2	Parameters of the BSC equation
k, k_{CK}, k_{DM}, k_{GT}, k_{JH}, k_{kw}	Parameters of various $T_g(w)$ functions
k_b	Amount of backbone bonds per repeat unit
k_β	Boltzmann constant
L, l	Length
l_k	Kuhn length
l_b	Length of the average backbone bond
$M*$	Complex modulus
M_0	Monomer (or repeat-unit) molar mass
M_c	Molar mass of chains between cross-links
M_n	Molar mass (number average)
m	Mass; fragility parameter (steepness index)
m_T	Thermodynamic fragility (parameter)
N_A	Avogadro's number
N_i	Number of segments of the ith polymer
n	Exponent (various models)
P	Pressure
P_{av}	Average probability
p_c	Critical configurons concentration
Q	Partition function; heat
q	Rate of temperature change; parameter (Kwei equation)
R	Gas constant
S	Entropy

S_c	Configurational entropy
s_c^*	Critical configurational entropy
t	Time
T	Absolute temperature
T_c	Crystallization temperature
T_{cc}	Cold crystallization temperature
T_{MCT}	Critical temperature (MCT, RFOT)
T_{crit}	Critical temperature (Kovacs' model)
T_f	Fictive temperature
T_g	Glass-transition temperature
T_K	Kauzmann temperature
T_{LL}	Liquid–liquid transition temperature
T_m	Melting temperature
T_r	Reference temperature
T_s	Sample temperature
T_V	Vogel temperature
T_0, T_2	S_c-vanishing temperatures
T_b, T_{1e}, T_{2e}, T_e	Different marks of glass-transition temperature in a DSC curve
$T_{1\rho}$(H)	Proton spin-lattice relaxation time in the rotational frame
$\tan\delta$	Loss tangent (E''/E', G''/G', $\varepsilon''/\varepsilon'$)
V	Volume
V_α	Cooperativity volume
V_f	Free volume
V_f^*	Free volume at $T < T_g$
V_0	Hardcore (or incompressible) molecular volume
w	Mass (or weight) fraction
x	Mole fraction
z	Size of CRR (Adam–Gibbs model)
z^*	Critical size of CRR

Greek Symbols

α	Coefficient of volumetric thermal expansion
α	Primary relaxation, dynamic glass transition
α_c	Degree of cure
α_f	Coefficient of free-volume thermal expansion
α_L	Coefficient of linear thermal expansion
α_T	Temperature shift factor; thermal expansion coefficient
β, γ, δ	Secondary relaxations
β_{KWW}	KWW function exponent
γ	Exponent (MCT)
γ_i	Number of flexible bonds per repeating unit
ΔC_p	Heat capacity change at the transition

ΔH	Heat of transition
ΔT	$T_r - T_s$
ΔT_g	Difference of components' T_g in a binary system ($T_{g,2} - T_{g,1}$)
ΔT_g^*	Shift of polymer's T_g under confinement ($T_g^{conf.} - T_g^{bulk}$)
$\Delta V^\#$	Activation volume (at T_g)
$\Delta\mu$	Activation energy (Adam–Gibbs model)
$\Delta\nu$	Difference of OH vibrational frequencies ($\nu_{free} - \nu_{inter\text{-}assoc.}$)
$\Delta\nu*$	Difference of OH vibrational frequencies ($\nu_{self\text{-}assoc.} - \nu_{inter\text{-}assoc.}$)
δ	Phase lag
δ_i	Solubility parameters
ε	Strain, permittivity
ε_0	Permittivity of free space
ε_∞	Permittivity at very large frequencies
η	Viscosity
κ_T	Compressibility
ν	Vibrational frequency
ξ_α	Cooperativity length scale of molecular motions
$\xi*$	Length scale of entropic droplets (RFOT)
Π_E	Ehrenfest ratio
ρ	Density
σ	Stress; conductivity
σ_{dc}	Direct current conductivity
τ	Relaxation time
Φ	Relaxation function
φ	Volume fraction
φ_{eff}	Effective local concentration
φ_{self}	Self-concentration
χ_{12}	Flory–Huggins binary interaction parameter
ω	Angular frequency

References

1 Sperling, L.H. (2006) *Introduction to Physical Polymer Science*, 4th edn, John Wiley & Sons, Inc., Hoboken, NJ.

2 Utracki, L.A. (ed.) (2002) *Polymer Blends Handbook*, vol. **1**, Kluwer, Dordrecht.

3 Robeson, L.M. (2007) *Polymer Blends: A Comprehensive Review*, Hanser, München, Germany.

4 Arrighi, V., Cowie, J.M.G., Fuhrmann, S., and Youssef, A. (2010) Miscibility Criterion in Polymer Blends and its Determination, in *Encyclopedia of Polymer Blends, Volume 1: Fundamentals* (ed. A.I. Isayev), John Wiley & Sons, Chapter 5, pp. 153–198.

5 Menczel, J.D., Judovits, L., Prime, R.B., Bair, H.E., Reading, M., and Swier, S. (2009) Differential scanning calorimetry (DSC), in *Thermal Analysis of Polymers, Fundamentals and Applications* (eds J.D. Menczel and R.B. Prime), John Wiley & Sons, Inc., Hoboken, NJ, Chapter 2, pp. 7–239.

6 Angell, C.A. (2004) Glass transition, in *Encyclopedia of Materials: Science and Technology*, 2nd edn, (Editors-in-Chief K.H.J. Buschow, R.W. Cahn, M.C.

Flemings, and B. Ilschner) (print) E.J. Kramer, S., Mahajan, and P. Veyssière, (updates), Elsevier, Oxford, pp. 1–11.
7 Plazek, D.J. and Ngai, K.L. (1996) The glass temperature, in *Physical Properties of Polymers Handbook* (ed. J.E. Mark), AIP Press, Woodbury, N.Y., p. 139.
8 Gutzow, I.S. and Schmelzer, J.W.P. (2011) Basic properties and the nature of glasses, in *Glasses and the Glass Transition* (eds J.W.P. Schmelzer and I.S. Gutzow), Wiley VCH Verlag GmBH, Weinheim, Chapter 2.
9 Van den Mooter, G. (2012) *Drug Discov. Today Technol.*, **9**, e79–e85; Meeus, J., Scurr, D.J., Chen, X., Amssoms, K., Davies, M.C., Roberts, C.J., and Van den Mooter, G. (2015) *Pharm. Res.*, **32**, 1407–1416; Demirdirek, B. and Uhrich, K.E. (2015) *J. Drug Target.* **23**, 716–724; Dubois, J.N.L. and Lavignac, N. (2014) *Polym. Chem.* **5**, 1586–1592.
10 Kalogeras, I.M. (2011) *Eur. J. Pharm. Sci.*, **42**, 470–483; Kim, Y., Liemmawal, E.D., Pourgholami, M.H., Morris, D.L., and Stenzel, M.H. (2012) *Macromolecules* **45**, 5451–5462.
11 Hill, J.J., Shalaev, E.Y., and Zografi, G. (2014) *J. Pharm. Sci.*, **103**, 2605–2614.
12 Kalogeras, I.M. and Hagg Lobland, H.E. (2012) *J. Mater. Ed.*, **34**, 69–94.
13 Ngai, K.L. (1979) *Com. Solid State Phys.*, **9**, 127; Ngai, K.L. and Rendell, R.W. (1993) *J. Mol. Liq.*, **56**, 199–214; Ngai, K.L. (2000) *J. Phys.: Condens. Matter*, **12**, 6437–6451; Ngai, K.L. (2007) All standard theories and models of glass transition appear to be inadequate: missing some essential physics, in *Soft Matter under Exogenic Impacts* (eds S.J. Rzoska and V.A. Mazur), Springer, Dordrecht, pp. 91–111.
14 McKenna, G.B. and Simon, S.L. (2002) The glass transition – its measurement and underlying physics, in *Handbook of Thermal Analysis and Calorimetry*, vol. **3**, Applications to Polymers and Plastics (ed. S.Z.D. Cheng), Elsevier, Amsterdam, Chapter 2, pp. 49–110.
15 Menard, K.P. (2008) *Dynamic Mechanical Analysis: A Practical Introduction*, 2nd edn, CRC Press, Boca Raton, FL.
16 Hedvig, P. (1977) *Dielectric Spectroscopy of Polymers*, Adam Hilger, Bristol.
17 Chartoff, R.P. and Sircar, A.K. (2005) Thermal analysis of polymers, in *Encyclopedia of Polymer Science and Technology*, John Wiley & Sons, Inc., Hoboken, NJ.
18 Prigogine, I. and Defay, R. (1954) *Chemical Thermodynamics*, Longmans, Green and Co., New York.
19 Ribeiro, M.C.C., Scopigno, T., and Ruocco, G. (2009) *J. Phys. Chem. B*, **113**, 3099–3104; Schmelzer, J.W.P. (2012) *J. Chem. Phys.*, **136**, 074512.
20 Kovacs, A.J. (1958) *J. Polymer Sci.*, **30**, 131–147.
21 Öttinger, H.C. (2006) *Phys. Rev. E*, **74**, 011113.
22 Cohen, M.H. and Turnbull, D. (1964) *Nature*, **203**, 964; Herlach, D., Holland-Moritz, D. and Gelenko, P. (2007) *Metastable Solids from Undercooled Melts*, Elsevier, Amsterdam.
23 Kauzmann, W. (1948) *Chem. Rev.*, **43**, 219–256.
24 Stillinger, F.H. and Weber, T.A. (1982) *Phys. Rev. A*, **25**, 978–989; Stillinger, F.H. and Weber, T.A. (1983) *Phys. Rev. A*, **28**, 2408–2416; Debenedetti, P.G. and Stillinger, F.H. (2001) *Nature*, **410**, 259–267.
25 Berthier, L. and Biroli, G. (2011) *Rev. Mod. Phys.*, **83**, 577–645.
26 Yun, M., Jung, N., Yim, C., and Jeon, S. (2011) *Polymer*, **52**, 4136–4140.
27 Struik, L.C.E. (1978) *Physical Aging of Amorphous Polymers and Other Materials*, Elsevier, New York.
28 Tool, A.Q. (1946) *J. Am. Ceram. Soc.*, **29**, 240–253.
29 Davies, R.O. and Jones, G.O. (1953) *Adv. Phys.*, **2**, 370–410.
30 Kovacs, A.J., Aklonis, J.J., Hutchinson, J.M., and Ramos, A.R. (1979) *J. Polymer Sci. B*, **17**, 1097–1162.
31 Hong, L., Begen, B., Kisliuk, A., Novikov, V.N., and Sokolov, A.P. (2010) *Phys. Rev. B*, **81**, 104207.
32 Simmons, D.S. and Douglas, J.F. (2011) *Soft Matter*, **7**, 11010–11020.
33 Ngai, K.L., Sokolov, A., and Steffen, W. (1997) *J. Chem. Phys.*, **107**, 5268–5272.

34 Hong, L., Novikov, V.N., and Sokolov, A.P. (2011) *J. Non-Cryst. Solids*, **357**, 351–356.

35 Stevenson, J. and Wolynes, P. (2010) *Nat. Phys.*, **6**, 62.

36 Johari, G.P. and Goldstein, M. (1970) *J. Chem. Phys.*, **53**, 2372; (1970) *J. Phys. Chem.*, **74**, 2034; (1971) *J., Chem., Phys.*, **55**, 4245; (1972) *J. Chem., Phys.*, **56**, 4411.

37 Williams, G. and Watts, D.C. (1971) *Trans. Faraday Soc.*, **67**, 1971–1979.

38 Kudlik, A., Tschirwitz, C., Blochowicz, T., Benkhof, S., and Rossler, E. (1998) *J. Non-Cryst. Solids*, **235–237**, 406–411.

39 Schmidt-Rohr, K., Kulik, A.S., Beckham, H.W., Ohlemacher, A., Pawelzik, U., Boeffel, C., and Spiess, H.W. (1994) *Macromolecules*, **27**, 4733–4745.

40 Gilroy, K.S. and Phillips, W.A. (1981) *Phil. Mag. B*, **43**, 735.

41 Donth, E. (1982) *J. Non-Cryst. Solids*, **53**, 325; Donth, E. (1991) *J. Non-Cryst. Solids*, **131–133**, 204; Donth, E., Kahle, S., Korus, J., and Beiner, M. (1997) *J. Phys. I France*, **7**, 581–598; Donth, E. (2001) *The Glass Transition. Relaxation Dynamics in Liquids and Disordered Materials*, Springer, Berlin.

42 Cohen, M.H. and Crest, G.S. (1959) *Phys. Rev. B*, **20**, 1077; Stillinger, F.H. and Hodgdon, J.A. (1994) *Phys. Rev. E*, **50**, 2064; Stillinger, F.H. and Hodgdon, J.A. (1996) *Phys. Rev. E*, **53**, 2995.

43 Schröter, K. (2009) *J. Therm. Anal. Calorim.*, **98**, 519–599.

44 Adam, G. and Gibbs, J.H. (1965) *J. Chem. Phys.*, **43**, 139–146.

45 Hempel, E., Hempel, G., Hensel, A., Schick, C., and Donth, E. (2000) *J. Phys. Chem. B*, **104**, 2460–2466.

46 Sastry, S. (2006) *J. Indian Inst. Sci.*, **86**, 731–749.

47 Sillescu, H. (1999) *J. Non-Cryst. Solids*, **243**, 81–108.

48 Williams, M.L., Landel, R.F., and Ferry, J.D. (1955) *J. Am. Chem. Soc.*, **77**, 3701–3707.

49 Vogel, H. (1921) *Phys. Z.*, **22**, 645; Fulcher, G.S. (1925) *J. Am. Ceram. Soc.*, **8**, 339, 789; Tammann, G. and Hesse, W. (1926) *Z. Anorg. Allg. Chem.*, **156**, 245.

50 Hodge, I.M. (1997) *J. Res. Natl Inst. Stand. Technol.*, **102**, 195–205.

51 Saiter, J.M., Grenet, J., Dargent, E., Saiter, A., and Delbreilh, L. (2007) *Macromol. Symp.*, **258**, 152–161; Bureau, E., Cabot, C., Marais, S., and Saiter, J.M. (2005) *Eur. Polymer J.*, **41**, 1152–1158.

52 Lubchenko, V. and Wolynes, P.G. (2007) *Annu. Rev. Phys. Chem.*, **58**, 235–266; Richert, R. and Wagner, H. (1998) *Solid State Ionics*, **105**, 167–173; Richert, R. and Wagner, H. (1997) *Polymer*, **38**, 255–261.

53 Ngai, K.L., Capaccioli, S., Paluch, M., and Provosto, D. (2014) *J. Phys. Chem. B*, **118**, 5608–5614; Kossack, W., Adrjanowicz, K., Tarnacka, M., Kipnusu, W.K., Dulski, M., Mapesa, E.U., Kaminski, K., Pawlus, S., Paluch, M., and Kremer, F. (2013) *Phys. Chem. Chem. Phys.*, **15**, 20641–20650; Hecksher, T., Nielsen, A.I., Olsen, N.B., and Dyre, J.C. (2008) *Nat. Phys.*, **4**, 737–741; O'Connell, P.A. and McKenna, G.B. (1999) *J. Chem. Phys.*, **110** 11054–11060.

54 Zhao, J. and McKenna, G.B. (2012) *J. Chem. Phys.*, **136**, 154901.

55 Zhao, J., Simon, S.L., and McKenna, G.B. (2013) *Nat. Commun.*, **4**, 1783.

56 Richert, R. and Angell, C.A. (1998) *J. Chem. Phys.*, **108**, 9016–9026.

57 DiMarzio, E.A. and Yang, A.J.M. (1997) *J. Res. Natl Inst. Stand. Technol.*, **102**, 135–157.

58 Angell, C.A. (1985) Strong and fragile liquids, in *Relaxations in Complex Systems* (eds K.L. Ngai and G.B. Wright), National Technical Information Service, U.S. Department of Commerce, Springfield, VA 22161, pp. 3–11.

59 Doremus, R.H. (2002) *J. Appl. Phys.*, **92**, 7619–7629.

60 Huang, D. and McKenna, G.B. (2001) *J. Chem. Phys.*, **114**, 5621–5630.

61 Bruning, R. and Sutton, M. (1996) *J. Non-Cryst. Solids*, **205–207**, 480–484.

62 Avramov, I. (2005) *J. Non-Cryst. Solids*, **351**, 3163–3173.

63 Moynihan, C.T. and Angell, C.A. (2000) *J. Non-Cryst. Solids*, **274**, 131–138.

64 Narayanaswamy, O.S. (1971) *J. Am. Ceram. Soc.*, **54**, 491; Moynihan, C.T., Macebo, P.B., Montrose, C.J., Gupta, P.K., DeBolt, M.A., Dill, J.F. *et al.* (1976) *N.Y. Ann. Acad. Sci.*, **279**, 15.

65 Angell, C.A., Ngai, K.L., McKenna, G.B., McMillan, P.F., and Martin, S.W. (2000) *J. Appl. Phys.*, **88**, 3113–3157.

66 Niss, K., Dalle-Ferrier, C., Tarjus, G., and Alba-Simionesco, C. (2007) *J. Phys.: Condens. Matter*, **19**, 076102; Zhang, C., Guo, Y., and Priestley, R.D. (2014) *ACS Macro Lett.*, **3**, 501–505.

67 Bohmer, R., Ngai, K.L., Angell, C.A., and Plazek, D.J. (1993) *J. Chem. Phys.*, **99**, 4201; Robertson, C.G. and Wilkes, G.L. (2001) *J. Polymer Sci. B*, **39**, 2118–2129.

68 Böhmer, R. and Angell, C.A. (1994) *Disorder Effects on Relaxational Processes* (eds R. Richert and A. Blumen), Springer, Berlin.

69 Vilgis, T.A. (1993) *Phys. Rev. B*, **47**, 2882–2885.

70 Novikov, V.N., Ding, Y., and Sokolov, A.P. (2005) *Phys. Rev. E*, **71**, 061501; Sokolov, A.P., Novikov, V.N., and Ding Y. (2007) *J. Phys.: Condens. Matter*, **19**, 205116.

71 Kunal, K., Robertson, C.G., Pawlus, S., Hahn, S.F., and Sokolov, A.P. (2008) *Macromolecules*, **41**, 7232–7238.

72 Roland, C.M., Santangelo, P.G., and Ngai, K.L. (1999) *J. Chem. Phys.*, **111**, 5593.

73 Cangialosi, D., Alegria, A., and Colmenero, J. (2006) *J. Chem. Phys.*, **124**, 024906.

74 Ngai, K.L. and Plazek, D.J. (1995) *Rubber Chem. Technol. Rubber Review*, **68**, 376–434; Angell, C.A., Richards, B.E., and Velikov, V. (1999) *J. Phys.: Condens. Matter*, **11**, A75.

75 Johari, G.P. (2000) *J. Chem. Phys.*, **112**, 8958.

76 Saiter, A., Saiter, J.M., and Grenet, J. (2006) *Eur. Polymer J.*, **42**, 213–219.

77 Glarum, S.H. (1960) *J. Chem. Phys.*, **33**, 639.

78 Turnbull, D. and Cohen, M.H. (1959) *J. Chem. Phys.*, **31**, 1164–1169; Turnbull, D. and Cohen, M.H. (1961) *J. Chem. Phys.*, **34**, 120–125.

79 Gibbs, J.H. and DiMarzio, E.A. (1958) *J. Chem. Phys.*, **28**, 373.

80 DiMarzio, E.A. (1981) *Ann. N.Y. Acad. Sci.*, **371**, 1.

81 Goldstein, M. (1969) *J. Chem. Phys.*, **51**, 3728–3739.

82 Stillinger, F.H. and Debenedetti, P.G. (2003) *Biophys. Chem.*, **105**, 211–220.

83 Bengtzelius, U., Gotze, W., and Sjolander, A. (1984) *J. Phys. C*, **17**, 5915–5934; Leutheusser, E. (1984) *Phys. Rev. A*, **29**, 2765–2773.

84 Debenedetti, P.G. (1996) *Metastable Liquids: Concepts and Principles*, Princeton University Press, Princeton.

85 Binder, K., Baschnagel, J., and Paul, W. (2003) *Prog. Polymer Sci.*, **28**, 115–172.

86 Kirkpatrick, T.R. and Wolynes, P.G. (1987) *Phys. Rev. A*, **35**, 3072–3080; (1987) *Phys. Rev. B*, **36**, 8552–8564; Kirkpatrick, T.R. and Thirumalai, D. (1987) *Phys. Rev. Lett.*, **58**, 2091–2094.

87 Ojovan, M.I. (2006) *J. Exp. Theor. Phys. Lett.*, **79**, 632–634; Ojovan, M.I. and Lee, W.E. (2006) *J. Phys.: Condens. Matter*, **18**, 11507–11520.

88 Ojovan, M.I., Travis, K.P., and Hand, R.J. (2007) *J. Phys.: Condens. Matter*, **19**, 415107.

89 Ojovan, M.I. (2008) *Entropy*, **10**, 334–364.

90 Ritord, F. and Sollich, P. (2003) *Adv. Phys.*, **52**, 219–342.

91 Garrahan, J.P., Sollich, P., and Toninelli, C. (2011) Kinettically constrained models, in *Dynamical Heterogeneities in Glasses, Colloids and Granular Media* (eds L. Berthier, G. Biroli, J.-P. Bouchaud, L. Cipelletti, and W. van Saarloos), Oxford University Press, Oxford, Chapter 10, pp. 341–369.

92 Nelson, D.R. (1983) *Phys. Rev. Lett.*, **50**, 982–985; (1983) *Phys. Rev. B*, **28**, 5515–5535.

93 Tarjus, G. (2011) An overview of the theories of the glass transition, in *Dynamical Heterogeneities in Glasses, Colloids and Granular Media* (eds L. Berthier, G. Biroli, J.-P. Bouchaud, L. Cipelletti, and W. van Saarloos), Oxford University Press, Oxford, Chapter 2, pp. 39–67.

94 Ediger, M.D., Angell, C.A., and Nagel, S.R. (1996) *J. Phys. Chem.*, **100**, 13200–13212.

95 Chandler, D. and Garrahan, J.P. (2010) *Annu. Rev. Phys. Chem.*, **61**, 191.

96 Doliwa, B. and Heuer, A. (2003) *Phys. Rev. E*, **67**, 031506.

97 Heuer, A. (2008) *J. Phys.: Condens. Matter*, **20**, 373101.

98 Mauro, J.C., Loucks, R.J., Varshneya, A.K., and Gupta, P.K. (2008) *Sci. Model Simul.*, **15**, 241–281.

99 Stillinger, F.H. (1988) *J. Chem. Phys.*, **88**, 7818–7825.

100 Huang, D., Simon, S.L., and McKenna, G.B. (2003) *J. Chem. Phys.*, **119**, 3590–3593.

101 Kohlrausch, R. (1854) *Pogg. Ann. Phys.*, **91**, 179–213; Williams, G. and Watts, D.C. (1970) *Trans. Faraday Soc.*, **66**, 80–85.

102 Doolittle, A.K. (1951) *J. Appl. Phys.*, **22**, 1471–1479.

103 Simha, R. and Somcynsky, T. (1969) *Macromolecules*, **2**, 342–350.

104 Sanchez, I.C. and Stone, M.T. (2000) Statistical thermodynamics of polymer solutions and blends, in *Polymer Blends Volume 1: Formulation* (eds D.R. Paul and C.B. Bucknall), John Wiley & Sons Inc., New York.

105 Frenkel, J. (1946) *Kinetic Theory of Liquids*, Clarendon, Oxford; Chow, T.S. (1984) *Polymer Eng. Sci.*, **24**, 1079–1086.

106 Bair, H.E., Akinay, A.E., Menczel, J.D., Prime, R.B., and Jaffe, M. (2009) Thermomechanical analysis (TMA) and thermodilatometry (TD), in *Thermal Analysis of Polymers, Fundamentals and Applications* (eds J.D. Menczel and R.B. Prime), John Wiley & Sons, Inc., Hoboken, NJ, Chapter 4, pp. 319–385; Price, D.M. (1998) *Thermochim. Acta*, **315**, 11–18.

107 Chartoff, R.P., Menczel, J.D., and Dillman, S.H. (2009) Dynamic mechanical analysis (DMA), in *Thermal Analysis of Polymers, Fundamentals and Applications* (eds J.D. Menczel and R.B. Prime), John Wiley & Sons, Inc., Hoboken, N J, Chapter 5, pp. 387–495.

108 Chu, P.P. and Wu, H.-D. (2000) *Polymer*, **41**, 101–109.

109 Fox, T.G. and Flory, P.J. (1950) *J. Appl. Phys.*, **21**, 581; (1954) *J., Polymer Sci.*, **14**, 315.

110 Simha, R. and Boyer, R.F. (1962) *J. Chem. Phys.*, **37**, 1003–1007.

111 Dlubek, G., Kilburn, D., and Alam, M.A. (2004) *Electrochim. Acta*, **49**, 5241–5247.

112 Kobayashi, Y., Haraya, K., Kamiya, Y., and Hattori, S. (1992) *Bull. Chem. Soc. Jpn*, **65**, 160–163.

113 Flory, P. (1942) *J. Chem. Phys.*, **10**, 51–61.

114 Huggins, M.L. (1942) *J. Am. Chem. Soc.*, **64**, 1712–1719.

115 Sastry, S. (2001) *Nature*, **409**, 164–167.

116 Cavagna, A. (2009) *Phys. Rep.*, **476**, 51.

117 Kirkpatrick, T.R., Thirumalai, D., and Wolynes, P.G. (1989) *Phys. Rev. A*, **40**, 1045.

118 Bouchaud, J.-P. and Biroli, G. (2004) *J. Chem. Phys.*, **121**, 7347.

119 Lubchenko, V. and Wolynes, P.G. (2007) *Ann. Rev. Phys. Chem.*, **58**, 235.

120 Ashtekar, S., Scott, G., Lyding, J., and Gruebele, M. (2010) *J. Phys. Chem. Lett.*, **1**, 1941.

121 Kivelson, D., Kivelson, S.A., Zhao, X.-L., Nussinov, Z., and Tarjus, G. (1995) *Physica A*, **219**, 27; Tarjus, G., Kivelson, S.A., Nussinov, Z., and Viot, P. (2005) *J. Phys.: Condens. Matter*, **17**, R1143.

122 Coslovich, D. and Pastore, G. (2007) *J. Chem. Phys.*, **127**, 124504; Tanaka, H., Kawasaki, T., Shintani, H., and Watanabe, K. (2010) *Nat. Mater.*, **9**, 324; Pedersen, U.R., Schroder, T.B., Dyre, J.C., and Harrowell, P. (2010) *Phys. Rev. Lett.*, **104**, 105701.

123 Medvedev, N.N., Geiger, A., and Brostow, W. (1990) *J. Chem. Phys.*, **93**, 8337; Naberukhin, Yu.I., Voloshin, V.P., and Medvedev, N.N. (1991) *Mol. Phys.*, **73**, 919.

124 Kondo, T. and Tsumuraya, K. (1990) *J. Chem. Phys.*, **94**, 8220.

125 Douglas, R.W. (1949) *J. Soc. Glass Technol.*, **33**, 138–162.

126 Tanaka, H. (2005) *J. Non-Cryst. Solids*, **351**, 3371–3384, 3385–3395, 3396–3413.

127 Freed, K.F. (2011) *Acc. Chem. Res.*, **44**, 194–203 (and cited references).

128 Katritzky, A.R., Kuanar, M., Slavov, S., Hall, C.D., Karelson, M., Kahn, I., and Dobchev, D.A. (2010) *Chem. Rev.*, **110**, 5714–5789; Le, T., Epa, V.C., Burden, F.R., and Winkler, D.A. (2012) *Chem. Rev.*, **112**, 2889–2919.

129 Liu, W.Q. and Cao, C.Z. (2009) *Colloid Polymer Sci.*, **287**, 811–818.

130 Barrat, J.L., Baschnagel, J., and Lyulin, A. (2010) *Soft Matter*, **6**, 3430–3446.

131 Hamerton, I., Howlin, B.J., and Kamyszek, G. (2012) *PLoS One*, **7**, e38424.

132 Mhlanga, P., Hassan, W.A.W., Hamerton, I., and Howlin, B.J. (2013) *PLoS One*, **8**, e53367.

133 Karasz, F.E. and MacKnight, W.T. (1968) *Macromolecules*, **1**, 537.
134 Mark, J.E. (ed.) (1999) *Polymer Data Handbook*, Oxford University Press, New York.
135 O'Reilly, J.M., Bair, H.E., and Karasz, F.E. (1982) *Macromolecules*, **15**, 1083–1088.
136 Rogers, S.S. and Mandelkern, L. (1957) *J. Phys. Chem.*, **61**, 985–990.
137 Shetter, J.A. (1963) *J. Polymer Sci. B Polymer Lett.*, **1**, 209–213.
138 Shen, M.C. and Eisenberg, A. (1970) *Rubber Chem. Technol.*, **43**, 95, 156.
139 Lal, J. and Trick, G.S. (1964) *J. Polymer Sci. A2*, **2**, 4559–4572.
140 Haldon, R.A., Schell, W.J., and Simha, R. (1967) *J. Macromol. Sci. B*, **1**, 759–775.
141 Stukalin, E.B., Douglas, J.F., and Freed, K.F. (2009) *J. Chem. Phys.*, **131**, 114905–114913.
142 Vincent, P.I. (1965) *The Physics of Plastics* (ed. P.D. Ritchie), D. Van Nostrand Co., Inc., Princeton, NJ, Chapter 2.
143 Allcock, H.R., Connolly, M.S., Sisko, J.T., and Al-Shali, S. (1988) *Macromolecules*, **21**, 323–334.
144 Wisian-Neilson, P., Huang, L., Islam, M.Q., and Crane, R.A. (1994) *Polymer*, **35**, 4985–4989.
145 Foucher, D.A., Ziembinski, R., Ben-Zhong, T., Macdonald, P.M., Massey, J., Jaeger, C.R., Vansco, G.J., and Manners, I. (1993) *Macromolecules*, **26**, 2878.
146 Somcynsky, T. and Patterson, D. (1962) *J. Polymer Sci.*, **62**, 151.
147 Pezzin, G., Zilio-Grandi, F., and Sanmartin, P. (1970) *Eur. Polymer J.*, **6**, 1053–1061.
148 Gedde, U.W. (1995) *Polymer Physics*, Chapman & Hall, London.
149 Schmieder, K. and Wolf, D. (1953) *Kolloid Z.*, **134**, 149.
150 Roland, C.M. and Casalini, R. (2005) *Macromolecules*, **38**, 8729–8733; Roland, C.M., Hensel-Bielowka, S., Paluch, M., and Casalini, R. (2005) *Rep. Prog. Phys.*, **68**, 1405–1478; Karlou, K. and Schneider, H.A. (2000) *J. Thermal Anal. Calorim.*, **59**, 59–69.
151 Schwartz, G.A., Paluch, M., Alegría, A., and Colmenero, J. (2009) *J. Chem. Phys.*, **131**, 044906; Roland, C.M. (2008) *Soft Matter*, **4**, 2316–2322; Roland, C.M. and Casalini, R. (2007) *Macromolecules*, **40**, 3631–3639.
152 Speedy, R.J. (1999) *J. Phys. Chem. B*, **103**, 8128–8131.
153 Goldstein, M. (1973) *J. Phys. Chem.*, **77**, 667–673.
154 Andersson, S.P. and Andersson, O. (1998) *Macromolecules*, **31**, 2999–3006.
155 Cheng, S.Z.D. and Jin, S. (2002) Crystallization and melting of metastable crystalline polymers, in *Handbook of Thermal Analysis and Calorimetry, Vol. 3: Applications to Polymers and Plastics* (ed. S.Z.D. Cheng), Elsevier, Amsterdam, Chapter 3, pp. 167–195.
156 Calleja, G., Jourdan, A., Ameduri, B., and Habas, J.-P. (2013) *Eur. Polymer J.* **49**, 2214–2222; Wunderlich, B. (2005) *Thermal Analysis of Polymeric Materials*, Springer Berlin; Wunderlich, B. (2003) *Prog. Polymer Sci.*, **28**, 383–450.
157 Alves, N.M., Mano, J.F., Balaguer, E., Meseguer Duenas, J.M., and Gómez Ribelles, J.L. (2002) *Polymer*, **43**, 4111–4122.
158 Griffith, J.H. and Rånby, B.G. (1960) *J. Polymer Sci.*, **44**, 369–381.
159 Miller, R.W. and Murayama, T. (1984) *J. Appl. Polymer Sci.*, **29**, 933–939.
160 Garrett, P.D. and Grubb, D.T. (1988) *J. Polymer Sci. B*, **26**, 2509.
161 Shen, M.C. and Tobolsky, A.V. (eds) (1965) Glass transition temperature of polymers – effect of plasticizer, chain ends, and comonomer, in *Plasticization and Plasticizer Processes*, vol. **48** (ed. N.A.J. Platzer), ACS, Washington.
162 Shtarkman, B.P. and Razinskaya, I.N. (1983) *Acta Polym.*, **34**, 514–520.
163 Riggleman, R.A., Douglas, J.F., and de Pablo, J.J. (2010) *Soft Matter*, **6**, 292–304.
164 Pittia, P. and Sacchetti, G. (2008) *Food Chem.*, **106**, 1417–1427.
165 Pena, J.R., Hidalgo, M., and Mijangos, C. (2000) *J. Appl. Polymer Sci.*, **75**, 1303–1312.
166 Rothon, R.N. (ed.) (2003) *Particulate-Filled Polymer Composites*, 2nd edn, Rapra Technology Ltd, Shrewsbury, UK.
167 Mohomed, K., Gerasimov, T.G., Abourahma, H., Zaworotko, M.J., and Harmon, J.P. (2005) *Mater. Sci. Eng. A Struct.*, **409**, 227.

168 Ash, B.J., Siegel, R.W., and Schadler, L.S. (2004) *J. Polymer Sci. B*, **42**, 4371–4383.

169 Sargsyan, A., Tonoyan, A., Davtyan, S., and Schick, C. (2007) *Eur. Polymer J.*, **43**, 3113–3127; Davtyan, S.P., Tonoyan, A.O., Varderesyan, A.Z., and Müller, S.C. (2014) *Eur. Polymer J.*, **54**, 182–186.

170 Klonos, P., Panagopoulou, A., Bokobza, L., Kyritsis, A., Peoglos, V., and Pissis, P. (2010) *Polymer*, **51**, 5490–5499.

171 Fragiadakis, D., Pissis, P., and Bokobza, L. (2005) *Polymer*, **46**, 6001–6008.

172 Srivastava, S. and Basu, J.K. (2007) *Phys. Rev. Lett.*, **98**, 165701.

173 Srivastava, S., Kandar, A.K., Basu, J.K., Mukhopadhyay, M.K., Lurio, L.B., Narayanan, S., and Sinha, S.K. (2009) *Phys. Rev. E*, **79**, 021408.

174 Rittigstein, P. and Torkelson, J.M. (2006) *J. Polymer Sci. B*, **44**, 2935–2943.

175 Fragiadakis, D., Bokobza, L., and Pissis, P. (2011) *Polymer*, **52**, 3175–3182.

176 Fox, T.G. and Loshaek, S. (1955) *J. Polymer Sci.*, **15**, 371–390.

177 DiBenedetto, A.T. (1987) *J. Polymer Sci. B*, **25**, 1949–1969.

178 Pascault, J.P. and Williams, R.J.J. (1990) *J. Polymer Sci. B*, **28**, 85.

179 Venditti, R.A. and Gillham, J.K. (1997) *J. Appl. Polymer Sci.*, **64**, 3–14.

180 Prolongo, M.G., Arribas, C., Salom, C., and Masegosa, R.M. (2007) *J. Appl. Polymer Sci.*, **103**, 1507–1516.

181 Schick, C. (2010) *Eur. Phys. J. Special Topics*, **189**, 3–36; Arabeche, K., Delbreilh, L., Adhikari, R., Michler, G.H., Hiltner, A., Bear, E., and Saiter, J.-M. (2012) *Polymer*, **53**, 1355–1361.

182 McKenna, G.B. (2010) *Eur. Phys. J. Special Topics*, **189**, 285–302.

183 Anastasiadis, S.H., Karatasos, K., Vlachos, G., Manias, E., and Giannelis, E.P. (2000) *Phys. Rev. Lett.*, **84**, 915; Vaia, R.A., Sauer, B.B., Tse, O.K., and Giannelis, E.P. (1997) *J. Polymer Sci. B*, **35**, 59.

184 Ao, Z.M. and Jiang, Q. (2006) *Langmuir*, **22**, 1241–1246.

185 Pham, J.Q. and Green, P.F. (2003) *Macromolecules*, **36**, 1665–1669.

186 Boiko, Y.M. (2010) *Colloid Polymer Sci.*, **288**, 1757–1761.

187 Mok, M.M., Kim, J., Marou, S.R., and Torkelson, J.M. (2010) *Eur. Phys. J. E*, **31**, 239–252.

188 Kalogeras, I.M. (2005) *Acta Mater.*, **53**, 1621–1630; Kalogeras, I.M. and Neagu, E.R. (2004) *Eur. Phys. J. E*, **14**, 193–204.

189 Alcoutlabi, M. and McKenna, G.B. (2005) *J. Phys.: Condens. Matter*, **17**, R461–R524; Roth, C.B. and Dutcher, J.R. (2005) *J. Electroanal. Chem.*, **584**, 13–22.

190 Richert, R. (2011) *Ann. Rev. Phys. Chem.*, **62**, 65–84; D. Cangialosi (2015) Effect of confinement geometry on out-of-equilibrium glassy dynamics, in *Non-equilibrium Phenomena in Confined Soft Matter, Soft and Biological Matter* (S. Napolitano, ed.), Springer, Basel, Chapter 12, pp. 265–298.

191 Zheng, W. and Simon, S.L. (2007) *J. Chem. Phys.*, **127**, 194501.

192 Jackson, C.L. and McKenna, G.B. (1991) *J. Non-Cryst. Solids*, **131–133**, 221.

193 Trofymluk, O., Levchenko, A.A., and Navrotsky, A. (2005) *J. Chem. Phys.*, **123**, 194509.

194 Schönhals, A., Goering, H., and Schick, Ch. (2002) *J. Non-Cryst. Solids*, **305**, 140; He, F., Wang, L.-M., and Richert, R. (2005) *Phys. Rev. B*, **71**, 144205; Arndt, M., Stannarius, R., Gorbatchow, W., and Kremer, F. (1996) *Phys. Rev. E*, **54**, 5377.

195 Fakhraai, Z. and Forrest, J.A. (2008) *Science*, **319**, 600–604; Dutcher, J.R. and Ediger, M.D. (2008) *Science*, **319**, 577–578; Xia, W., Mishra, S., Keten, S. (2013) *Polymer* **54**, 5942–5951.

196 Fukao, K. and Miyamoto, Y. (2000) *Phys. Rev. E.*, **61**, 1743–1754; Fakharaai, Z. and Forrest, J.A. (2005) *Phys. Rev. Lett.*, **95**, 025701.

197 Keddie, J.L., Jones, R.A.L., and Cory, R.A. (1994) *Europhys. Lett.*, **27**, 59.

198 de Gennes, P.G. (2000) *Eur. Phys. J. E*, **2**, 201–205.

199 Park, C.H., Kim, J.H., Ree, M., Sohn, B.-H., Jung, J.C., and Zin, W.-C. (2004) *Polymer*, **45**, 4507–4513; Forrest, J.A. and Dalnoki-Veress, K. (2001) *Adv. Colloid Polymer Sci.*, **94**, 167–195.

200 Priestley, R.D., Mundra, M.K., Barnett, N.J., Broadbelt, L.J., and Torkelson, J.M. (2007) *Aust. J. Chem.*, **60**, 765–771; Rittigstein, P., Priestley, R.D., Broadbelt,

L.J., and Torkelson, J.M. (2007) *Nat. Mater.*, **6**, 278–282.

201 Zhao, H.Y., Yu, Z.N., Begum, F., Hedden, R.C., and Simon, S.L. (2014) *Polymer*, **55**, 4959–4965.

202 Priestley, R.D., Rittigstein, P., Broadbelt, L.J., Fukao, K., and Torkelson, J.M. (2007) *J. Phys.: Condens. Matter*, **19**, 205120.

203 Zanotto, A., Spinella, A., Nasillo, G., Caponetti, E., and Luyt, A.S. (2012) *Express Polymer Lett.*, **6**, 410–416.

204 Tran, T.A., Said, S., and Grohens, Y. (2005) *Macromolecules*, **38**, 3867.

205 Ouaad, K., Djadoun, S., Ferfera-Harrar, H., Sbirrazzuoli, N., and Vincent, L. (2011) *J. Appl. Polymer Sci.*, **119**, 3227–3233.

206 John, J., Klepac, D., Didović, M., Sandesh, C.J., Liu, Y., Raju, K.V.S.N., Pius, A., Valić, S., and Thomas, S. (2010) *Polymer*, **51**, 2390–2402.

207 Priestley, R.D., Ellison, C.J., Broadbelt, L.J., and Torkelson, J.M. (2005) *Science*, **309**, 456–459.

208 Brady, R.F. and Charlesworth, J.M. (1994) *Prog. Org. Coat.*, **24**, 1.

209 Forrest, J.A., Dalnoki-Veress, K., and Dutcher, J.R. (1997) *Phys. Rev. E*, **56**, 5705–5716.

210 DeMaggio, G.B., Frieze, W.E., Gidley, D.W., Zhu, M., Hristov, H.A., and Yee, A.F. (1997) *Phys. Rev. Lett.*, **78**, 1524–1527.

211 Gorbunov, V.V., Grandy, D., Reading, M., and Tsukruk, V.V. (2009) Micro- and nanoscale local thermal analysis, in *Thermal Analysis of Polymers, Fundamentals and Applications* (eds J.D. Menczel and R.B. Prime), John Wiley & Sons, Inc., Hoboken, NJ, Chapter 7, pp. 615–649.

212 Turi, E.A. (ed.) (1997) *Thermal Characterization of Polymeric Materials*, 2nd edn, Academic Press, New York.

213 Vassilikou-Dova, A. and Kalogeras, I.M. (2009) Dielectric analysis (DEA), in *Thermal Analysis of Polymers, Fundamentals and Applications* (eds J.D. Menczel and R.B. Prime), John Wiley & Sons, Inc., Hoboken, NJ, Chapter 6, pp. 497–610.

214 Rieger, J. (2001) *Polymer Test.*, **20**, 199–204.

215 Kalogeras, I.M., Pallikari, F., Vassilikou-Dova, A., and Neagu, E.R. (2006) *Appl. Phys. Lett.*, **89**, 172905; (2007) *J. Appl. Phys.*, **101**, 094108.

216 Moynihan, C.T., Easteal, A.J., DeBolt, M.A., and Tucker, J. (1976) *J. Am. Ceram. Soc.*, **59**, 12–16.

217 Badrinarayanan, P., Zheng, W., Li, Q., and Simon, S.L. (2007) *J. Non-Cryst. Solids*, **353**, 2603–2612.

218 Reading, M. (1993) *Trends Polymer Sci.*, **8**, 248–253; Lacey, A.A., Price, D.M., and Reading, M. (2006) Theory and practice of modulated temperature differential scanning calorimetry, in *Modulated-Temperature Differential Scanning Calorimetry, Theoretical and Practical Applications in Polymer Characterisation. Series: Hot Topics in Thermal Analysis and Calorimetry*, vol. 6 (eds M. Reading and D.J. Hourston), Springer, New York, pp. 1–79.

219 Silva, G.G., Machado, J.C., Song, M., and Hourston, D.J. (2000) *J. Appl. Polymer Sci.*, **77**, 2034–2043.

220 www.tainst.com: Applications Library, Thermal Solutions – Determination of polymer blend composition (TS-22A).

221 Maldonado-Santoyo, M., Ortiz-Estrada, C., Luna-Barcenas, G., Sanchez, I.C., Cesteros, L.C., Katime, I., and Nuno-Donlucas, S.M. (2004) *J. Polymer Sci. B*, **42**, 636–645; Maldonado-Santoyo, M., Cesteros, L.C., Katime, I., and Nuno-Donlucas, S.M. (2004) *Polymer*, **45**, 5591–5596.

222 Maldonado-Santoyo, M., Nuno-Donlucas, S.M., Cesteros, L.C., and Katime, I. (2004) *J. Appl. Polymer Sci.*, **92**, 1887–1892.

223 Chakrabarti, R., Das, M., and Chakraborty, D. (2004) *J. Appl. Polymer Sci.*, **93**, 2721–2730; Patricio, P.S.O., Silva, G.G., and Machado, J.C. (2007) *J. Appl. Polymer Sci.*, **105**, 641–646.

224 Heijboer, J. (1978) *Molecular Basis of Transitions and Relaxations* (ed. D.J. Meier), Gordon and Breach, New York.

225 Aouachria, K., Belhaneche-Bensemra, N., and Massardier-Nageotte, V. (2011) *J. Vinyl Addit. Technol.*, **17**, 156–163.

226 Kremer, F. and Schönhals, A. (2003) *Broadband Dielectric Spectroscopy*, Springer, Berlin; Yin, H. and Schönhals, A. (2014) Broadband dielectric spectroscopy on polymer blends, in

Polymer Blends Handbook (eds L.A. Utracki and C.A. Wilkie), Springer, Dordrecht, pp. 1299–1356.
227 van den Berg, O., Sengers, W.G.F., Jager, W.F., Pichen, S.J., and Wübbenhorst, M. (2004) *Macromolecules*, **37**, 2460–2470.
228 Sengers, W.G.F., van den Berg, O., Wübbenhorst, M., Gotsis, A.D., and Pichen, S.J. (2005) *Polymer*, **46**, 6064–6074.
229 Jonscher, A.K. (1983) *Dielectric Relaxation in Solids*, Chelsea Dielectrics Press, London.
230 Havriliak, S. and Negami, S. (1967) *Polymer*, **8**, 161.
231 Kalogeras, I.M., Roussos, M., Vassilikou-Dova, A., Spanoudaki, A., Pissis, P., Savelyev, Y.V., Shtompel, V.I., and Robota, L.P. (2005) *Eur. Phys. J. E*, **18**, 467.
232 Nishi, T., Wang, T.T., and Kwei, T.K. (1975) *Macromolecules*, **8**, 227–234; Wagler, T., Rinaldi, P.L., Han, C.D., and Chun, H. (2000) *Macromolecules*, **33**, 1778–1789.
233 Koningsveld, R., Kleintjens, L., and Schoffeleers, H. (1974) *Pure Appl. Chem.*, **39**, 1–32.
234 Higgins, J.S., Lipson, J.E.G., and White, R.P. (2010) *Phil. Trans. R. Soc. A*, **368**, 1009–1025.
235 Urakawa, O., Fuse, Y., Hori, H., Tran-Cong, Q., and Yano, O. (2001) *Polymer*, **42**, 765–773.
236 Guo, Q. and Liu, Z. (2000) *J. Therm. Anal. Calorim.*, **59**, 101–120.
237 Sy, J.W. and Mijovic, J. (2000) *Macromolecules*, **33**, 933–946.
238 Kim, C.K. and Paul, D.R. (1992) *Polymer*, **33**, 1630–1639.
239 Araki, O., Zheng, Q., Takahashi, M., Takiwaga, T., and Masuda, T. (1995) *Mater. Sci. Res. Int.*, **1**, 144–149.
240 Chang, L.L. and Woo, E.M. (2001) *Polymer J.*, **33**, 13–17.
241 Kim, J.K., Lee, H.H., Son, H.W., and Han, C.D. (1998) *Macromolecules*, **31**, 8566–8578.
242 Coleman, M.M. and Painter, P.C. (1995) *Prog. Polymer Sci.*, **20**, 1–59.
243 Painter, P.C., Veytsman, B., Kumar, S., Shenoy, S., Graf, J.F., Xu, Y., and Coleman, M.M. (1997) *Macromolecules*, **30**, 932–942; Pruthtikul, R., Coleman, M., Painter, P.C., and Tan, N.B. (2001) *Macromolecules*, **34**, 4145–4150; Park, Y., Veytsman, B., Coleman, M., and Painter, P. (2005) *Macromolecules*, **38**, 3703–3707.
244 Utracki, L.A. (1965) *Adv. Polymer Sci.*, **5**, 33–39.
245 Sanchez-Cabezudo, M., Masegosa, R.M., Salom, C., and Prolongo, M.G. (2010) *J. Therm. Anal. Calorim.*, **102**, 1025–1033.
246 Thirtha, V., Lehman, R., and Nosker, T. (2006) *Polymer*, **47**, 5392–5401.
247 Xue, M.-L., Yu, Y.-L., Sheng, J., Chuah, H.H., and Geng, C.-H. (2005) *J. Macromol. Sci. B*, **44**, 317–329.
248 Li, D. and Brisson, J. (1996) *Macromolecules*, **29**, 868–874; Zhang, S.H. and Runt, J. (2004) *J. Polymer Sci. B*, **42**, 3405–3415.
249 Zhang., X., Takegoshi, K., and Hikichi, K. (1991) *Macromolecules*, **24**, 5756–5762.
250 Savin, D.A., Larson, A.M., and Lodge, T.P. (2004) *J. Polymer Sci. B*, **42**, 1155–1163.
251 Kratochvil, J., Sturcova, A., Sikova, A., and Dybal, J. (2011) *J. Polymer Sci. B*, **49**, 1031–1040.
252 Chung, G.C., Kornfield, J.A., and Smith, S.D. (1994) *Macromolecules*, **27**, 5729–5741.
253 Colmenero, J. and Arbe, A. (2007) *Soft Matter*, **3**, 1474–1485.
254 Song, M., Hourston, D.J., Pollock, H.M., and Hammiche, A. (1999) *Polymer*, **40**, 4763–4767.
255 Zheng, S., Huang, J., Li, Y., and Guo, Q. (1997) *J. Polymer Sci. B*, **35**, 1383–1392.
256 Gordon, M. and Taylor, J.S. (1952) *Appl. Chem. (USSR)*, **2**, 493.
257 Wood, L.A. (1958) *J. Polymer Sci.*, **28**, 319–330.
258 Kelley, F.N. and Bueche, F. (1961) *J. Polymer Sci.*, **50**, 549–556.
259 DiMarzio, E.A. and Gibbs, J.H. (1959) *J. Polymer Sci.*, **40**, 121–131.
260 DiMarzio, E.A. (1990) *Polymer*, **31**, 2294–2298.
261 Fox, T.G. (1956) *Bull. Am. Phys. Soc.*, **1**, 123–125.
262 Kalogeras, I.M. and Brostow, W. (2009) *J. Polymer Sci. B*, **47**, 80–95.

263 Kalogeras, I.M. (2010) *Thermochim. Acta*, **509**, 135–146.

264 Khougaz, K. and Clas, S.-D. (2000) *J. Pharm. Sci.*, **89**, 1325–1334.

265 Konno, H. and Taylor, L.S. (2006) *J. Pharm. Sci.*, **95**, 2692–2705.

266 Kovacs, A.J. (1963) *Adv. Polymer Sci.*, **3**, 394–507.

267 Braun, G., Kovacs, A.J., and Prim, J.A. (eds) (1966) *Physics of Non-Crystalline Solids*, North-Holland, Amsterdam, p. 303.

268 Aubin, M. and Prud'homme, R.E. (1988) *Polymer Eng. Sci.*, **28**, 1355–1361; (1988) *Macromolecules*, **28**, 2945–2949.

269 Feldstein, M.M. (2001) *Polymer*, **42**, 7719–7726.

270 Chang, C.-S., Woo, E.M., and Lin, J.-H. (2006) *Macromol. Chem. Phys.*, **207**, 1404–1413.

271 Pedrosa, P., Pomposo, J.A., Calahorra, E., and Cortazar, M. (1994) *Macromolecules*, **27**, 102–109.

272 Coleman, M.M., Xu, Y., and Painter, P.C. (1994) *Macromolecules*, **27**, 127–134; Serman, C.J., Painter, P.C., and Coleman, M.M., *Polymer* (1991) **32**, 1049–1058.

273 Mpoukouvalas, K., Floudas, G., Zhang, S.H., and Runt, J. (2005) *Macromolecules*, **38**, 552–560.

274 Park, M.S. and Kim, J.K. (2002) *J. Polymer Sci. B*, **40**, 1673–1681.

275 Couchman, P.R. and Karasz, F.E. (1978) *Macromolecules*, **11**, 117–119.

276 Couchman, P.R. (1987) *Macromolecules*, **20**, 1712–1717.

277 Couchman, P.R. (1991) *Macromolecules*, **24**, 5772–5774.

278 Pochan, J.M., Beatty, C.L., and Pochan, D.F. (1979) *Polymer*, **20**, 879–886.

279 An, L., He, D., Jing, J., Wang, Z., Yu, D., and Jiang, B. (1997) *Eur. Polymer J.*, **33**, 1523–1528.

280 Pinal, R. (2008) *Entropy*, **10**, 207–223.

281 Painter, P.C., Graf, J.F., and Coleman, M.M. (1991) *Macromolecules*, **24**, 5630–5638.

282 Pomposo, J.A., Cortazar, M., and Calahorra, E. (1994) *Macromolecules*, **27**, 245–251.

283 Yang, Z. and Han, C.D. (2008) *Macromolecules*, **41**, 2104–2118.

284 ElMiloudi, K., Djadoun, S., Sbirrazzuoli, N., and Geribaldi, S. (2009) *Thermochim. Acta*, **483**, 49–54; Hamou, A.S.H., ElMiloudi, K., and Djadoun, S. (2009) *J. Polymer Sci. B*, **47**, 2074–2082; Abdellaoui-Arous, N., Hadj-Hamou, A.S., and Djadoun, S. (2012) *Thermochim. Acta*, **547**, 22–30.

285 Masser, K.A., Zhao, H.Q., Painter, P.C., and Runt, J. (2010) *Macromolecules*, **43**, 9004–9013.

286 ElMiloudi, K. and Djadoun, S. (2009) *J. Polymer Sci. B*, **47**, 923–931.

287 Kuo, S.W. (2005) *J. Polymer Res.*, **15**, 459–486.

288 Kim, J.H., Min, B.R., and Kang, Y.S. (2006) *Macromolecules*, **39**, 1297–1299.

289 Lu, X. and Weiss, R.A. (1991) *Macromolecules*, **24**, 4381–4385; Lu, X. and Weiss, R.A. (1992) *Macromolecules*, **25**, 3242–3246.

290 Chun, Y.S. and Weiss, R.A. (2004) *J. Appl. Polymer Sci.*, **94**, 1227–1235.

291 Jenckel, E. and Heusch, R. (1953) *Kolloid Z.*, **130**, 89–105.

292 Kanig, G. (1963) *Kolloid Z.*, **190**, 1–10.

293 Kwei, T.K. (1984) *J. Polymer Sci. Lett.*, **22**, 307.

294 Brekner, M.-J., Schneider, A., and Cantow, H.-J. (1988) *Makromol. Chem.*, **189**, 2085–2097.

295 Schneider, H.A. (1997) *J. Res. Natl Inst. Stand. Technol.*, **102**, 229–248.

296 Kalogeras, I.M., Stathopoulos, A., Vassilikou-Dova, A., and Brostow, W. (2007) *J. Phys. Chem. B*, **111**, 2774–2782.

297 Alegría, A., Tellería, I., and Colmenero, J. (1994) *J. Non-Cryst. Solids*, **172**, 961–965.

298 Roland, C.M. and Casalini, R. (2007) *Macromolecules*, **40**, 3631–3639.

299 Brostow, W., Chiu, R., Kalogeras, I.M., and Vassilikou-Dova, A. (2008) *Mater. Lett.*, **62**, 3152–3155.

300 Urakawa, O., Ujii, T., and Adachi, K. (2006) *J. Non-Cryst. Solids*, **352**, 5042–5049.

301 Stoelting, J., Karasz, F.E., and MacKnight, W.J. (1970) *Polymer Eng. Sci.*, **10**, 133–138; Lau, S.F., Pathak, J., and Wunderlich, B. (1982) *Macromolecules*, **15**, 1278–1283.

302 Lodge, T.P., Wood, E.R., and Haley, J.C. (2006) *J. Polymer Sci. B*, **44**, 756–763.

303 Zhao, J., Ediger, M.D., Sun, Y., and Yu, L. (2009) *Macromolecules*, **42**, 6777–6783.

304 Lorthioir, C., Alegría, A., and Colmenero, J. (2003) *Phys. Rev. E*, **68**, 031805; Leroy, E., Alegría, A., and Colmenero, J. (2002) *Macromolecules*, **35**, 5587. Leroy, E., Alegría, A., and Colmenero, J. (2003) *Macromolecules*, **36**, 7280–7288.

305 Miwa, Y., Sugino, Y., Yamamoto, K., Tanabe, T., Sakaguchi, M., Sakai, M., and Shimada, S. (2004) *Macromolecules*, **37**, 6061–6068.

306 Miwa, Y., Usami, K., Yamamoto, K., Sakaguchi, M., Sakai, M., and Shimada, S. (2005) *Macromolecules*, **38**, 2355–2361.

307 Kumar, S.K., Shenogin, S., and Colby, R.H. (2007) *Macromolecules*, **40**, 5759–5766.

308 Zetsche, A. and Fischer, E. (1994) *Acta Polym.*, **45**, 168–175.

309 Kumar, S.K., Colby, R.H., Anastasiadis, S.H., and Fytas, G. (1996) *J. Chem. Phys.*, **105**, 3777–3788.

310 Arrese-Igor, S., Alegria, A., Moreno, A.J., and Colmenero, J. (2011) *Macromolecules*, **44**, 3611–3621.

311 Lodge, T.P. and McLeish, T.C.B. (2000) *Macromolecules*, **33**, 5278–5284.

312 Herrera, D., Zamora, J.-C., Bello, A., Grimau, M., Laredo, E., Müller, A.J., and Lodge, T.P. (2005) *Macromolecules*, **38**, 5109–5117.

313 Gaikwad, A.N., Wood, E.R., Ngai, T., and Lodge, T.P. (2008) *Macromolecules*, **41**, 2502–2508.

314 Evans, C.M. and Torkelson, J.M. (2012) *Polymer*, **53**, 6118–6124.

315 Evans, C.M., Sandoval, R.W., and Torkelson, J.M. (2011) *Macromolecules*, **44**, 6645–6648.

316 Crispim, E.G., Rubira, A.F., and Muniz, E.C. (1999) *Polymer*, **40**, 5129–5135.

317 Lutz, T.R., He, Y., Ediger, M.D., Pitsikalis, M., and Hadjichristidis, N. (2004) *Macromolecules*, **37**, 6440–6448.

318 Sakaguchi, T., Taniguchi, N., Urakawa, O., and Adachi, K. (2005) *Macromolecules*, **38**, 422–428.

319 Haley, J.C., Lodge, T.P., He, Y., Ediger, M.D., Von Meerwall, E.D., and Mijovic, J. (2003) *Macromolecules*, **36**, 6142–6151.

320 Haley, J.C. and Lodge, T.P. (2004) *Colloid Polymer Sci.*, **282**, 793–801.

321 He, Y., Lutz, T.R., Ediger, M.D., Pitsikalis, M., and Hadjichristidis, N. (2005) *Macromolecules*, **38**, 6216–6226.

322 Schneider, H.A. and Breckner, M.-J. (1985) *Polymer Bull.*, **14**, 173–178.

323 He, Y., Lutz, T.R., and Ediger, M.D. (2003) *J. Chem. Phys.*, **119**, 9956–9965.

324 Zheng, W. and Simon, S.L. (2008) *J. Polymer Sci. B*, **46**, 418–430.

325 Balsamo, V., Newman, D., Gouveia, L., Herrera, L., Grimau, M., and Laredo, E. (2006) *Polymer*, **47**, 5810–5820.

326 Song, M. and Long, F. (1991) *Eur. Polymer J.*, **27**, 983–986.

327 Hsu, W.P. (2004) *J. Appl. Polymer Sci.*, **91**, 35–39.

328 Zawada, J.A., Ylitalo, C.M., Fuller, G.G., Colby, R.H., and Long, T.E. (1992) *Macromolecules*, **25**, 2896–2902.

329 Li, X. and Hsu, S.L. (1984) *J. Polymer Sci. B*, **22**, 1331–1342.

330 Zhang, S.H., Jin, X., Painter, P.C., and Runt, J. (2004) *Polymer*, **45**, 3933–3942.

331 Zhang, S.H., Painter, P.C., and Runt, J. (2002) *Macromolecules*, **35**, 9403–9413.

332 Zhang, S.H., Jin, X., Painter, P.C., and Runt, J. (2002) *Macromolecules*, **35**, 3636–3646.

333 Song, M., Hammiche, A., Pollock, H.M., Hourston, D.J., and Reading, M. (1995) *Polymer*, **36**, 3313–3316.

334 Tanaka, S., Nishida, H., and Endo, T. (2009) *Macromolecules*, **42**, 293–298.

335 Kuo, S.W., Huang, C.F., and Chang, F.C. (2001) *J. Polymer Sci. B*, **39**, 1348–1359.

336 Li, X.D. and Goh, S.H. (2003) *J. Polymer Sci. B*, **41**, 789–796.

337 Chiang, W.-J. and Woo, E.M. (2007) *J. Polymer Sci. B*, **45**, 2899–2911.

338 Benabdelghani, Z. and Etxeberria, A. (2011) *J. Appl. Polymer Sci.*, **121**, 462–468.

339 ElMiloudi, K., Hamou, A.S.H., and Djadoun, S. (2008) *Polymer Eng. Sci.*, **48**, 458–466.

340 Hamou, A.S.H. and Djadoun, S. (2007) *J. Appl. Polymer Sci.*, **103**, 1011–1024.

341 M. A., deAraujo., Stadler, R., and Cantow, H.-J. (1988) *Polymer*, **29**, 2235–2243.

342 Bouslah, N., Haddadine, N., Amrani, F., and Hammachin, R. (2008) *J. Appl. Polymer Sci.*, **108**, 3256–3261.

343 Habi, A. and Djadoun, S. (2008) *Thermochim. Acta*, **469**, 1–7.
344 Tanaka, S., Nishida, H., and Endo, T. (2009) *Macromol. Phys.*, **210**, 1235–1240.
345 Lorthior, C., Alegría, A., and Colmenero, J. (2003) *Phys. Rev. B*, **68**, 031805 (1–9).
346 Sanchis, A., Masegosa, R.M., Rubio, R.G., and Prolongo, M.G. (1994) *Eur. Polymer J.*, **30**, 781–787.
347 Kuo, S.W. and Chang, F.C. (2001) *Macromolecules*, **34**, 5224–5228.
348 Qin, C., Pires, A.T.N., and Belfiore, L.A. (1990) *Polymer Commun.*, **31**, 177–182.
349 Qiu, Z., Komura, M., Ikehara, T., and Nishi, T. (2003) *Polymer*, **44**, 8111–8117.
350 Qiu, Z., Fujinami, S., Komura, M., Nakajima, K., Ikehara, T., and Nishi, T. (2004) *Polymer*, **45**, 4515–4521.
351 Xing, P., Dong, L., An, Y., Feng, Z., Avella, M., and Martuscelli, E. (1997) *Macromolecules*, **30**, 2726–2733.
352 Hsu, W.-P. (2002) *J. Appl. Polymer Sci.*, **83**, 1425–1431.
353 Zhang, L., Goh, S., and Lee, S. (1999) *J. Appl. Polymer Sci.*, **74**, 383–388.
354 Lee, L.-T., Woo, E.M., Chen, W.-T., Chang, L., and Yen, K.-C. (2010) *Colloid Polymer Sci.*, **288**, 439–448.
355 Meaurio, E., Zuza, E., and Sarasua, J.-R. (2005) *Macromolecules*, **38**, 1207–1215.
356 Meaurio, E., Zuza, E., and Sarasua, J.-R. (2005) *Macromolecules*, **38**, 9221–9228.
357 Lee, L.T. and Woo, E.M. (2004) *Polymer Int.*, **53**, 1813–1820; (2006) *J. Polymer Sci. B*, **44**, 1339, 1350.
358 Yi, J.Z., Goh, S.H., and Wee, A.T.S. (2001) *Macromolecules*, **34**, 7411–7415.
359 Li, X.-D. and Goh, S.H. (2003) *J. Polymer Sci. B*, **41**, 789–796.
360 Kuo, S.-W. (2009) *J. Appl. Polymer Sci.*, **114**, 116–124.
361 Goh, S.H. and Siow, K.S. (1987) *Polymer Bull.*, **17**, 453–458.
362 Hill, D.J.T., Whittaker, A.K., and Wong, K.W. (1999) *Macromolecules*, **32**, 5285–5291.
363 Arrighi, V., Cowie, J.M.G., Ferguson, R., McEwen, I.J., McGonigle, E.-A., Pethrick, R.A., and Princi, E. (2005) *Polymer Int.*, **55**, 749–756.
364 Lee, J.Y. and Han, J.Y. (2004) *Macromol. Res.*, **12**, 94–99.
365 Alata, H., Zhu, B., and Inoue, Y. (2007) *J. Appl. Polymer Sci.*, **106**, 2025–2030.
366 Yang, F., Qiu, Z., and Yang, W. (2009) *Polymer*, **50**, 2328–2333.
367 Sotele, J.J., Soldi, V., and Nunes Pires, A.T. (1997) *Polymer*, **38**, 1179–1185.
368 Papageorgiou, G.Z., Bikiaris, D.N., and Panayiotou, C.G. (2011) *Polymer*, **52**, 4553–4561.
369 Landry, M.P., Massa, D.J., Mandry, C.J.T., Teegarden, D.M., Colby, R.H., Long, T.E., and Henrichs, P.M. (1994) *J. Appl. Polymer Sci.*, **54**, 991.
370 Zhang, X.Q., Takegoshi, K., and Hikichi, K. (1992) *Macromolecules*, **25**, 4871.
371 Zhang, X.Q., Takegoshi, K., and Hikichi, K. (1991) *Macromolecules*, **24**, 5756–5762.
372 Hirose, Y., Urakawa, O., and Adachi, K. (2004) *J. Polymer Sci. B*, **42**, 4084–4094.
373 Huang, C.-F. and Chang, F.-C. (2003) *Polymer*, **44**, 2965–2974.
374 Mandal, T.K. and Woo, E.M. (1999) *Polymer J.*, **31**, 226–232; Woo, E.M. and Mandal, T.K. (1999) *Macromol. Rapid Commun.*, **20**, 46–49.
375 Bélorgey, G. and Prud'homme, R.E. (1982) *J. Polymer Sci. B*, **20**, 191–203.
376 Chiu, F.-C. and Min, K. (2000) *Polymer Int.*, **49**, 223–234.
377 Cheung, Y.W. and Stein, R.S. (1994) *Macromolecules*, **27**, 2512–2519.
378 Princi, E. and Vicini, S. (2010) *J. Polymer Sci. B*, **48**, 2129–2139.
379 Madbouly, S.A., Abdou, N.Y., and Mansour, A.A. (2006) *Macromol. Chem. Phys.*, **207**, 978–986.
380 Rim, P.B. and Runt, J.P. (1983) *Macromolecules*, **16**, 762–768.
381 Moskala, E.J., Varnell, D.F., and Coleman, M.M. (1985) *Polymer*, **26**, 228.
382 Kuo, S.W. and Chang, F.C. (2001) *Macromolecules*, **34**, 7737–7743.
383 Wang, J., Cheung, M.K., and Mi, Y. (2002) *Polymer*, **43**, 1357–1364.
384 Prolongo, M.G., Salom, C., and Masegosa, R.M. (2002) *Polymer*, **43**, 93–102.
385 Zhang, H., Bhagwagar, D.E., Graf, J.F., Painter, P.C., and Coleman, M.M. (1994) *Polymer*, **35**, 5378–5397.

386 Scott, R.L. (1949) *J. Chem. Phys.*, **17**, 279.

387 Tompa, H. (1949) *Trans. Farad. Soc.*, **45**, 1142–1152.

388 Kwei, T.K., Frisch, H.L., Radigan, W., and Vogel, S. (1977) *Macromolecules*, **10**, 157–160; Pomposo, J.A., Cortazar, M., and Calahorra, E. (1994) *Macromolecules*, **27**, 252–259.

389 Kuo, S.W., Lin, C.L., and Chang, F.C. (2002) *Macromolecules*, **35**, 278–285.

390 Guo, Q. (1996) *Eur. Polymer J.*, **32**, 1409–1413.

391 Ponoit, D. and Prud'homme, R.E. (2002) *Polymer*, **43**, 2321–2328.

392 Min, K.E., Chiou, J.S., Barlow, J.W., and Paul, D.R. (1987) *Polymer*, **28**, 172.

393 Goh, S.H. and Ni, X. (1999) *Polymer*, **40**, 5733–5735.

394 Woo, E.M. and Tseng, Y.C. (2000) *Macromol. Chem. Phys.*, **201**, 1877–1886.

395 Yau, S.N. and Woo, E.M. (1996) *Macromol. Rapid Commun.*, **17**, 615–621.

396 Lee, S.C. and Woo, E.M. (2002) *J. Polymer Sci. B*, **40**, 747–754.

397 Hong, B.K., Kim, J.Y., Jo, W.H., and Lee, S.C. (1997) *Polymer*, **38**, 4373–4375.

398 Hsu, W.P. (2007) *Thermochim. Acta*, **454**, 50–56.

399 Rabeony, M., Siano, D.B., Peiffer, D.G., Siakali-Kioulafa, E., and Hadjichristidis, M. (1994) *Polymer*, **35**, 1033.

400 Kuo, S.W., Chan, C.S.-C., Wu, H.-D., and Chang, F.-C. (2005) *Macromolecules*, **38**, 4729–4736.